BIOGEOCHEMISTRY OF CO_2 SYSTEM AND NET COMMUNITY PRODUCTION DURING MESOSCALE CYCLONIC EDDIES IN THE LEE OF HAWAII

by

FEIZHOU CHEN

(Under the Direction of Wei-Jun Cai)

ABSTRACT

This dissertation characterizes how cyclonic eddy events affect air-sea CO_2 exchange and surface water dissolved inorganic carbon (DIC) budget in the lee of Hawaii, an oligotrophic open ocean region in the subtropical North Pacific Gyre. Local steep sea-floor topography and dominant northeasterly trade winds make the lee of main islands of Hawaii an excellent field for eddy study (Seki, et al., 2001; Benitez-Nelson, 2002; Bidigare et al., 2003; Lumpkin, 1998). Three consecutive E-Flux cruises were conducted in November 2004, January 2005 and March 2005, respectively. Discrete water samples were collected with Niskin bottles at individual stations over about 12 discreet depths for pH, Alkalinity and DIC analysis as well as other related biogeochemical parameters. Underway pCO_2 measurements were conducted along all transects and at process stations both at the center of an eddy or places affected by eddy (IN) and at places which are outside of eddy (OUTER), providing instant real time information of pCO_2 changes in surface water. Based on above measurements, I: 1) discuss the controlling factors of regional CO_2 air-sea exchange across cyclonic eddies; 2) estimate regional air-sea CO_2 exchange rate by mapping of the difference between surface water pCO_2 and atmospheric pCO_2 (ΔpCO_2) and other parameters; 3) estimate the influence of cyclonic eddies on surface water CO_2 budget

at selected stations in the lee of Hawaii; 4) examine whether cold-core cyclonic eddies can significantly improve net community production (NCP) due to the upwelling of nutrients-rich deep water up to the shallower layer based on the inorganic carbon budget.

INDEX WORDS: Mesoscale processes, Cyclonic eddies, Dissolved inorganic carbon (DIC), Net community production (NCP), Carbon cycle, CO_2, CO_2 fluxes, Global warming, the lee of main Hawaiian Islands, Subtropical North Pacific Ocean, E-Flux

BIOGEOCHEMISTRY OF CO_2 SYSTEM AND NET COMMUNITY PRODUCTION DURING MESOSCALE CYCLONIC EDDIES IN THE LEE OF HAWAII

by

FEIZHOU CHEN

B.S., Xiamen University, P. R. China, 1992

PhD, Xiamen University, P. R. China, 1997

A Dissertation Submitted to the Graduate Faculty of The University of Georgia in Partial Fulfillment of the Requirements for the Degree

DOCTOR OF PHILOSOPHY

ATHENS, GEORGIA

2008

BIOGEOCHEMISTRY OF CO_2 SYSTEM AND NET COMMUNITY PRODUCTION DURING MESOSCALE CYCLONIC EDDIES IN THE LEE OF HAWAII

by

FEIZHOU CHEN

Major Professor: Wei-Jun Cai

Committee: Claudia R. Benitez-Nelson
Richard A. Jahnke
Ming-Yi Sun
Chuanlun Zhang

Electronic Version Approved:

Maureen Grasso
Dean of the Graduate School
The University of Georgia
May 2008

ACKNOWLEDGEMENTS

First of all, I want to thank my major advisor, Dr. Wei-Jun Cai for his continuous instruction and great help all these years. I want to thank all my committee members, who have made valuable suggestions to this work. Special thanks to Dr. Benitez-Nelson for inviting us to the E-Flux cruises and her great help in editing my publications related to this dissertation.

I wish to thank all E-Flux collaborators, especially Dr. R. Bidigare and Yoshimi Rii for providing nutrients, TOC, and DON data for this dissertation. Many thanks to Dr. T. Dickey, W. Black, F. Nencioli, Dr. V. Kuwahara, Dr. K. Maiti, P. McAndrew, J. Becker, Dr. T. Bibby, and Dr. Michael Landry's group for their great help for me to access the shipboard data and sampling collection.

I am grateful to C. L. Leonard and the NOAA Ocean Watch Central Pacific for the satellite SST image. Thank the crews of R/V *Ka'imikai-O-Kanaloa* (*KOK*) and R/V *Wecoma* for providing supports for our sampling cruises.

Gratitude to all the colleagues in my lab for their great help all these years, especially, Dr. Yongchen Wang and Ms. Guirong Han for their laboratory support for sample analysis and for their mental support. I would also like to thank Li-Qing Jiang, Justin Hartmann, Dr. Xinping Hu, and Wei-Jen Huang for their great help all these years.

I am grateful to all the friends and colleagues in our department, especially Dr. James Hollibaugh, Dr. Mary Ann Moran, Cedric Fichot, Dr. Sarah Cooley, Paul McKay, Dr. Daniela Di Iorio, Dr. Charles Tilburg, Erin Biers, and Weidong Zhao for their diverse help to my dissertation.

TABLE OF CONTENTS

Page

LIST OF TABLES

Page

LIST OF FIGURES

Page

CHAPTER 1

INTRODUCTION

A significant fraction (~ 30-50 %) of the anthropogenic CO_2 emitted by fossil-fuel burning and deforestation (~ 7 Pg C yr^{-1}) (Sarmiento, 1993; Siegenthaler and Sarmiento, 1993; Takahashi et al., 1997; Bakker and Watson, 2001; Feely et al., 2001; Sarmiento and Gruber, 2002) is absorbed by oceans and terrestrial ecosystems (Sarmiento, 1993; Siegenthaler and Sarmiento, 1993; Bakker and Watson, 2001; Sarmiento and Gruber, 2002; Sabine et al., 2004). While it appears that the "missing" carbon may be equally divided between these major sinks (Quay et al., 1992; Takahashi et al., 1997; Bakker and Watson, 2001; Sarmiento and Gruber, 2002), there is still substantial uncertainty. Recent study (Sabine et al., 2004) indicates that the ocean sink accounts for ~48 % of the total fossil-fuel emissions for the period from 1800 to 1994, while/whereas the terrestrial biosphere was a net source of CO_2 for this period. These all suggest that a more precise oceanic carbon budget is desired to evaluate the capacity of CO_2 uptake in the ocean and land. Therefore, as key step to assess carbon budget in the global ocean, more comprehensive understanding to air-sea CO_2 exchange and upper ocean CO_2 cycle is essential.

Global air-sea CO_2 exchange fluxes can be estimated based on the disequilibrium between atmospheric and sea surface CO_2 concentrations, which primarily drives oceanic CO_2 uptake. Although wind speed can determine the magnitude of air-sea gas exchange, it is ΔpCO_2 (atmospheric pCO_2 minus sea surface pCO_2) that determines the flux direction (Fig. 1.1). Since variation in atmospheric pCO_2 is minor and much less than that of sea surface pCO_2, the

prediction of sea surface pCO_2 is thus critical for the accurate estimates of global oceanic CO_2 uptake.

A significant correlation exists between surface water pCO_2 and sea surface temperature (SST) in the open ocean so that limited in situ oceanic CO_2 and SST observations were computed spatially and temporally to obtain global air-sea CO_2 fluxes. However, sea surface pCO_2-SST relationships are affected by a combination of factors, such as thermodynamics (e.g. temperature effects on CO_2 dissociation and solubility), physical transport (the influence of lateral and vertical mixing of water with different concentrations of total inorganic carbon), and biological activity. Although these processes are all correlated both directly and indirectly with temperature, their relative effects may differ over geographical and temporal scales. Thus several different trends in pCO_2-SST relationship coexist within the world oceans (e.g., (Tans et al., 1990; Takahashi et al., 1993; Inoue et al., 1995; Metzl et al., 1995; Stephens et al., 1995; Landrum et al., 1996; Takahashi et al., 1997; Bates et al., 1998; Wanninkhof and Feely, 1998; Lefevre et al., 2002; Lefevre and Taylor, 2002; Takahashi et al., 2002; Cosca et al., 2003; Olsen et al., 2004). As a result, spatial, seasonal and interannual variability of oceanic CO_2 uptake is difficult to assess and there are large uncertainties in regional and global CO_2 budgets (Tans et al., 1990; Takahashi et al., 1997; Takahashi et al., 2002). Subtropical gyres represent about 60% of the global ocean area (Quay and Stutsman, 2003). A more comprehensive understanding of sea surface pCO_2-SST relationship and its controlling factors within the subtropical gyres is desired in order to more accurately estimate the global capacity of CO_2 uptake.

One of the key processes responsible for the removal of carbon from surface waters is governed by the quantity of carbon exported to the deep water via the biological pumps (Volk and Hoffert, 1985). In the subtropical open ocean, both production and community structure are

controlled to a large extent by the limited availability of macro and trace nutrients. As a result, much of the primary production (PP) in these systems uses recycled nutrients (i.e., regenerated production), and is dominated by a microbial food web (Dugdale and Goering, 1967). New production (NP) is by definition the portion of PP sustained by exogenous nutrients. At steady state, it is often equated with net community production (NCP, defined as net autotrophic production minus community respiration) and to be balanced by the sinking of organic matter from the euphotic zone (Platt et al., 1989; Williams, 1993). Within the oligotrophic subtropical ocean, however, basin wide geochemical estimates of NP are substantially higher than that which can be explained by direct biological and physical estimates of PP and nutrient supply (Shulenberger and Reid, 1981; Jenkins and Goldman, 1985; Oschlies and Garcon, 1998). A possible explanation of this inconsistency is due to the fact that direct measurements may miss the episodic nutrient injections (McGillicuddy and Robinson, 1997; McGillicuddy et al., 1998; Oschlies and Garcon, 1998; Williams and Follows, 1998).

Several studies suggest that mesoscale eddies are potentially one of major pathways for supplying new nutrients to the worldwide upper ocean, thereby enhance PP rates and particle export (Eppley and Peterson, 1979; Falkowski et al., 1991; McGillicuddy and Robinson, 1997; McGillicuddy et al., 1998; Siegel et al., 1999; McGillicuddy et al., 2003; McGillicuddy et al., 2007). It is hypothesized that only a few eddy events are necessary to provide the nutrients required for the annual NP in oligotrophic systems such as the Sargasso Sea (Jenkins, 1988; McGillicuddy et al., 1998). This hypothesis, however, remains controversial, for example, modeling studies argue that the contribution from mesoscale eddy-induced nutrient supply is not sufficient to maintain the observed PP in the subtropical ocean (Oschlies and Garcon, 1998; Oschlies, 2002).

Although few in number, most studies of eddy biogeochemistry have focused on the upwelling of new nutrients (e.g., nitrogen), increases in PP, and shifts in phytoplankton community structure (Falkowski et al., 1991; Olaizola et al., 1993; Allen et al., 1996; Anderson et al., 1996; Seki et al., 2001; Vaillancourt et al., 2003). In contrast, the overall effect of episodic eddies on CO_2 air-sea exchange and inorganic carbon cycling remains vague. The major portion of this dissertation study includes three consecutive cruises under the E-Flux project, a multidisciplinary effort to improve our fundamental understanding of physical, chemical and biological characteristics of cold-core cyclonic eddies that form in the lee of main Hawaiian Islands (Fig. 1.1) (Benitez-Nelson et al., 2007; Dickey et al., 2008). We will focus on analyzing and interpreting the variability of sea surface pCO_2 and dissolved inorganic carbon (CO_2 dynamics) during cold-core cyclonic eddy events. We will interpret how cold-core mesoscale eddies in the lee of main Hawaiian Islands affect the inorganic carbon biogeochemistry and to quantify the contribution of net community production (NCP) to the surface water CO_2 budget in the subtropical ocean. This dissertation consists of four chapters. Chapter one is Introduction. Chapter two provides a summary of the three field experiments, which lasted approximately three weeks each, between November 4, 2004 and March 28, 2005. Chapters 3 and 4 are two main parts of this dissertation. Chapter five is the summary of this dissertation.

Chapter three will focus on sea surface pCO_2 variability and its relationship with other environmental parameters, in particularly, how cyclonic eddies affect pCO_2-SST relationship since several competing effects will coexist during an eddy event. By analyzing CO_2 spatial distribution and temporal changes, this chapter provides an excellent opportunity to study the effects of cyclonic eddies on air-sea CO_2 exchange and CO_2 temporal variation due to different seasons and eddy phases.

Chapter four will discuss the dynamics of dissolved inorganic carbon (DIC) and processes controlling NCP during cyclonic eddy events in the lee of main Hawaiian Islands using the inorganic carbon data during three consecutive cruises. In addition to data analysis and presentation, the discussion will focus on several aspects. First, we will discuss DIC data at OUT-stations (in the absence of the mesoscale eddies) in the lee of main Hawaiian Islands and compare to Station ALOHA, site of the Hawaii Ocean time-series program (HOT) 100 km due North of Oahu. Second, we will propose a two end-member mixing model by using salt budget. This model will be applied to estimate NCP at the eddy center by using mass balances of several biogeochemical parameters. Third, we will compare these results to the NCP estimates without the influence of the eddy at OUT-stations by using one-box mixed-layer model.

Finally, Chapter five will summarize the main findings in Chapters 3 and 4 in terms of carbon cycle during mesoscale-eddy processes in the oligotrophic subtropical gyres. Although "a two end-member mixing model" may oversimplify the situations with the mesoscale cyclonic eddies, it does provide a conceptual model that generalizes how mesoscale cyclonic eddy events affect hydrological and chemical characteristics and the biological response to these events, which will play a critical role in temporal and spatial variability of the CO_2 system in this otherwise nutrient-deficit ocean dissert.

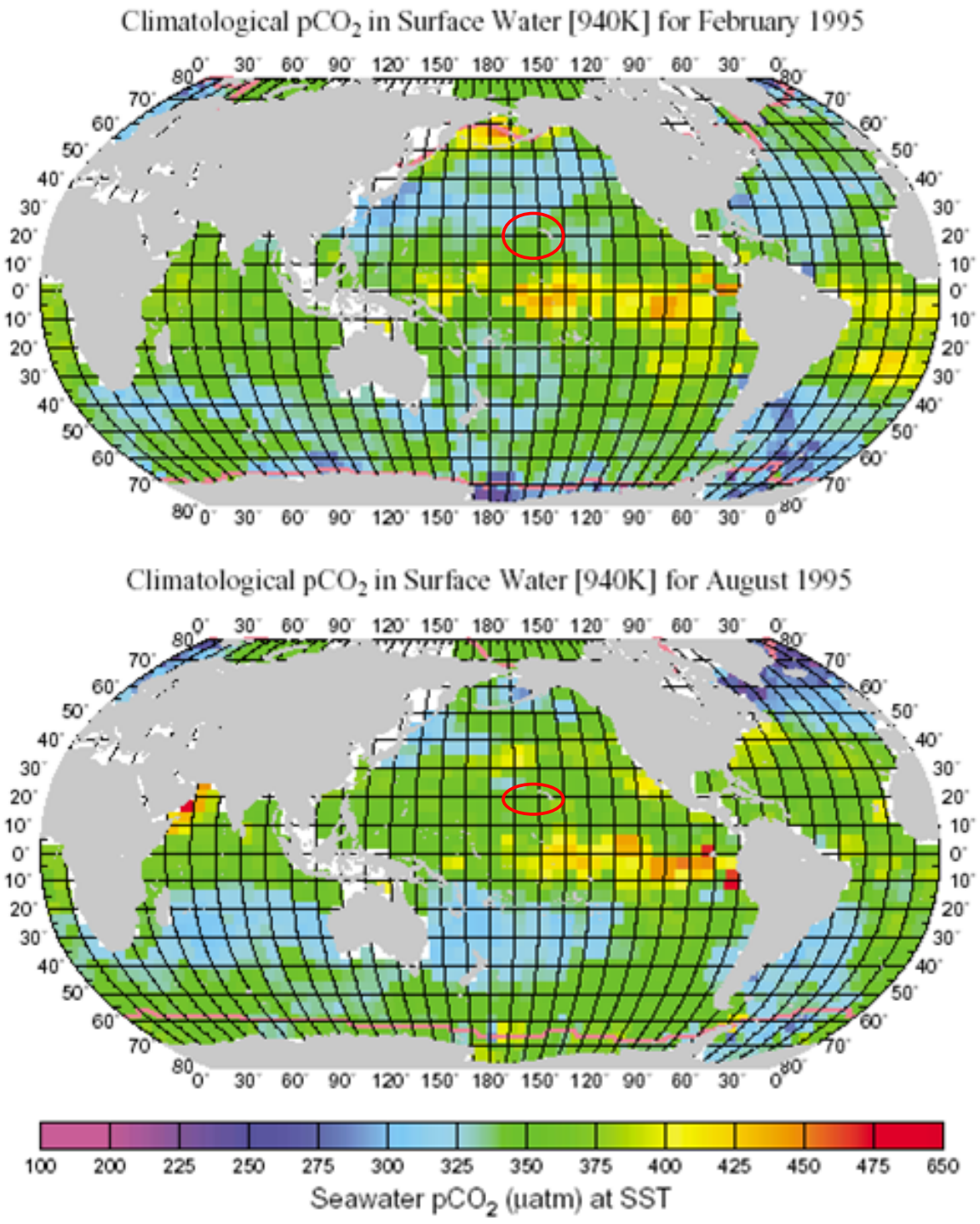

Fig. 1.1 Climatological mean seasonal distribution of sea surface pCO_2. Note that Hawaiian lee eddy area is circled and the spatial resolution of 4° x 5° pixels is insufficient to describe the mesoscale eddy-induced sea surface pCO_2 variation (adapted from Takahashi et al. 2002).

CHAPTER 2

SITE DESCRIPTION AND RESEARCH METHODS

The E-Flux Program was a multidisciplinary effort to understand the physical, chemical and biological characteristics of subtropical cyclonic eddies that form in the lee of main Hawaiian Islands (Benitez-Nelson et al., 2007; Dickey et al., 2008). In this region, island topography and prevailing northeasterly trade winds combine to generate mesoscale eddies in the ‘Alenuihaha Channel between the islands of Maui and Hawaii (Fig. 2.1 adopted from Winn et al. (1998)). They are formed at all times of the year (mean generation frequency = 60 d), but most frequently during periods of high trade wind activity (i.e., late summer through winter). Spanning an average diameter of 180 km, these ephemeral features have typical life spans of 2 to 8 months (Patzert, 1969; Lumpkin, 1998; Chavanne et al., 2002; Dickey et al., 2008). This area thus serves as an ideal natural laboratory providing excellent opportunities for examining eddy biogeochemistry at various stages of eddy development and decay (Falkowski et al., 1991; Seki et al., 2001; Bidigare et al., 2003; Vaillancourt et al., 2003). Please note that Station ALOHA, site of the Hawaii Ocean time-series program (HOT), is located 100 km north of Oahu and ~ 300 km north E-Flux field experiment area (Fig. 2.1). This also provides an excellent opportunity to compare our DIC data to Station ALOHA, which is typical for subtropical waters in the North Pacific Ocean. In this study, we focused on examining NCP and inorganic carbon biogeochemistry in two first baroclinic mode cyclonic eddies, subsequently named Cyclone Noah and Opal, during two cruises of the E-Flux Program (E-Flux I and III). Data from E-Flux

II, an earlier cruise than E-Flux III, prior to formation of Cyclone Opal are also used to assess hydrographic changes through time and also to make inferences about initial conditions.

Description of three E-Flux cruises and sampling strategy

Three consecutive E-Flux cruises were conducted to sample mesoscale cyclonic eddies in the lee of main Hawaiian Islands. Of which, two cyclonic eddies, Cyclone Noah and Opal, were caught during E-Flux I and III, respectively. Cyclone Noah was surveyed during E-Flux I between 4 and 22 November 2004 aboard the University of Hawaii's R/V *Ka'imikai-O-Kanaloa* (*KOK*). Cyclone Opal was sampled during E-Flux III between 10 and 28 March 2005 aboard Oregon State University's R/V *Wecoma*. About one and a half months before E-Flux III field experiment, E-Flux II experiment was conducted between 10 and 28 January 2005 aboard the R/V *Wecoma*. No mesoscale eddies were observed due to the lack of northeasterly trade winds from late December 2004 through the E-Flux II cruise period (Dickey et al., 2008). Thus, the data from this cruise are used to compare with the data at OUT-stations during E-Flux cruises as needed.

To determine the locations and track the cyclonic eddies during ship-based observation, several methodologies on eddy tracking were applied to E-Flux cruises and were described in detail by Dickey et al. (2008). Before each cruise, satellite measurements were available. Sea surface temperature (SST) imagery was obtained from NOAA's Geostationary Operational Environmental Satellites (GOES) radiance sensors (via the Ocean Watch Central Pacific program website at http://oceanwatch.pifsc.noaa.gov/) and NASA's Moderate Resolution Imaging Spectroradiometer (MODIS), which were sent to research vessels and used to determine the initial sampling locations. In addition, drifters were deployed in proximal centers to track the fluid motion of the eddy during E-Flux experiments. Signal of geographic coordinates of drifter

were obtained through satellite system and transmitted to the Ocean Physics Laboratory in University of California in Santa Barbara. These position data were then forwarded to research vessels for near real-time tracking of the drifter. Thirdly, the current data measured by Acoustic Doppler Current Profiler (ADCP) (VM150 KHz Narrow Band manufactured by RDI) were provided by R/V *Ka'imikai-O-Kanaloa* (*KOK*) and R/V *Wecoma*. ADCP current data were used not only to determine the spatial dimensions of the eddy but also to monitor the positions of the eddy centers and to choose the transect paths that intersected the eddy centers.

Cyclone Noah in E-Flux I

Based on satellite sea surface temperature (SST) imagery obtained from Geostationary Operational Environmental Satellite (GOES) radiance sensors, a first baroclinic mode cyclonic eddy, Cyclone Noah, first appeared to the southwest of the Alenuihaha Channel between August 13 and 20th, 2004 with its center located at ~ 20.2ºN, 156.4ºW (Dickey et al., 2008). Cyclone Noah intensified and drifted slowly southward for a brief time after its formation, but then remained near 19.6ºN, 156.5ºW (~ 74 km to the south from its initial satellite-determined center) for most of the E-Flux I cruise sampling period (Dickey et al., 2008; Kuwahara et al., 2008). E-Flux I experiment was conducted during November 4 – 20th, 2004 aboard the R/V *KOK*. Cyclone Noah was at least 2.5 months old by the time of sampling in E-Flux I since eddies could have spun up prior to detection of a surface feature (Dickey et al., 2008). Time-series GOES SST imagery prior to the ship survey (between 4 and 15 October 2004, Fig. 2.2) showed that its surface expression had been rotating as an elliptical shaped eddy, possibly indicative of relaxation and "decay" phase (Kuwahara et al., 2008). The surface expression of Cyclone Noah was less apparent from satellite SST imagery three days prior to the beginning of survey (Fig. 2.3A), which also suggested that Cyclone Noah may have begun to physically decay. However,

this can be caused by factors such as diurnal heating as well (Chavanne et al., 2002; Kuwahara et al., 2008).

During the first week of the cruise (4 to 11 November 2004), an OUT-station (well removed from Cyclone Noah) was sampled at first on 5 November 2004. Then a series of four shipboard transects averaging ~ 150 km in length (in a star configuration) were performed to identify the eddy center and to track Noah's spatial structure (Fig. 2.4 and Table 2.1). Transects 1 (station 1-8, Fig. 2.4), 2 (station 8-17, Fig. 2.4 and Table 2.1), and 4 (station 29-38, Fig. 2.4 and Table 2.1) were characterized by repeat CTD casts. Transect 3 (station 18-27, Fig. 2.4 and Table 2.1) was intensively sampled for a suite of biogeochemical parameters including nutrients and carbon parameters (see Section 2.2). Inorganic carbon samples were also collected for other three transects. Cyclone Noah is in semi-elliptical shape for the upper 200 m with ~ 144 km long in the major axis (Transect 2: ~ 130 km, Transcet 3: ~ 144 km) and ~ 90 km wide in the minor axis (Transect 1: 95 km, Transect 4: ~ 90 km) (Dickey et al., 2008; Kuwahara et al., 2008). The density surface of σ_t = 24.0 kg·m^{-3} was uplifted to ~ 83 m in the center from about 132 m in waters unaffected by the eddy (Kuwahara et al., 2008).

After the transect survey, the best estimate of the center of the eddy was determined to be at station 13 (19.67ºN, 156.52ºW, Fig. 2.4 and Table 2.1) (Kuwahara et al., 2008). Subsequently, we planed to stay at this eddy center, i.e., IN-stations, for more intensive sampling. ADCP velocity data were applied to evaluate if a hydrographic cast was positioned close enough to the eddy to be considered as an IN-station (Dickey et al., 2008; Kuwahara et al., 2008). Angular velocity (defined as the tangential velocity divided by the radial distance from the eddy center) did not remain constant at distinct distances from the center, indicating that solid body rotation (i.e., the portion of water mass isolated from surrounding waters) did not occur beyond ~ 10 km

from the estimated geometric center (Kuwahara et al., 2008). Stations determined to be very near the eddy center (IN-station: IN1) including casts 49-57 were sampled on 12 November 2004. On the next day (13 November 2004), another IN-station (IN2), which is a bit west, was sampled (Fig. 2.4 and Table 2.1). However, only one day later (14 November 2004), wind gusts increased substantially as a front passed, necessitating the cessation of shipboard station sampling (Dickey et al., 2008; Kuwahara et al., 2008). Thus, only IN1 and probably IN2 are really IN-stations which were in the eddy center (Fig. 2.4 and Table 2.1). Another two IN-stations sampled after the storm, i.e., IN3 and IN4, were sampled in the high velocity zone and the eddy edge, respectively. Then R/V *KOK* transited to controlling stations (OUT-stations) well outside the eddy flow field (Fig. 2.4 and Table 2.1) and they were sampled during the last two days (November 19 and 20).

E-Flux II

The E-Flux II field campaign was conducted during January 10 – 28th, 2005 aboard the R/V *Wecoma*, approximately 6 weeks prior to E-Flux III field experiment. A series of six transects were conducted. No mesoscale eddies were observed due to the lack of northeasterly trade winds from late December 2004 throughout the sampling period (Dickey et al., 2008). Thus, the data from this cruise, considered to be somewhat representative of the initial waters from which Cyclone Opal was derived, are used for comparison purposes with other E-Flux cruises as needed. Process stations (IN- and OUT-stations) and Transect 6 (Fig. 2.5 and Table 2.2) was intensively sampled for a suite of biogeochemical parameters including nutrients and carbon parameters (see Section 2.2). Please note that IN- and OUT-stations during E-Flux II are essentially the same since there is no eddy available during this time. They are named so because their geographical locations are more close to IN- and OUT-stations during E-Flux I and III.

Cyclone Opal in E-Flux III

Cyclone Opal first appeared in sea surface temperature (SST) imagery obtained from GOES to the southwest of the Alenuihaha Channel between February 18 and 25, 2005, as a result of the return of strong and persistent northeasterly trade winds in early February (Fig. 2.6A) (Benitez-Nelson et al., 2007; Dickey et al., 2008). Sampling occurred during the E-Flux III field experiment from March 10 - 28, 2005 aboard the R/V *Wecoma*, approximately 4-6 weeks after Opal's first appearance. During the first week of sample collection (March 10 to 15), a series of five ~180 km long transects were conducted across the eddy center to define Cyclone Opal's physical and initial biological characteristics (Dickey et al., 2008; Nencioli et al., 2008). Transects 1, 2, 4, and 5 were characterized by repeat CTD casts. Transect 3 (Fig. 2.6B and Table 2.3) was intensively sampled for a suite of biogeochemical parameters including nutrients and carbon parameters (see Section 2.2). Results suggested that Opal's diameter was ~160 - 180 km wide and circular in shape (Nencioli et al., 2008). A deep chlorophyll maximum layer (DCML) occurred between the σ_t = 24.2 and 24.4 kg m^{-3} isopycnal surfaces (Rii et al., 2008), shoaling from 110 m at the eddy edge to 70-90 m at the eddy center with >2-fold increase in chlorophyll concentrations (Rii et al., 2008). This preliminary measurements suggested that Cyclone Opal was in a physically and biologically mature phase of eddy development (Sweeney et al., 2003).

A 7 time-series of process studies were then conducted at the eddy center (IN-stations) from March 16-22 to describe the temporal biogeochemical evolution of Cyclone Opal during the course of a decaying diatom bloom (Benitez-Nelson et al., 2007). During this period, Cyclone Opal moved rapidly to the south (average translational speed of 0.33 km h^{-1}) by ~160 km from its initial location (e.g., traveled from IN1 to IN7, Table 2.3 and Fig. 2.6B) (Nencioli et al., 2008). ADCP data, SST, and satellite observations were used to evaluate if each

hydrographic cast was positioned close enough to the eddy center (tangential velocity ≤ 25 cm s^{-1} as a threshold value) to be considered as an IN-station (Nencioli et al., 2008). As a result, 9 out of the 51 CTD casts were excluded, including cast 49 (i.e., IN1 in Table 2.3 and Fig. 2.6B). Once completed, a series of three control stations (OUT-stations) were sampled during March 24 – 27 at a location well removed from the eddy flow field (>200 km north of IN7, Fig. 2.6B), but still within the lee of the Hawaiian Islands (Dickey et al., 2008).

Brief introduction to the phases of life cycle for Cyclones Noah and Opal

From the data collected at the Bermuda Atlantic Time-series Study (BATS) site in the Sargasso Sea, Sweeney et al. (2003) proposed a conceptual model that hypothesized three main stages of the life cycle of a cyclonic eddy (Sweeney et al., 2003). This model assumes mesoscale eddies to be fundamentally closed system with respect to horizontal material exchanges with the surrounding waters. The first stage is the "intensification" or "spin-up" phase which occurs when an eddy is spinning up. On continuous isopycnal doming associated with the spin-up process, significant amounts of nutrients were upwelled into the euphotic zone. The enhanced availability of nutrients in the euphotic zone is likely to stimulate biological responses subsequently (i.e., increase in primary productivity, pigment concentration, and biomass). The second stage is the "mature" phase, which is characterized by maximum production rates and maximal isopycnal doming. During this phase, phytoplankton concentrations at the deep chlorophyll maximum layer (DCML) are expected to increase significantly and shifts in phytoplankton communities may occur, so that larger size phytoplankton (e.g., diatom) may dominate the bloom. The third stage or "decay" phase is initiated when the isopycnal doming begins to level off or relax. This phase is characterized by a reduced availability of nutrients at the eddy center within the euphotic zone and a consequent decay of the phytoplankton bloom and an increase in the export of organic

carbon below the euphotic zone (Goldman, 1993; Seki et al., 2001; Bidigare et al., 2003). According to this close-system model, the biogeochemical evolution of mesoscale eddies are closely dependent on their age.

Based on Sweeney et al. (2003)'s conceptual model and observation of physical and hydrological characteristics, Cyclones Opal and Noah represent "mature" phase and "decay" phase, respectively (Kuwahara et al., 2008; Nencioli et al., 2008; Rii et al., 2008). In the following chapters, we will discuss Cyclone Opal first and then Cyclone Noah by following the order of temporal evolution of cyclonic eddies.

Cyclone Opal in E-Flux III is in the physical "mature" phase that began to 'decay' biologically after a diatom bloom. Nencioli et al. (2008) deduced a solid body rotation at the eddy center which is isolated from surrounding surface waters based on angular velocities and the potential field data. However, such a solid body rotation was only ~ 70-90 m in depth, at greater depths, there are significant radial movements of water between the center and outer portions along the density surfaces between σ_t = 23.6 and 24.4 kg m^{-3} especially during the periods when Opal's translational migration was significant (Nencioli et al., 2008). Therefore, below the solid body rotation, this "open-bottom/horizontal leaky system" hypothesis provided additional upwelling of nutrients at Cyclone Opal's center, rather than being limited to only a single nutrient injection at the time when Cyclone Opal was initially formatted from Sweeney et al. (2003)'s model.

In the description of E-Flux I cruise, we already presented the reasons why Cyclone Noah was in the "decay" phase, e.g., elliptical shaped eddy from GOES SST imagery and Transects data, less apparent surface expression of Cyclone Noah from satellite SST imagery, only moderate enhancement in biogeochemical properties and ambient phytoplankton communities

(Kuwahara et al., 2008). If we review two cyclonic eddies: Cyclones Opal and Noah, Opal was in a more biological productive phase whereas Noah was in a declining phase. A major difference between these two Cyclones was their translational speeds. Opal had significant southward immigration whereas Noah was relatively stationary during E-Flux I cruise. Thus, in the case of Cyclone Noah, below the solid body rotation, contributions of nutrients to the eddy core via lateral exchange along density surfaces were much limited comparing to Cyclone Opal.

Sample collection and analyses

Sample collection

Discrete water samples were collected over the upper 350 m for pH, total alkalinity (TAlk), DIC, inorganic nutrients (including nitrate and nitrite (N+N)), total organic carbon (TOC), and dissolved organic nitrogen (DON) using a SeaBird SBE 9/11 + CTD system with rosette sampler (Table 2.1-2.3 and Fig. 2.4-2.6). Samples were collected at selected transects and process stations (IN- and OUT-stations) (Table 2.1-2.3 and Fig. 2.4-2.6). A large range of additional measurements were also conducted by other researchers (e.g., Benitez-Nelson et al., 2007; Dickey et al., 2008; Rii et al., 2008). Here, only the hydrographic data and biogeochemical parameters related to this paper are described.

Sample analysis

Underway sea surface pCO_2

Underway samples were collected continuously by the flow-through system on board of the R/V *KOK* and *Wecoma* during all three consecutive cruises as part of the E-Flux study (Figs. 2.4-2.6). Underway pCO_2 measurements were conducted along all transects and at process stations (including IN-stations (at the center of the eddy) and OUT-stations (outside the eddy) during E-Flux I and III) by using a combined laminate-flow and shower-head equilibrator

coupled to an infrared CO_2 analyzer (Li-Cor 6252) system (Wang and Cai, 2004). Underway salinity and temperature data were available from R/V *KOK* and *Wecoma* during all three cruises. Underway uncorrected fluorescence data (voltage) were available only from R/V *Wecoma* during E-Flux II and III.

Inorganic carbon parameters

Inorganic carbon parameters were measured using standard protocols. pH was measured at a constant temperature (25ºC) with a Ross combination glass pH electrode (Orion Research). The calibration was conducted by using three NBS pH buffers (pH = 4, 7, 10) to calculate its response slope and a tris buffer at salinity 35 to derive a seawater pH scale. The relative accuracy was ±0.01 pH units. TAlk was determined by Gran titration using 0.1 μM HCl on board ship (Cai and Wang, 1998; Wang and Cai, 2004). The titration was calibrated with a certified reference material (CRM) from A. G. Dickson. Under constant temperature condition (25ºC), the precision and accuracy of the titration was 0.1 %. On shipboard condition, the fluctuation of laboratory temperature is more than 1 ºC. Therefore, the imprecision and inaccuracy were about 0.3% or ±7 $\mu mol \cdot kg^{-1}$. Water samples for DIC analysis were collected in 20-ml vials and preserved with 10 μl mercuric chloride. The samples were stored refrigerated prior to analysis (Cai and Wang, 1998; Wang and Cai, 2004). Based on replicate analysis, DIC imprecision was determined to be within ±2 $\mu mol\ kg^{-1}$. The accuracy of the analysis is assured by the calibration against the CRM. pCO_2 in Fig. 2H was calculated (to within ± 10-15 μatm of the underway pCO_2 data) from measured pH and DIC data under 25 ºC and 1 atm conditions by using the carbonic acid dissociation constants of Mehrbach et al. (1973) as refitted by Dickson and Millero (1987) (Mehrbach et al., 1973; Dickson and Millero, 1987). Underway sea surface pCO_2 measurements were conducted along all transects and at process stations.

Nutrients

Water samples for inorganic nutrients (including N+N) and DON were frozen immediately and stored frozen at ~ -20 ºC until analysis (see Rii et al, 2008 and Mahaffey et al., 2008 for more detail). Samples for inorganic nitrogen were analyzed by Joe Jennings at Oregon State University using a continuous segmented flow system consisting of components of both a Technicon Autoanalyzer II™ and an Alpkem RFA 300™ (Gordon et al., 1994). Inorganic nitrogen precision was estimated to be 0.2 μM.

DON and DOC

DON was calculated as the difference between total dissolved nitrogen (TDN) and inorganic nitrogen. TDN was measured at Dr. Craig Carlson's laboratory at the University of California, Santa Barbara (Mahaffey *et al.*, 2008). The precision for TDN and DON is ±0.5 μM. Samples for total organic carbon (TOC) (unfiltered water samples frozen until measurement) were analyzed via high temperature combustion using a Shimadzu TOC-V at Dr. Carlson's laboratory as well. The operating conditions of the Shimadzu TOC-V were slightly modified from the manufacturer's model system (Carlson et al., 2004). The precision for TOC measurement is ± 1 μM.

Supplemental data (Atmospheric CO_2 and wind data)

Atmospheric CO_2 (in dry air) was measured periodically throughout three cruises. But only the measurement during E-Flux III (March 2005) was successful and averaged ~ 380.2 ppm ((±2 ppm). After a 100% humidity correction, the average value is ~ 369.4 μatm (±2 μatm). Although atmospheric pCO_2 values were not available from E-Flux I and II, atmospheric CO_2 concentrations were derived monthly from in situ dry air samples collected at Mauna Loa Observatory, Hawaii (beside E-Flux field area, Fig. 2.1) by Keeling and Whorf (Fig. 2.7A-B).

The data can be downloaded via website http://www.esrl.noaa.gov/gmd/ccgg/trends/. From Fig. 2.7A-B, monthly atmospheric pCO_2 values in November 2004, January and March 2005 are 375.8, 378.3, and 381.0 ppm, respectively. The results from our air CO_2 measurement in March 2005 are consistent with Keeling and Whorf's measurement (~ 380.2 ppm (±2 ppm) versus 381.0 ppm). This also supported the reliability of our results. After a 100% humidity correction, the values for E-Flux I and II are ~ 365.1 and 367.5 μatm, respectively.

One of the desired goals of this study is to estimate the regional CO_2 air-sea flux. To accomplish this, it is essential to have the wind speed data in the studied area. The monthly average wind was chosen from the meteorological data on NDBC buoy 51003 (location: 19.16º N and 160.74º W) (Figs. 2.8 and 2.9). The data can be downloaded at http://www.ndbc.noaa.gov/maps/Hawaii.shtml. From Fig. 2.1, we can see that the location of NDBC buoy 51003 is ~ 3º Longitude west of the E-Flux field area. Thus, we need to assure that the wind speed data from NDBC buoy 51003 are also representative for the E-Flux field area. Please note that NASA's QuikScat scattermeter provided the satellite wind data within the E-Flux field area outside the 'Alenuihaha Channel at 20.1º N, 156.4º W (Fig. 2.1). QuikScat, which is a polar orbiting satellite, provided data over an 1800 km wide swath for our study region (Dickey et al., 2008). The retrievals of wind speed and direction from QuikScat give twice-daily data with spatial resolution of 25 km X 25 km on the earth's surface. These satellite wind speed data are accessible at http://podaac.jpl.nasa.gov/DATA_PRODUCT/OVW/index.html#quikscat. Besides, shipboard underway wind speed data were also available during the cruise period. These data are all presented and compared in Figs 2.8 and 2.9. In general, wind speed data from NDBC buoy 51003 are consistent with the satellite and shipboard data.

Please note that satellite wind data are only available under good weather conditions. In Figs. 2.8A and 2.9A, there are many points (in red color) with zero wind speed. These mean there were no data available during those days. We should also mention that NDBC buoy wind data were measured at 5 m above sea level and shipboard wind data were measured at 20 m above sea level. They were all converted to wind speed at 10 m above sea level by factors of 1.06 and 0.95, respectively (Wanninkhof, personal communication).

Table 2.1 Stations and casts information for E-Flux I cruise

Station #	Longitude (°W)	Latitude (°N)	Sampling time	Cast # (DIC)	Cast # (NUTS)
Transect stations					
8	156.31.55	18.49.97	11/7/2004	17	N/A
10	156.31.46	19.9.92	11/7/2004	19	N/A
13 [a)]	156.31.46	19.40.05	11/8/2004	22	N/A
14	156.31.55	19.49.91	11/8/2004	23	N/A
15	156.31.40	20.0.28	11/8/2004	24	N/A
16	156.31.42	20.9.98	1/8/2004	25	N/A
17	156.31.52	20.20.02	11/8/2004	26	N/A
18	157.9.48	20.15.34	11/8/2004	27	27
20	156.54.52	20.1.26	11/9/2004	29	29
22	156.39.60	19.47.09	11/9/2004	31	31
23	156.32.10	19.40.01	11/9/2004	32	32
24	156.24.39	19.32.93	11/9/2004	33	33
25	156.16.95	19.25.86	11/9/2004	34	34
27	156.1.00	19.29.98	11/10/2004	36	36
29	156.2.14	20.8.63	11/10/2004	39	N/A
30	156.9.23	20.1.32	11/10/2004	40	N/A
31	156.16.98	19.54.14	11/10/2004	41	N/A
32	156.24.52	19.47.18	11/10/2004	42	N/A
33	156.31.95	19.40.07	11/10/2004	43	N/A
35	156.39.47	19.32.89	11/11/2004	45	N/A
36	156.46.82	19.25.82	11/11/2004	46	N/A
37	156.54.37	19.18.72	11/11/2004	47	N/A
38	157.1.88	19.11.59	11/11/2004	48	N/A
IN-stations and OUT-stations					
IN1	156.31.98	19.40.05	11/12/2004	55	51
IN2	156.37.10	19.39.97	11/13/2004	60	60
IN3 [b)]	156.47.09	19.53.92	11/16/2004	63	N/A
IN4 [c)]	156.29.23	19.1.69	11/17/2004	69	N/A
OUT1	157.15.26	20.27.70	11/5/2004	4	N/A
OUT2	157.12.88	20.32.53	11/19/2004	75	75
OUT3	157.12.51	20.31.54	11/19/2004	77	77

a) This station was sampled at the eddy center and are considered as IN-stations.

b) IN3 was sampled at high velocity region.

c) IN4 is at the edge of the Cyclone Noah to see if there was increased biological production in the shear zone.

Table 2.2 Stations and casts information for E-Flux II cruise

Station #	Longitude (°W)	Latitude (°N)	Sampling time	Cast # (DIC)	Cast # (NUTS)	Cast # (TOC/DON)
Transect stations						
44	157.0.05	20.20.00	1/18/2005	57	57	N/A
46	156.52.66	20.12.86	1/18/2005	59	59	N/A
48	156.46.72	20.7.01	1/18/2005	61	61	N/A
49	156.44.52	20.4.87	1/18/2005	62	62	N/A
50	156.42.01	20.2.42	1/19/2005	63	63	N/A
51	156.39.84	20.0.26	1/19/2005	64	64	N/A
52	156.36.14	19.56.64	1/19/2005	65	65	N/A
54	157.5.94	20.25.77	1/19/2005	67	67	N/A
IN-stations and OUT-stations [a)]						
IN1	156.42.09	20.2.31	1/16/2005	47	47	47
IN2	156.42.02	20.2.38	1/17/2005	52	52	52
IN3	156.48.89	20.9.20	1/20/2005	70	N/A	N/A
IN4	156.48.95	20.9.18	1/21/2005	74	N/A	N/A
IN5	156.56.28	20.16.90	1/22/2005	79	79	79
IN6	156.56.34	20.16.41	1/23/2005	85	85	85
OUT1	157.29.95	20.29.97	1/25/2005	89	89	89
OUT2	157.30.02	20.30.00	1/26/2005	96	96	96

a) There were no real IN-stations during this cruise since the absence of eddy.

Table 2.3 Stations and casts information for E-Flux III cruise

Station #	Longitude (°W)	Latitude (°N)	Sampling time	Cast # (DIC)	Cast # (NUTS)	Cast # (TOC/DON)
Sampled transect						
26	156.22.40	20.11.32	3/13/2005	13	13	N/A
28	156.37.46	19.57.22	3/13/2005	15	15	N/A
29	156.44.98	19.50.14	3/13/2005	16	16	N/A
30	156.52.47	19.43.04	3/13/2005	17	17	N/A
31	156.59.98	19.36.00	3/13/2005	18	18	N/A
32	157.4.92	19.31.38	3/13/2005	19a	19a	N/A
34	157.22.46	19.14.78	3/13/2005	23	23	N/A
36	157.37.44	19.00.70	3/13/2005	25	25	N/A
IN-stations and OUT-stations						
IN0 [a)]	157.4.92	19.31.38	3/13/2005	19a	19a	N/A
IN1 [b)]	157.4.77	19.21.37	3/16/2005	49	N/A	N/A
IN2	157.6.00	19.10.00	3/17/2005	63	63	59
IN3	157.02.70	19.06.70	3/18/2005	67	67	67
IN4	157.01.53	19.01.80	3/19/2005	74	73	73
IN5	156.53.8	18.56.19	3/20/2005	86	82	82
IN6	156.51.59	18.55.78	3/21/2005	93	88	88
IN7	156.51.57	18.55.83	3/22/2005	N/A	94	94
OUT1	157.35.36	20.37.33	3/24/2005	111	111	111
OUT2	157.35.42	20.37.33	3/25/2005	119	119	119
OUT3	157.35.43	20.37.32	3/26/2005	127	127	127

a) IN0 is cast 19a at station 32. We call it IN0 since it has the characteristics of IN-stations.

b) IN1 is not considered as IN-station from velocity analysis by using ADCP data.

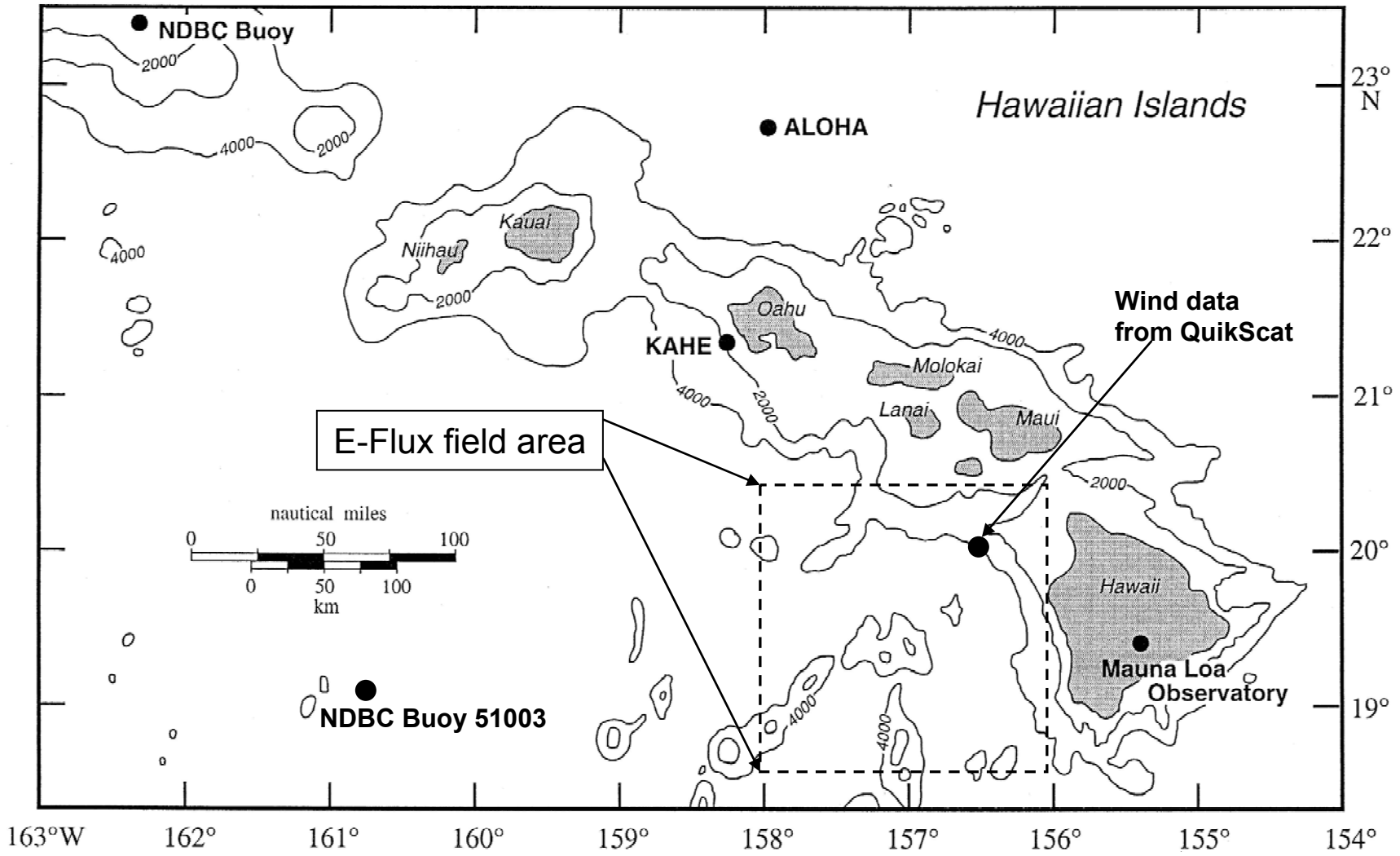

Fig. 2.1 Location of the E-Flux field area in the lee of Hawaii (see dashed-line box). Also shown are the locations of NDBC buoy 51003 at 19.16º N, 160.74º W and the Hawaii Mauna Loa Observatory. Wind data from NASA's QuikScat scattermeter is pointed on 20.1º N, 156.4º W (modified from Winn et al., 1998).

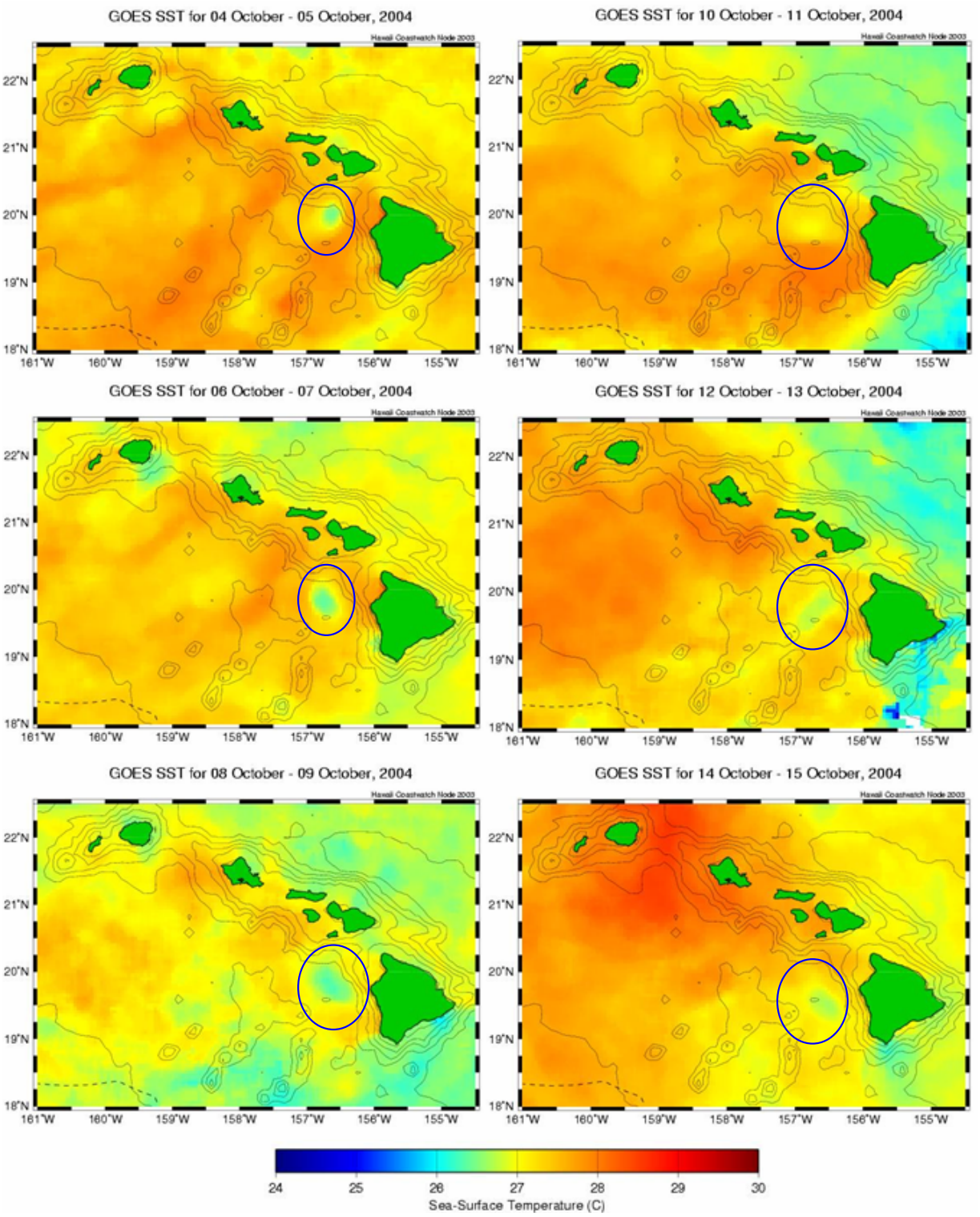

Fig. 2.2 Time-series remote sensing of GOES SST image in the lee of Hawaii area about one month before the E-Flux I cruise. Black circles highlight the cold core of Cyclone Noah.

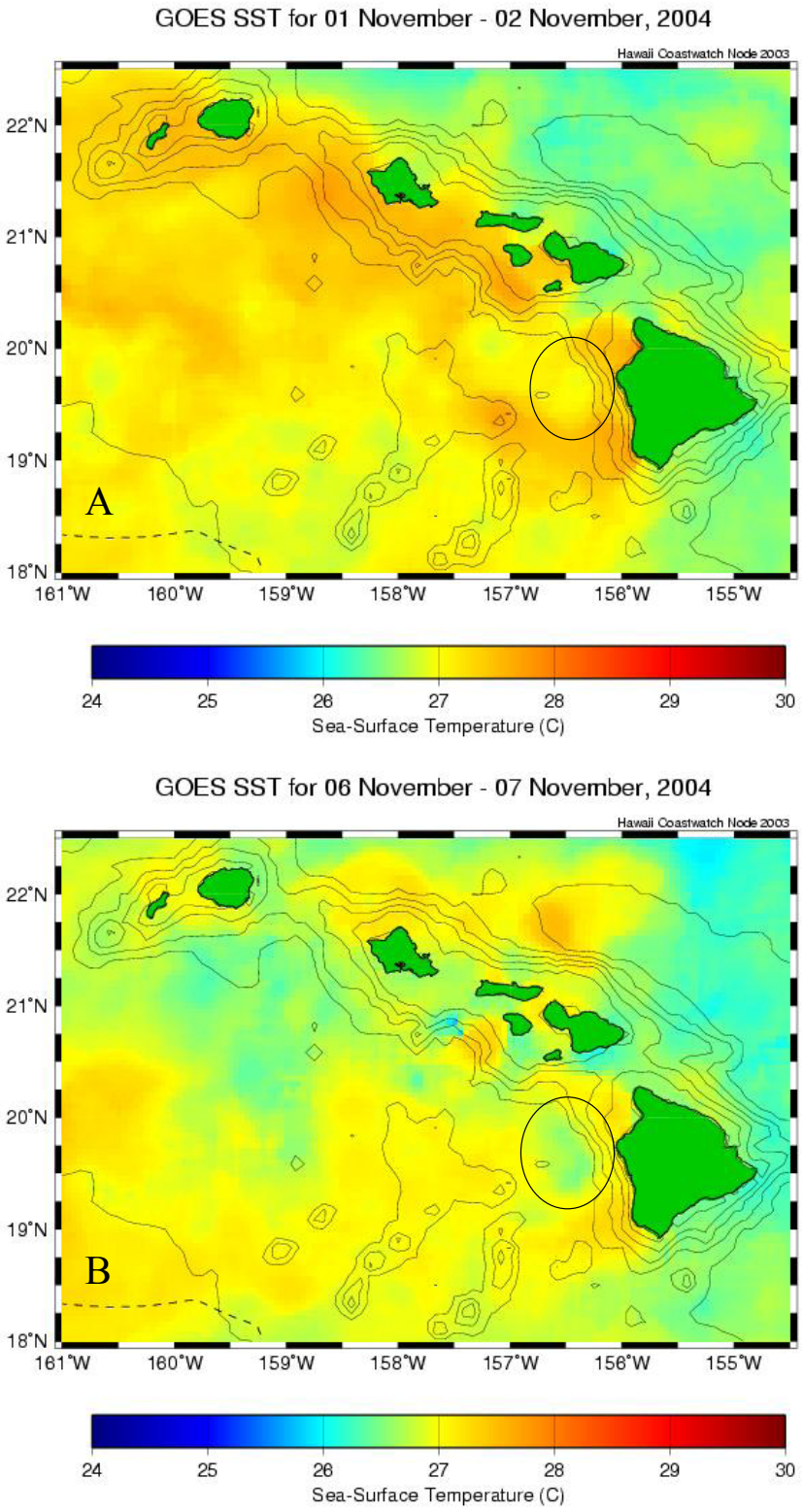

Fig. 2.3 Time-series remote sensing of GOES SST image in the lee of Hawaii area at the beginning of the E-Flux I cruise. Black circles highlight the cold core of Cyclone Noah.

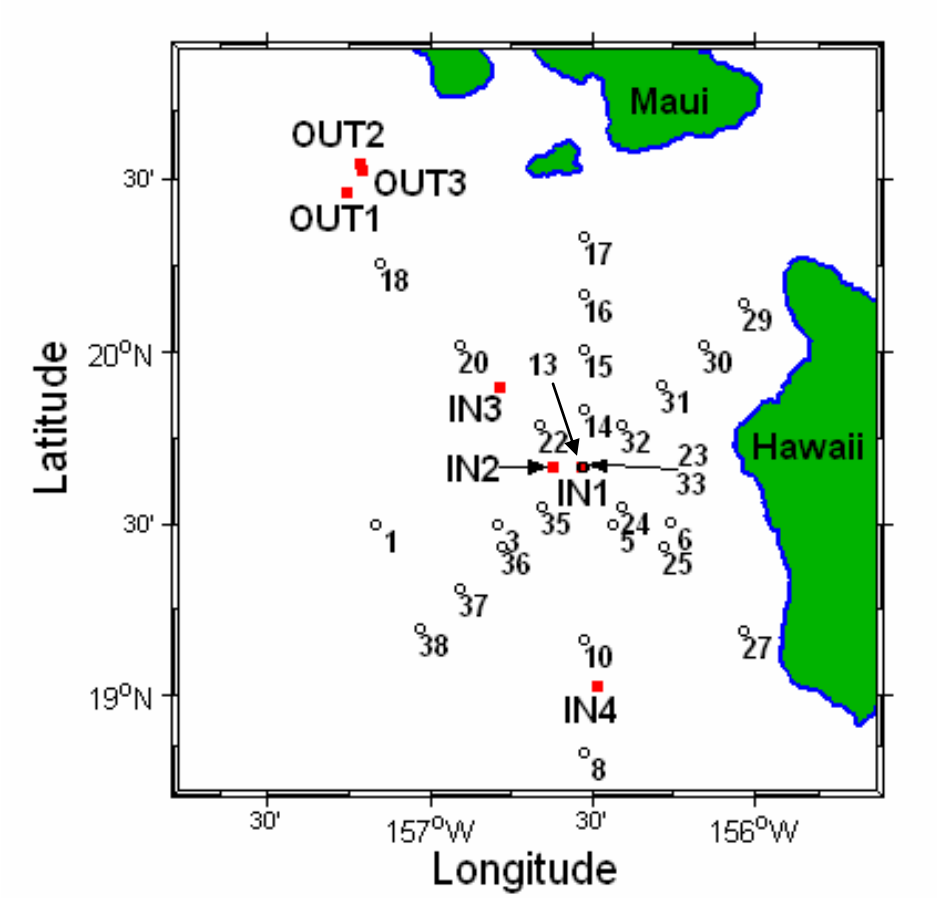

Fig. 2.4 Location of sampling stations map for the E-Flux I cruise in November 2004 in the lee of Hawaii, including Transects stations from 1-4 (Transect 1: stations 1 to 6; Transect 2: stations 8 to 17; Transect 3: stations 18 to 27; Transect 4: stations 29 to 38), IN-stations, and OUT-stations. Detail information is available in Table 2.1.

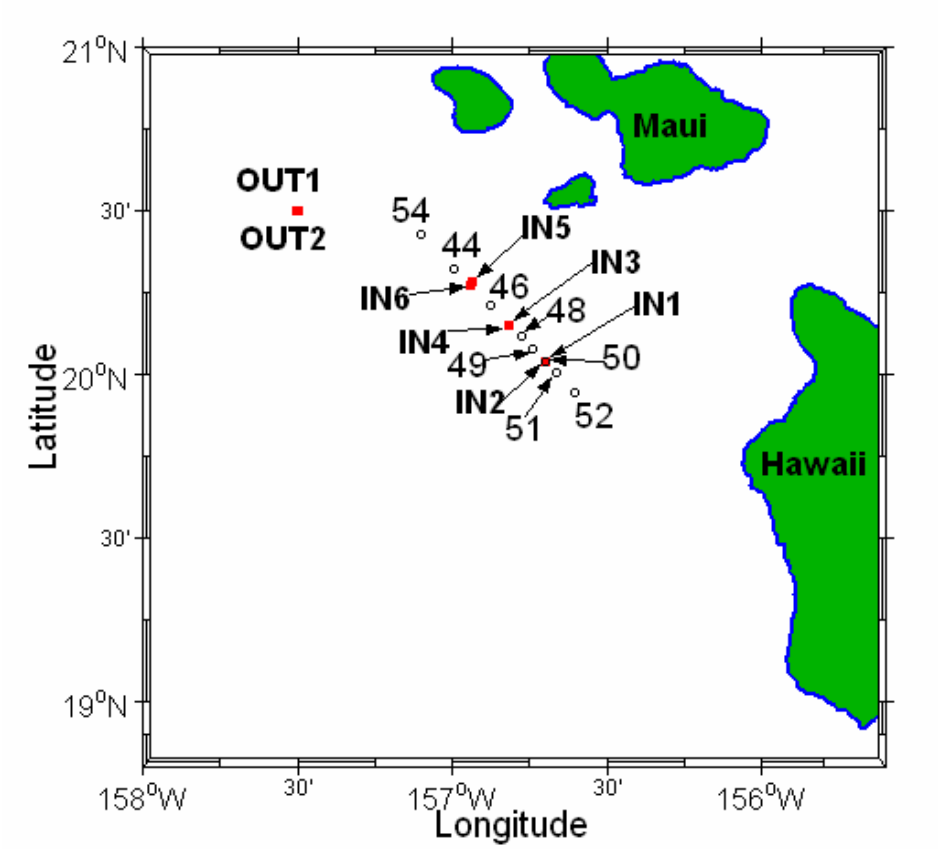

Fig. 2.5 Location of sampling stations map for the E-Flux II cruise in January 2005 in the lee of Hawaii, including Transect-6 stations (stations 44 to 54), IN-stations, and OUT-stations. Detail information is available in Table 2.2.

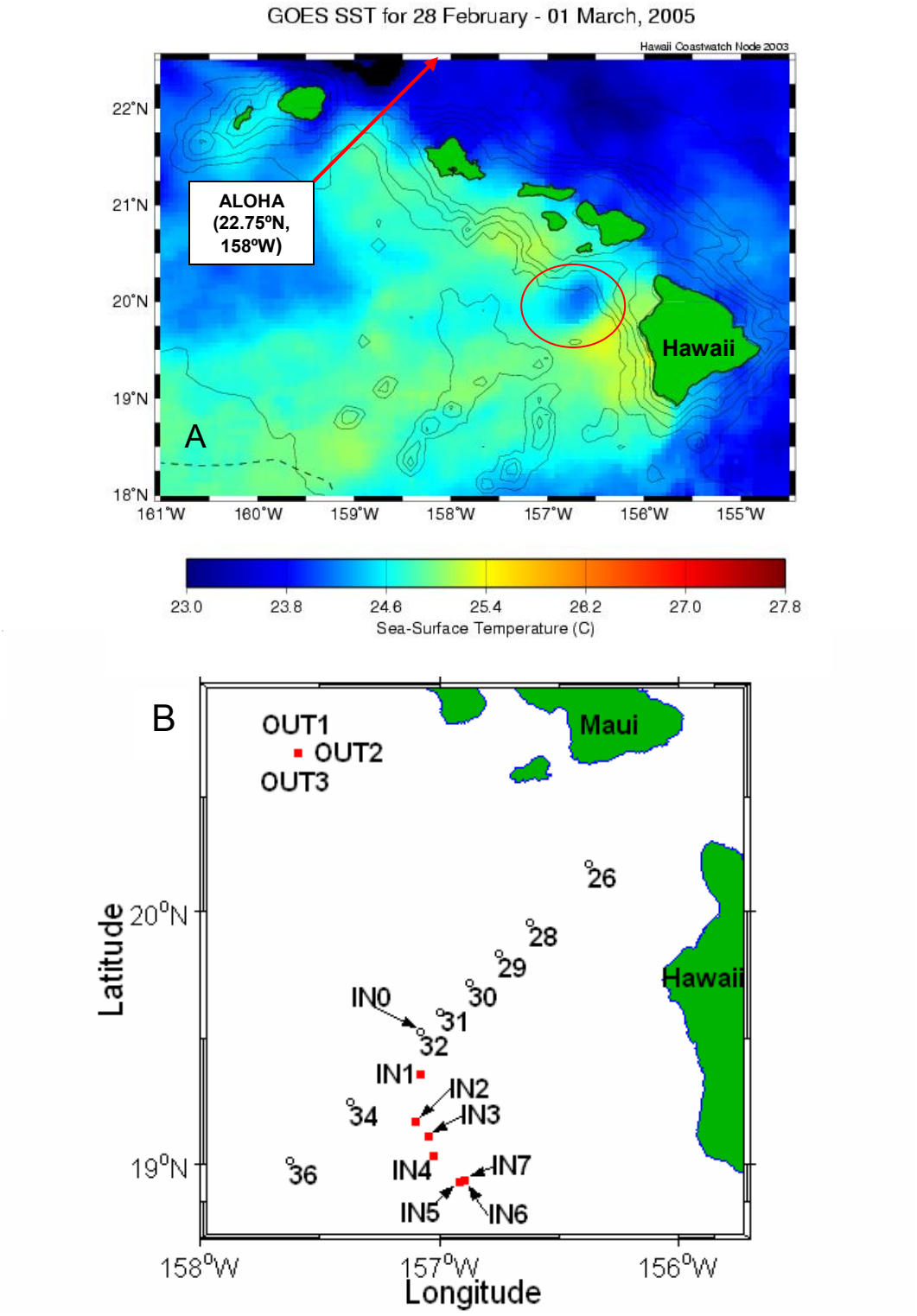

Fig. 2.6 Area map for the E-Flux III cruise in March 2005 in the lee of Hawaii. (A) Remote sensing of GOES SST image, red circle highlights the cold core of Cyclone Opal. (B) Location of sampling stations, including Transect-3 stations (stations 26 to 36), IN-stations, and OUT-stations. Detail information is available in Table 2.3.

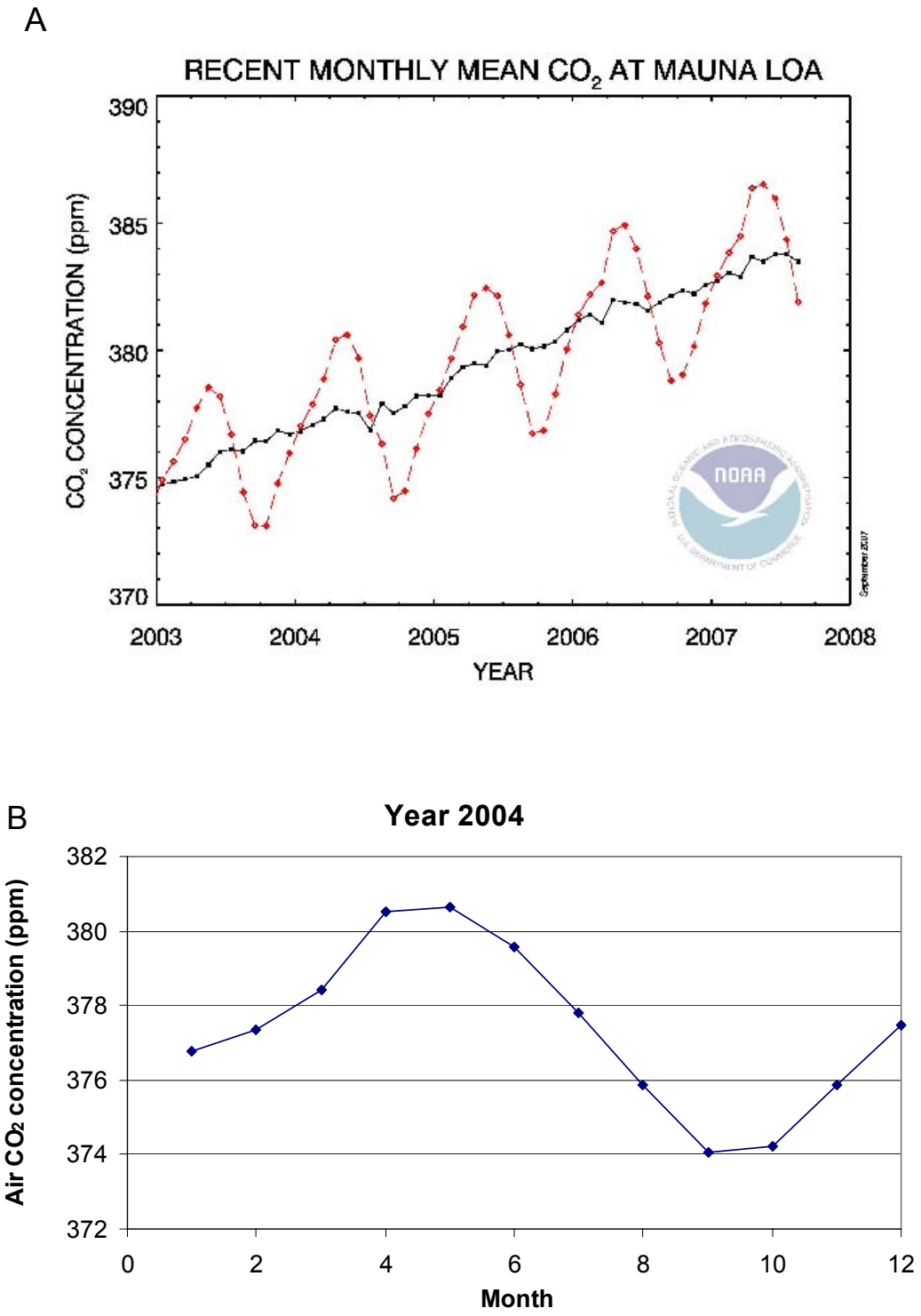

Fig. 2.7 Recent monthly atmospheric pCO_2 values expressed in parts per million (ppm) (A. From year 2003 to 2007; B. Year 2004). The monthly values have been adjusted to the 15th of each month. Atmospheric CO_2 concentrations were derived from in situ air samples collected at Mauna Loa Observatory, Hawaii by Keeling and Whorf. The data are available at http://www.esrl.noaa.gov/gmd/ccgg/trends/

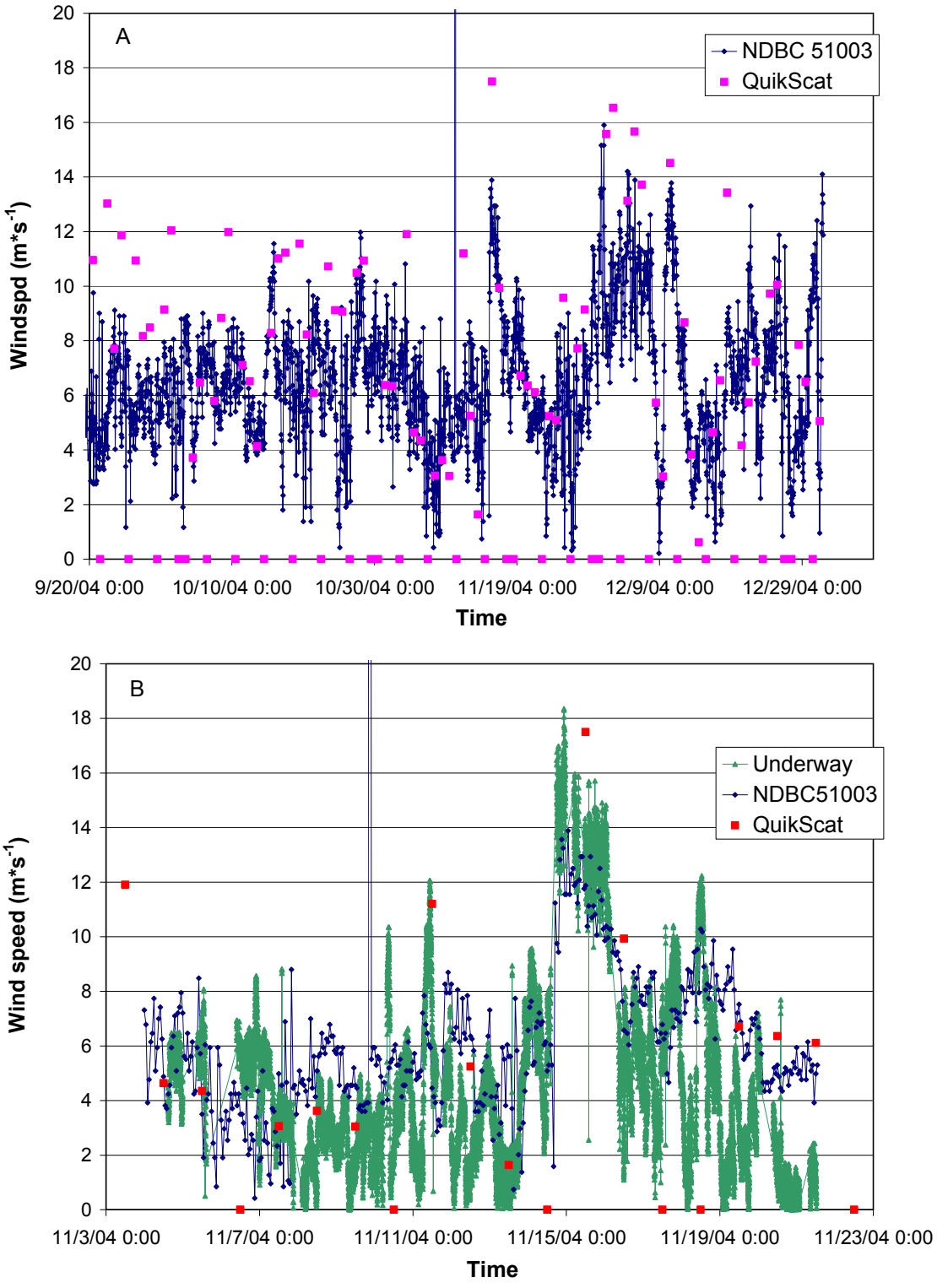

Fig. 2.8 Time-series wind data in the E-Flux field area in the lee of Hawaii in 2004 ((A). Wind data from NDBC buoy 51003 at 19.16º N, 160.74º W and NASA's QuikScat scattermeter pointed on 20.1º N, 156.4º W; (B). Wind data from NDBC buoy 51003 and QuikScat as well as the shipboard underway wind data).

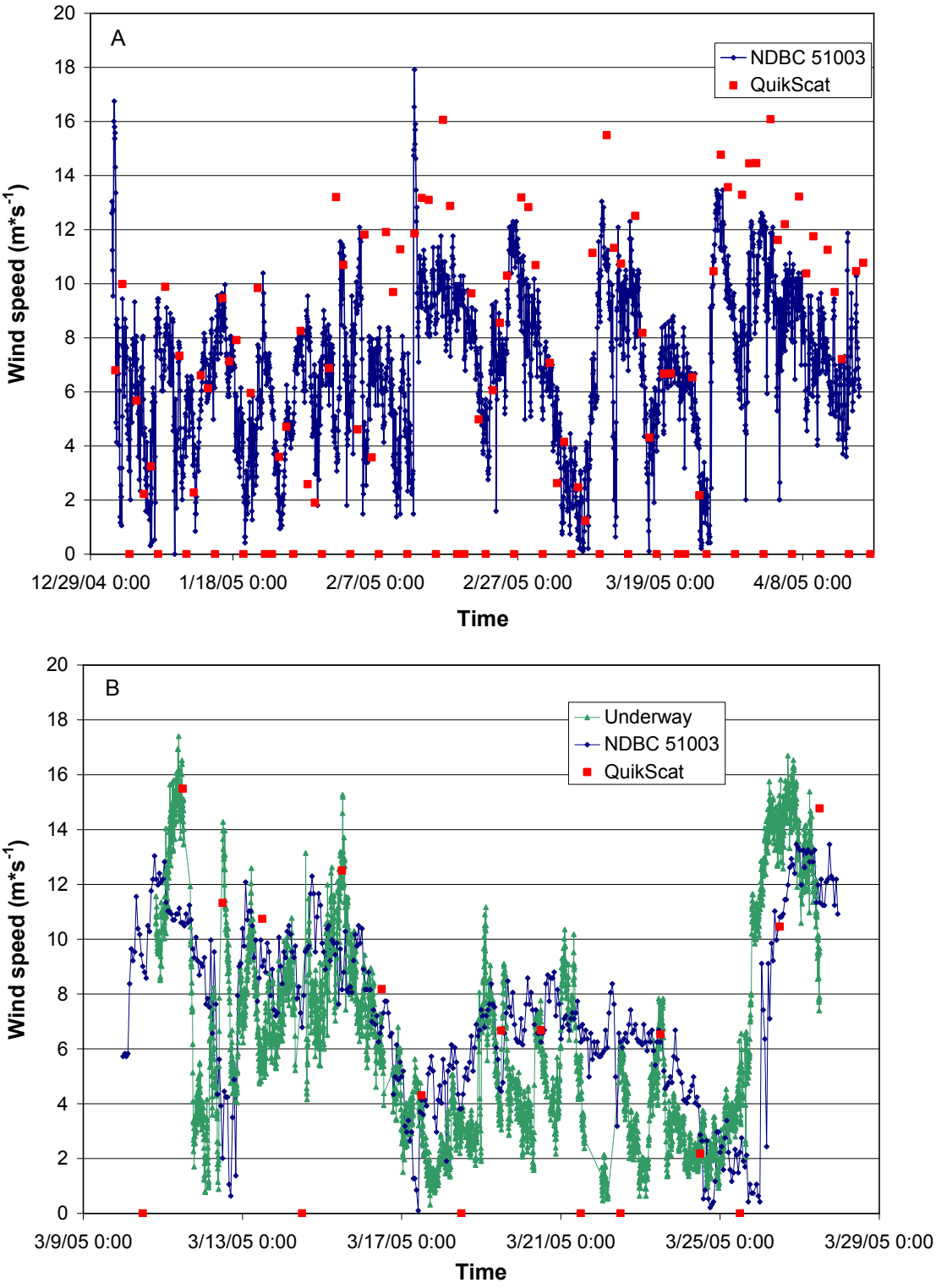

Fig. 2.9 Time-series wind data in the E-Flux field area in the lee of Hawaii in 2005 ((A). Wind data from NDBC buoy 51003 at 19.16º N, 160.74º W and NASA's QuikScat scattermeter pointed on 20.1º N, 156.4º W; (B). Wind data from NDBC buoy 51003 and QuikScat as well as the shipboard underway wind data).

CHAPTER 3 SEA SURFACE pCO_2-SST RELATIONSHIPS ACROSS COLD-CORE CYCLONIC EDDIES: IMPLICATIONS FOR UNDERSTANDING REGIONAL VARIABILITY AND AIR-SEA GAS EXCHANGE[1]

[1] Part of this chapter (from Section 3.1) was published (Chen, F., W.-J. Cai, C. Benitez-Nelson, Y. Wang (2007), *Geophysical Research Letters*, 34, L10603, doi: 10.1029/2006GL028058). Permission granted by American Geophysical Union.

Introduction

Background

Large scale pCO_2-SST relationships often miss episodic and mesoscale events. For example, the spatial resolution for climatological global surface ocean pCO_2 is based on 4° x 5° pixels (Fig. 1.1) (Takahashi et al., 2002). Therefore, the climatological distributions of sea surface pCO_2 constructed by interpolating spatially and temporally limited oceanic CO_2 observations may inaccurately represent the regional mean, particularly within the subtropical gyres (Takahashi et al., 1997; Takahashi et al., 2002; Mahadevan et al., 2004). The net global flux of oceanic CO_2 uptake is determined by a small difference between large in- and out-fluxes in the world oceans. Thus, it is sensitive to variability in these different regional estimates (Mahadevan et al., 2004). As a result, the global CO_2 air-sea fluxes obtained may involve significant errors (Takahashi et al., 1997). Although such error could be ideally reduced by greatly increasing sampling density and frequency, this sampling strategy is difficult to implement due to limited resources. More mechanistic or process-oriented approaches are required to link CO_2 concentration to other parameters.

Several studies suggested that mesoscale eddy-driven events may be a major process for supplying new nutrients to the upper ocean of oligotrophic subtropical gyres (McGillicuddy and Robinson, 1997; McGillicuddy et al., 1998; Williams and Follows, 1998; Mahadevan and Archer, 2000). This upwelling of subsurface water likely results in a strong initial degassing of CO_2 followed by a CO_2 drawdown due to enhanced biological activity (Lefevre et al., 2002). Thus, during an eddy event, several competing effects that influence pCO_2-SST relationships will be expected to coexist within subtropical oligotrophic waters that are generally influenced by thermodynamic rules alone (Lee et al., 1998). The gas exchange of CO_2 across eddies,

particularly in oligotrophic waters, remains poorly understood. This study examines several pCO_2-SST relationships and CO_2 air-sea exchange during different phases of cold-core cyclonic eddies, Cyclone Noah and Opal, which formed in the lee of the main Hawaiian Islands, an oligotrophic open ocean region in the subtropical North Pacific Gyre. This area serves as a natural laboratory with vigorous and continuous mesoscale eddies formed throughout the year, providing excellent opportunities for the study of the effects of eddies on surface water CO_2 (Seki et al., 2001; Bidigare et al., 2003).

Since the sampled Cyclone Opal was in its spin-up or mature phase and Cyclone Noah was sampled in its spin-down or decay phase (Dickey et al., 2008; Kuwahara et al., 2008; Nencioli et al., 2008), we will discuss pCO_2-SST relationships and air-sea CO_2 exchange across Cyclone Opal during E-Flux III cruise in Section 3.1 first. In Section 3.2, we will discuss sea surface pCO_2 and air-sea gas exchange across Cyclone Noah. At last, data from these two Cyclones will be compared to E-Flux II cruise which was absent of the eddy.

Estimation of air-sea CO_2 exchange fluxes

Whether a regional marine ecosystem is relatively a sink or source for atmospheric carbon dioxide has been a primary motivation to quantify the flux of air-sea CO_2 exchange. This flux is governed by:

$$F_{air-sea} = k * \alpha_{CO2} * (pCO_2^{SW} - pCO_2^{Air}) \qquad (3.1)$$

where $F_{air\text{-}sea}$ is the flux, k is gas exchange coefficient (or piston velocity), α is the CO_2 solubility in seawater (Weiss, 1974), pCO_2^{SW} and pCO_2^{Air} are the partial pressure of CO_2 in the seawater and overlaying air, respectively, at 100% humidity. For this study, pCO_2 data in surface water and air come from direct measurement with limited uncertainty. We did not obtain satisfied air pCO_2 data during the first two cruises. During those two cruises, we will use atmospheric CO_2

data at Hawaii Mauna Loa Observatory. More detail discussion is presented in Chapter 2. The value of α is calculated from known thermodynamic equations from given temperature and salinity (Weiss, 1974; Wanninkhof, 1992). The largest uncertainty may come from the determination of k, gas exchange coefficient, since direct measurement of k is not available. Previous studies (Liss and Merlivat, 1986; Wanninkhof, 1992; Wanninkhof and McGillis, 1999; Nightingale et al., 2000a; Nightingale et al., 2000b; McGillis et al., 2001) have proposed empirical relationships between k and wind speed for open ocean systems. We will use these formulas to bracket the flux values.

Section 3.1 Cyclone Opal

SST imagery from the NOAA satellite GOES showed that a first baroclinic cold-core cyclonic eddy, Cyclone Opal, outcropped at the surface by the end of February 2005 and persisted for 4~6 weeks ((Benitez-Nelson et al., 2007); Fig. 2.6). Underway samples were collected from Cyclone Opal by the flow-through system on board of the R/V *Wecoma* during March 10th - 28th, 2005 as part of the E-Flux study (Fig. 2.6; Fig. 3.1). Underway pCO_2 measurements were conducted along all transects and at process stations (including six IN-stations (at the center of the eddy) and three OUT-stations (outside the eddy)). Atmospheric CO_2 (in dry air) was measured periodically throughout the cruise, and averaged ~ 369.4 μatm (±2 μatm) after a 100% humidity correction.

pCO_2-SST relationships

Two very different relationships were observed in surface waters between underway salinity, temperature, and pCO_2 (Figs. 3.2 and 3.3A). Sea surface pCO_2 collected outside the eddy (OUT-pCO_2; blue diamonds in Figs. 3.2 and 3.3A) is clearly distinguished from that collected at process stations within the eddy core (IN-pCO_2; red triangles in Figs. 3.2 and 3.3A).

Outside the eddy, a positive linear relationship exists between the natural logarithms of sea surface pCO_2 and SST:

$$\ln pCO_2 = 0.0408 * SST + 4.8288 \qquad (3.2)$$

($n = 1110$, $r^2 = 0.84$, $p<0.0001$, root mean square error (RMSE) = 0.0074)

We categorized the data in this region as Group-I data (Fig. 3.3A). The RMSE in the pCO_2 prediction is within 3 μatm. The tight correlation suggests that temperature is a primary factor controlling sea surface pCO_2 outside the eddy and the calculated slope, or temperature factor ($\partial \ln pCO_2/\partial T$), is 0.0408. This is essentially the same for isochemical seawater determined by Takahashi et al. (1993) for a much larger database and temperature range (0.0423 $°C^{-1}$ between 2-28°C). This also suggests that other factors (e.g., DIC, TAlk, and salinity) are generally constant at our reference sites (where most of the OUT-pCO_2 was measured) (Takahashi et al., 1993; Takahashi et al., 2002). Please note that this dataset does not include data collected during the transect survey (dark pink color in Fig. 3.1, see below).

The SST is much lower, and the salinity is much higher for the IN-pCO_2 relative to the OUT-pCO_2 (Fig. 3.2). Surface waters with lower temperature and higher salinity, as well as higher pCO_2 at the center of Cyclone Opal, are consistent with the eddy outcropping at the surface. We categorize the negative relationship between pCO_2 and SST as Group-II data (Fig. 3.3A) and suggest that it is primarily controlled by physical transport-upwelling processes. Note, however that the relationship between pCO_2 and SST within the eddy is not as straightforward as that observed outside Cyclone Opal. We believe that this is due to enhanced biological activity associated with the upwelling of new nutrients into the euphotic zone. These two processes act in opposition, where upwelling water enriched in DIC can be a potential CO_2 source, and biological uptake, which consumes DIC, may be a sink due to the decrease of sea surface pCO_2. Closer

inspection of the IN-pCO_2 data reveals a subset within the eddy core characterized by intermediate pCO_2 values (between 344 and 350 μatm) and very low SST (< 24°C). Given the high rates of biological productivity observed(Benitez-Nelson et al., 2007), we believe that this subset reflects a combination of upwelling and biological uptake and is denoted as Group-III data (Fig. 3.3A). Please note that Groups II and III are not clearly separated and the dividing line between them is somewhat arbitrary (Fig. 3.3A).

A better mechanistic understanding of how different processes may affect sea surface pCO_2 can be assessed by separating the relative roles of (1) upwelling induced mixing, (2) the thermodynamic effect (warming), (3) gas exchange, and (4) biological uptake as shown in Fig. 3B. The expected pCO_2 resulting from the mixing of the original surface seawater and upwelled deep water is 355.4±10.0 μatm, 16.8 μatm higher than that of the original surface water (Fig. 3.3B, also see Table 3.1). The mixed water mass was then warmed up from 22.94±0.28 to 23.86±0.19°C. Warming caused a 14 μatm increase of pCO_2. CO_2 uptake from the atmosphere contributed another 2.6±1.9 μatm increase in sea surface pCO_2. Thus, the expected pCO_2 is 372±10.9 μatm (Fig. 3.3B). The sea surface pCO_2 values calculated from measured DIC and TAlk (average is 351.1±15.9 μatm) and measured underway (between 340 and 368 μatm) at the IN-stations are much lower. Thus, the contribution of biological uptake to CO_2 drawdown is between 4-32 μatm and the average contribution is 21 μatm (Fig. 3.3B). The above analysis strongly supports our hypothesis that sea surface pCO_2 within the eddy is a combined result of upwelling, warming, and biological uptake.

Transect data across the eddy were subdivided by temperature into Transects_In (<24.5°C and a negative pCO_2-SST relationship, green diamonds) and Transects_Out (>24.5°C and a positive pCO_2-SST relationship, dark pink circles) (Fig. 3.1, Fig. 3.2, and Fig. 3.3A). The

pCO_2 data collected during the transects are consistent with our process stations results above. Transects_In links the IN-pCO_2 and OUT-pCO_2 data and is a transition from upwelled high salinity, cold temperature waters within the eddy center to warmer surrounding waters outside the eddy.

The negative correlation between sea surface pCO_2 and SST along Transects_In data is described by:

$$\ln pCO_2 = -0.0257 * SST + 6.4691 \qquad (3.3)$$

$$(n = 376, r^2 = 0.57, p<0.0001, RMSE = 0.0052)$$

Most of the IN-pCO_2 data (Group-II data) from the process study stations in the eddy center falls along the upper part of the regression line for the Transects_In data in Fig. 3.3A. Therefore, if these data are included in equation (3.3), the calculated slope would be more negative and comparable to the slope of -0.049 $°C^{-1}$ (represented by a broken line in Fig. 3.3A) reported in the upwelling zone of the Equatorial Pacific Ocean (Landrum et al., 1996). Such a negative slope is also consistent with the observed pCO_2-SST relationships (-0.06 $°C^{-1}$) for high-latitude surface waters due to winter mixing with water from below (Takahashi et al., 1993; Metzl et al., 1995; Lee et al., 1998).

Note that Group-III data (the subset of IN-pCO_2 data discussed above with intermediate pCO_2 and very low SST) are similar to Transects_In data. Group-III data would merge into Transects_In pCO_2 data if they are temperature-normalized (Fig. 3.4; see next session). Part of the Transects_In data are in the frontal zone (the confluence area of the cold eddy-core water and the surrounding warm oligotrophic water), where enhanced biological uptake relative to the surrounding waters is expected. Thus, Transects_In pCO_2 data are consistent with our earlier interpretation that the relatively low pCO_2 level in Group-III data is caused by biological uptake.

Upwelling versus Biological Uptake

It is interesting to point out that the pCO_2 minimum occurs around a temperature of 24.4-24.6°C in the frontal zone (Figs. 3.2 and 3.3A). As far as we know, such a pCO_2 minimum within the frontal zone has not yet been reported in mesoscale or sub-mesoscale eddies, except that noted in the Sargasso Sea (i.e., surface fCO_2 variability of ~ 5-25 μatm was observed across mesoscale cyclonic and anticyclonic eddies (Bates et al., 2000)). Similar patterns of a negative pCO_2-SST relationship below a key temperature and a positive pCO_2-SST relationship above that temperature have been reported elsewhere over larger spatial scales (e.g., (Takahashi et al., 1993; Landrum et al., 1996)). Takahashi et al. (1993 and 2002) observed a pCO_2 minimum zone along the confluence of poleward-flowing warm subtropical waters and cold nutrient-rich subpolar waters and attributed it to a combination of warm water cooling and biological uptake in subpolar waters.

Here, when cold nutrient-rich water from the eddy-core outcrops to the surface and flows away from the center of the eddy, it contacts and mixes with the surrounding oligotrophic waters. The cooling of this oligotrophic water may result in the decrease of sea surface pCO_2 outside the eddy. On the other hand, when the cold nutrient-rich eddy-core water flows away from the eddy center, it also warms and potentially results in higher pCO_2. But this warming effect on sea surface pCO_2 (increase in pCO_2) may be balanced and surpassed by the biological CO_2 uptake at the confluence areas (frontal zone). Thus, the seawater may become increasingly undersaturated with respect to the atmosphere in spite of the warming. The observed pCO_2 minimum in Fig. 3.3A is likely a consequence of the above processes in this frontal zone, where primary production is no longer limited by nutrient deficits.

In order to assess the effects of upwelling versus biological activity, we must first remove the temperature effect on *in situ* pCO_2. Sea surface pCO_2 data are normalized to a constant temperature of 24.51°C, the lowest SST value observed in the OUT-pCO_2 data and the mean temperature of the overall data. We apply the method developed by Takahashi et al. (2002) to calculate the temperature-normalized pCO_2 values:

$$(pCO_2 \text{ at } T_{mean}) = (pCO_2)_{obs} * \exp(0.0408 * (T_{mean} - T_{obs})) \quad (3.4)$$

where T is the temperature in °C, and the subscripts 'mean' and 'obs' indicate the chosen reference temperature and the *in situ* values, respectively. OUT-pCO_2 data are assumed to be controlled by temperature only and are considered to be isochemical seawater. We also used the slope ($\partial \ln pCO_2/\partial T$) of 0.0408 $°C^{-1}$ determined by our data rather than 0.0423 $°C^{-1}$ by Takahashi et al. (1993).

The results are shown in Fig. 3.3C. For pCO_2 data outside the eddy (OUT-pCO_2 and Transects_Out pCO_2), the temperature-normalized values are nearly independent of the temperature, as expected for a water mass that follows thermodynamic rules (Takahashi et al., 1993). For pCO_2 data inside the eddy (IN-pCO_2 and Transects_In pCO_2), a negative relationship between temperature-normalized pCO_2 and SST is observed when SST falls below 24.51°C. For the large scale global ocean, Takahashi et al. (2002) attributed the temperature-normalized pCO_2 drawdown via seasonal warming to biological uptake. In our case, the low temperature is, however, an indicator of upwelling. Thus, the temperature-normalized pCO_2 values increase by ~30 μatm from a nearly constant reference value outside the eddy to the highest values at the eddy core due to the upwelling of high pCO_2 deep water. Temperature-normalized pCO_2 values in the eddy core that are higher than the outside waters are also supported by observed DIC data (see electronic supplementary information). DIC concentrations in surface waters at the eddy

center are ~15 μmol·kg^{-1} (normalized to a constant salinity of 35, data not shown here) higher than regional surface waters. Using a Revelle factor of 8.5 (Takahashi et al., 1993), the observed difference in total DIC can be translated into a pCO_2 increase of nearly 30 μatm inside the eddy (changes in alkalinity are small).

There is a negative linear relationship between temperature-normalized pCO_2 and SST for transects data within the eddy (Transects_In data) (Fig. 3.3C)

$$(pCO_2 \text{ at } T_{mean}) = -23.332 * SST + 915.49 \qquad (3.5)$$

$$(n = 376, r^2 = 0.90, p<0.0001, RMSE = 1.84)$$

Using this equation removes the thermodynamic effect of temperature (i.e., CO_2 dissociation and solubility changes) on pCO_2 and links pCO_2 to upwelling. If we let $\Delta SST = (SST - 24.51)$ and rewrite equation (3.5) as

$$(pCO_2 \text{ at } T_{mean}) = -23.332 * \Delta SST + 343.62 \qquad (3.6)$$

$$(n = 376, r^2 = 0.90, p<0.0001, RMSE = 1.84)$$

then a general prediction of pCO_2 in eddy-influenced areas can be developed after further adjustment to parameters such as the slope and ΔSST. For example, here, a temperature of 24.51°C is used as the boundary condition to separate surface water inside the eddy from surrounding warmer subtropical surface waters. This boundary temperature and the slope in equation (3.6) could be seasonally and geographically different. Therefore, with further research, equation (3.6) combined with equation (3.4), may be useful for satellite assessments of sea surface pCO_2 distributions and air-sea fluxes of CO_2 in the future.

Sea surface pCO_2 and its relationship to physical-biological environmental variables

Multivariate analysis of sea surface pCO_2 and other environmental factors

Within Cyclone Opal, we identified three unique relationships between pCO_2 and sea surface temperature (SST) in previous discussion (Fig. 3.2-3.4). A significant positive correlation between pCO_2 and SST (Group-I data) was observed in the waters outside the eddy suggesting gas exchange is controlled primarily by thermodynamics (so-called solubility pump control). In contrast, a negative relationship was observed inside the eddy core (Group-II data), suggesting that physical dynamics, the upwelling of CO_2-enriched waters to the surface dominated. A third relationship with low temperature and intermediate pCO_2 existed within the eddy (Group-III data) suggesting a combination of physical upwelling and subsequent biological uptake (Fig. 3.3).

To access the regional and global CO_2 air-sea fluxes and relatively scarce pCO_2 data, previous studies have used empirical relationships to predict sea surface pCO_2 from underway temperature, salinity and chlorophyll (or fluorescence) measurements since biological and physical properties both contribute to the observed pCO_2 (Lefevre et al., 2002; Cosca et al., 2003; Ono et al., 2004). Furthermore, the empirical relationship between pCO_2 and SST may vary with region, thus, some studies even included location (latitude and longitude) of the corresponding pCO_2 measurements in the equation (Nelson et al., 2001; Lefevre and Taylor, 2002; Olsen et al., 2004). Here we applied a multiple linear regression algorithm to identify the pCO_2 variation at OUT-stations (OUT-pCO_2) relative to physical (temperature, salinity) and biological (we use fluorescence data as a proxy for biological parameters) variables:

$$pCO_2 = 14.266 * SST - 0.087*Fluo – 17.492*S + 604.435 \qquad (3.7)$$

$$(n = 1110, r^2 = 0.924, RMSE = 1.773, p<0.001)$$

where SST is sea surface temperature (°C), Fluo is fluorescence data (voltage), S is salinity. The predicted pCO_2 is similar to a simple linear regression predicted pCO_2 with equation:

$pCO_2 = 14.256 * SST - 9.151$ (n = 1110, $r^2 = 0.842$, RMSE = 2.553, $p<0.001$) (3.8)

However, biological uptake of CO_2 may be concealed without explicitly accommodating biological term by using the simple regression model (equation (3.8)). If we take Fluo = 60 (an intermediate number in the fluorescence dataset) into equation (3.7), roughly, a 5 μatm pCO_2 decrease on average will be expected attributed to biological uptake.

The limitation of our previous linear regression is that we already assume that SST, S and chlorophyll (or fluorescence) play major roles in pCO_2 variability. Recently, principal component analysis (PCA) was applied to environmental variables and regressed the derived orthogonal components against in situ pCO_2 in order to obtain an empirical relationship for satellite assessment of CO_2 air-sea fluxes (Dandonneau, 1995; Lohrenz and Cai, 2006). This method is useful in that it enables those components which are the most important contributors to observed pCO_2 variations to be identified. This enables a significant reduction in the number of considered variables. Here we apply a similar strategy and identify pCO_2 variations relative to physical and biological processes from orthogonal components derived from PCA analysis. In the first case, we applied the PCA analysis to Group-I data (the same dataset we use for previous regression exercise (n=1110), see equation 3.2). PCA analysis of SST, salinity, fluorescence (voltage), and wind speed (meter·sec^{-1}) data (They are chosen to be proxies of physical and biological variables) indicates that the first three orthogonal components account for more than 95% of the variation ($r^2 = 0.895$, Fig. 3.5A). We further tested the reliability of this technique by dividing our dataset into two sub-datasets by using systematic sampling. The first half served as test data to compute the regression relationship for pCO_2 (Fig. 3.5B). The results were then applied to the second half of the data (Fig. 3.5C). The match between predicted pCO_2 and in situ pCO_2 for the second half of the data revealed a generally good correlation ($r^2 = 0.842$).

Sea surface pCO_2 data within the eddy can be divided into Group-II (with low temperature and high pCO_2) and Group-III (with low temperature and intermediate pCO_2), respectively (Chen et al., 2007). In practice, it is difficult to separate these two-groups quantitatively. However, it is not meaningful to apply regression analysis to both groups without separation. Thus we applied PCA to all of the in situ pCO_2 data within the eddy core (IN- pCO_2). Unfortunately, the results were not satisfactory. Initially, four variables were included in the analysis, SST, salinity, fluorescence, wind speed. But the magnitude of the computed pCO_2 variability (343-360 μatm) was significantly less than the measured pCO_2 (340-368 μatm). As a result, we added two more variables, humidity and air temperature, but results remain almost the same. We believe that this is because that critical variable representing the upwelling processes is not included in the performed PCA exercise above.

Time series analysis of shipboard underway data

Time series analyses suggest that the relationships among pCO_2, SST and fluorescence are complicated within the eddy center. The same IN-pCO_2 underway data used in Fig. 3.3B with red color were plotted versus time in Figs. 3.6A-C. The fluorescence time series data mirrors the temperature data (Fig. 3.6A), which may reflect the fact that waters with lower temperatures are characterized by higher nutrients, and hence enhanced biomass. However, the relationship between pCO_2 and temperature is more complicated. Arrows in the Fig. 3.6B-C highlight the relationships between pCO_2 and temperature or between pCO_2 and fluorescence. Data sections pointed by red arrows in Fig. 3.6B represent the negative relationship between pCO_2 and SST, which should belong to Group-II data in Fig. 3.3 and are mainly controlled by physical processes (vertical upwelling). Data sections pointed by black arrows in Fig. 3.6C represent a negative relationship between pCO_2 and fluorescence, which may reflect the biological uptake in addition

to physical upwelling process. This phenomenon may explain the observed intermediate pCO_2 at low temperature (Group-III pCO_2 data) in Fig. 3.3.

These analyses allow us to explore the pattern of pCO_2 variability with temperature and fluorescence and to interpret Group-II versus Group-III data that are located within the eddy. These various sections also imply different responses in pCO_2 to local physical and biological processes within short spatial and temporal scale. Now let us further examine two spots in Fig. 3.6B and 3.6C, respectively: one spot (Fig. 3.6B, pointed by black arrow with green circle) on March 16th, 6am, location: Lat: 19.3567°N, Long: 157.0828°W; and the other spot (Fig. 3.6C, pointed by red arrow with green circle) on March 21th, 6am, location: Lat: 18.9698°N, Long: 156.8938°W. The straight distance between these two spots is ~ 20.6 km. If we assume that the ship track is covered by a square area, and take this distance as a diagonal line, the estimated area is about 200 km^2. This implies that patchy distribution of pCO_2 on a spatial scale of several kilometers influenced by a mesoscale eddy is likely. Our observation is consistent with the result of large (5-10 μatm) variation in pCO_2 over short distances (10 km) in the North Atlantic (Watson et al., 1991).

Furthermore, time-series analyses of underway pCO_2 data within the eddy reflect the fact that physical and biological components can be significantly uncoupled at different temporal and spatial scales. There are several possible interpretations. One possibility is the different ventilation time of deep water that was brought up to the sea surface. Cyclone Opal was in its mature phase during our sampling period. It was extremely dynamic when we maneuvered to stay within the eddy center (Dickey et al., 2008). We may have encountered some water during the underway pCO_2 measurements with a relatively short ventilation time, which is insufficient for substantial biological uptake. The result is therefore that we observed high sea surface pCO_2

at low temperatures. In contrast, we likely also encountered waters with a similar temperature, but much longer ventilation time. Thus the pCO_2 may have decreased due to biological uptake. Another possible explanation is that fluorescence may reflect biomass, but not necessarily photosynthetic rate as only active living biomass can uptake CO_2 effectively. This may explain why decreases in pCO_2 did not always occur with increasing fluorescence. Nevertheless, diurnal variations in pCO_2 should also be considered. Two processes may affect the diurnal pCO_2 variation, first is photosynthetic CO_2 uptake (decrease in pCO_2) which mostly takes place in the daytime, and second is due to heat balance at the air-sea interface (cooling at night (decreasing pCO_2) and warming in daytime (increasing pCO_2)). More quantitative analysis is desired in the future.

Diurnal variations in pCO_2 outside the eddy were observed, strongly following SST (Figs. 3.7A-C). A nearly constant temperature-normalized pCO_2 level outside the eddy confirms this pattern (Fig. 3.4). In this study, SST increased from the early morning and reached its peak in the afternoon. SST subsequently decreased and reached its lowest value typically before sunrise, which is a typical diurnal variation due to heat budget.

Air-sea Fluxes of CO_2

The overall average CO_2 sea-to-air fluxes over the entire area, within the eddy, and outside the eddy were estimated using several models (Table 3.2). Overall, CO_2 flux from W-92 (Wanninkhof, 1992) is about twice that estimated from LM-86 (Liss and Merlivat, 1986). The estimates from W-92 and W-99 (Wanninkhof and McGillis, 1999) are comparable. Other approaches (NG2000a (Nightingale et al., 2000a); NG2000b (Nightingale et al., 2000b); MG2001 (McGillis et al., 2001)) reached similarly intermediate values between LM-86 and W-92. Estimates from LM-86 and W-92 serve as the lower and higher limit for calculating CO_2 sea-

to-air fluxes. In the future discussion, we will use CO_2 sea-to-air fluxes calculated from Wanninkhof's equation in 1992, i.e., W-92, since this model has been widely applied by different researcher. Such that it is more appropriate to compare to other studies. The flux estimates are also not significantly different by using wind speeds from different sources (Table 3.2). The estimates from NDBC buoy51003 wind speed data are much closer to the results from average shipboard data, while the fluxes from NDBC buoy 51002 are a bit more negative. This supports our earlier decision that we choose wind speed data from NDBC buoy51003 to calculate CO_2 air-sea fluxes in Chapter 2.

The average wind speed from the meteorological data on NDBC buoy 51003 (location: 19.16°N and 160.74°W) was 6.6 $m \cdot s^{-1}$ in February and March 2005. CO_2 fluxes for summarization were calculated from this wind speed (adjusted to 10 m height), the ΔpCO_2 (difference in average pCO_2 between surface water and atmosphere) and W-92. The overall average sea-to-air CO_2 fluxes in the entire region, within the eddy core (In) and outside the eddy (Out) are estimated to be -2.6 (± 1.7), -2.4 (± 1.5) , and -2.9 (± 1.9) mmol C m^{-2} day^{-1}, respectively (see values in circle with red color, Table 3.2). In all cases, estimated sea-air fluxes are negative, and hence this area is a regional CO_2 sink throughout the cruise period as reported previously (Landrum et al., 1996; Dore et al., 2003). Interestingly, however, Cyclone Opal was less of a sink (i.e., a 17% reduction inside the eddy vs. the outside area). Furthermore, if we apply the general pCO_2-SST correlation outside the eddy (i.e., equation (3.2)) to the region inside the eddy, the predicted sea surface pCO_2 value would be about 333 μatm at 24 °C (the average value is indicated with a large open circle along the Group-I line in Fig. 3.3A). The predicted average sea-to-air CO_2 flux would be about -4.8 mmol C m^{-2} day^{-1}, which represents a 100% overestimation of the real CO_2 uptake inside the eddy. Therefore, although cyclonic eddies are

highly productive, their impact on the carbon cycling and sea surface CO_2 exchange with the atmosphere are complex and needs to be closely examined in light of low observed particle export rates(Benitez-Nelson et al., 2007). With an estimated annual average of 9 cyclonic eddies driven by trade winds in the lee of the main Hawaiian Islands (Lumpkin, 1998), the influence of eddies on CO_2 air-sea exchange deserves much greater attention and further research.

Section 3.2 Cyclone Noah

Based on satellite SST imagery obtained from GOES radiance sensors, a first baroclinic mode cyclonic eddy, Cyclone Noah, first appeared to the southwest of the Alenuihaha Channel between August 13 and 20, 2004 (Dickey et al., 2008; Kuwahara et al., 2008). Cyclone Noah was at least 2.5 months old by the time of sampling during E-Flux I (Dickey et al., 2008); Figs. 2.2-2.3). Underway samples were collected from Cyclone Noah by the flow-through system on board of the R/V *KOK* during November 4 - 20th, 2004 as part of the E-Flux study (Fig. 2.4). Underway pCO_2 measurements were conducted along all transects and at process stations (Table 2.1; Fig. 2.4). Atmospheric pCO_2 was not measured during E-Flux I. Based on in situ dry air samples collected at Mauna Loa Observatory, Hawaii (beside E-Flux field area, Fig. 2.1) by Keeling and Whorf (Fig. 2.7), atmospheric pCO_2 averaged ~365.1 μatm after a 100% humidity correction.

pCO_2-SST relationships

Underway sea surface pCO_2 and SST data were collected throughout the cruise. Thus, with regard to their relative locations to Cyclone Noah and weather conditions (as mentioned in Chapter 2), in Fig. 3.8, they were labeled as "IN1-2" (data from IN1 and IN2 at the center of Noah), "OUT" (at OUT-stations, well outside the eddy flow field), "IN3-4" (high velocity eddy zone and the eddy edge), and "Drift" (during the period of wind gusts time and cessation of

sampling). Similarly to E-Flux III, outside the eddy (OUT in Fig. 3.8), a positive linear SST-pCO_2 relationship between the natural logarithms of sea surface pCO_2 and SST is obtained:

$$\ln pCO_2 = 0.0394 * SST + 4.8236 \qquad (3.9)$$

($n = 2503$, $r^2 = 0.58$, $p<0.0001$, root mean square error (RMSE) = 0.0036)

The RMSE in the pCO_2 prediction is within 2 μatm. The calculated slope, i.e., temperature factor ($\partial \ln pCO_2/\partial T$), is 0.0394 $^oC^{-1}$. This is essentially the same as OUT-pCO_2 during E-Flux III (slope is 0.0408 $^oC^{-1}$, in Section 3.1), suggesting that temperature is the controlling factor on sea surface pCO_2 outside the eddy.

Sea surface pCO_2 at the center of Cyclone Noah (IN1-2-pCO_2) were about 7-8 μatm higher than other groups of pCO_2 data, including OUT-, IN3-4-, and Drift-pCO_2 (Fig. 3.8A). The pCO_2 data along the several transects are between IN1-2-pCO_2 and other groups labeled in Fig. 3.8A, although the transects-pCO_2 data are not shown there. This higher sea surface pCO_2 within the eddy core is consistent with the isopycnal uplift and contribution of significant DIC-rich deep water into the surface, which is the same as we mentioned for Cyclone Opal during E-Flux III. One would argue that significant decomposition of organic carbon may occur since Cyclone Noah was in its decay phase during the sampling period. However, we would expect such organic carbon decomposition mostly exists in the lower layer of the euphotic zone (Cochran et al., 1993; Amiel et al., 2002; Benitez-Nelson et al., 2007; Maiti et al., 2008; Rii et al., 2008).

There are at least two differences between Cyclone Opal and Noah with regard to the SST-pCO_2 relationships. First, we did not observe the negative SST-pCO_2 relationship within the center of Cyclone Noah except a group of data at the eddy edge after the wind gusts between November 14 and 15, 2004 (IN3-4). Instead, IN1-2 pCO_2 within the eddy core (IN1-2 in Fig. 3.8A) showed up a positive SST-pCO_2 relationship. The slope of IN1-2-pCO_2 data, $\partial \ln pCO_2/\partial T$

is similar to 0.04 ºC^{-1}, suggesting that sea surface pCO_2 within the eddy core of Cyclone Noah was primarily controlled by temperature as well during the sampling period. Such a different pattern in SST- pCO_2 relationship between Cyclone Opal and Noah implies the temporal evolution of cyclonic eddies and is consistent with their mature (or spin-up) phase and decay phase, respectively. This is to say the active pumping of cold DIC rich water from below can still be detected during sampling period for Cyclone Opal, whereas no active pumping from below can be detected for Cyclone Noah. Diurnal variations in pCO_2 for both the center of Cyclone Noah (IN1-2) and outside-eddy area (OUT-stations) were observed, strongly following SST (Figs. 3.9A-B). SST and sea surface pCO_2 increased from the early morning and reached its peak in the afternoon. SST subsequently decreased and reached its lowest value typically before sunrise, which is a typical diurnal variation due to heat budget. These results all indicate that with the temporal evolution of a cyclonic eddy, the influence of temperature on sea surface pCO_2 is getting more and more important.

Second, a closer comparison of SST across Cyclone Noah enables us to realize that there is essentially no difference in SST between the Cyclone Noah center and outside-eddy area during the sampling period (except some data with lower temperature from groups of "IN3-4" and "Drift" after the period of wind gust) (Fig. 3.8A). These phenomena indicate that the warming of the upwelled subsurface salinity maximum water was almost complete by the time of sampling for Cyclone Noah and this is consistent with the thermodynamic dominant pCO_2-SST at the eddy center (see equation 3.9). These unique characteristics also support the view that Cyclone Noah was indeed in a decay phase at the sampling time from hydrological and biological analysis (Kuwahara et al., 2008; Rii et al., 2008).

The same strategy as we applied to Cyclone Opal in Section 3.1 was applied here to access a better mechanistic understanding of how different processes, which may affect sea surface pCO_2, can be assessed by separating the relative roles of (1) upwelling induced mixing, (2) the thermodynamic effect (warming), (3) gas exchange, and (4) biological uptake as shown in Fig. 8B. The expected pCO_2 resulting from the mixing of the original surface seawater and upwelled deep water is 357.3±11.2 μatm, 10.1 μatm higher than that of the original surface water (Fig. 3.8B, also see Table 3.3). The mixed water mass was then warmed up from 23.527±0.445 to 26.901±0.127 °C. Warming caused a 51 μatm increase of pCO_2 in this case. CO_2 degassing to the atmosphere contributed a 13.8±7.2 μatm decrease in sea surface pCO_2. Thus, the expected pCO_2 is 394.7±12.8 μatm (Fig. 3.8B). The sea surface pCO_2 values calculated from measured DIC and TAlk (average is 367.5±12.4 μatm) and measured underway (most data are between 360 and 380 μatm, averaged 368.1±3.7 μatm) at the IN-stations (IN1-2) are much lower. Thus, the contribution of biological uptake to CO_2 drawdown is between ~15-35 μatm and the average contribution is 27 μatm (Fig. 3.3B).

Again, the above analysis strongly support our conclusion from Section 3.1 that sea surface pCO_2 within the cyclonic eddies is a combined result of upwelling, warming, and biological uptake. Furthermore, with the temporal evolution of a cyclonic eddy, especially when a cyclonic eddy evolves from mature phase to a decay phase, warming may become more significant and therefore cause more pCO_2 increase.

Air-sea Fluxes of CO_2

The overall average CO_2 sea-to-air fluxes over the entire area, within the eddy, along transects, and outside the eddy were estimated using several models as mentioned in Section 3.1 (Table 3.4). Estimates from LM-86 (Liss and Merlivat, 1986) and W-92 (Wanninkhof, 1992)

serve as the lower and higher limit for calculating CO_2 sea-to-air fluxes. As the reason mentioned in Section 3.1 and for consistency purpose, we will summarize the regional CO_2 sea-to-air fluxes calculated from W-92's equation and wind speed data from NDBC buoy51003.

The average wind speed from the meteorological data on NDBC buoy 51003 (location: 19.16°N and 160.74°W) was 6.3 m s^{-1} (adjusted to 10 m height) in Fall 2004 (the average of September, October, and the first two weeks of November). Similar to E-Flux III in Section 3.1, sea-to-air CO_2 fluxes were calculated from this wind speed, the ΔpCO_2 (difference in average pCO_2 between surface water and atmosphere) and several models (Table 3.4). Comparing to the results from different models, similar conclusion will be reached. Therefore, to be consistent, CO_2 fluxes from equation W-92 (Wanninkhof, 1992) were applied for discussion (Table 3.4). The overall average sea-to-air CO_2 fluxes in the entire E-Flux field area, within the eddy core (IN) and outside the eddy (OUT) are estimated to be -0.44 (± 0.36), 0.37 (± 0.48) , and -0.53 (± 0.30) mmol C m^{-2} day^{-1}, respectively (see values in square with red color, Table 3.4). Thus, the center of Cyclone Noah served as weak CO_2 source or neutral area while the entire area is small sink of CO_2. This is also clear when we compare IN1-2-pCO_2 data to atmospheric pCO_2 line in Fig. 3.8. On the other hand, the other parts for the E-Flux field area in the lee of Hawaii served as weak CO_2 sink or neutral area (Fig. 3.8).

Comparing to Cyclone Opal, an apparent difference between these two eddies, and subsequently a plausible description can be as follows: Cyclonic eddies serve as CO_2 sink during their spin-up or mature phase (e.g., Cyclone Opal) and neutral or weak CO_2 source during their decay phase (e.g., Cyclone Noah). On the other hand, a common feature in these two cyclones is that sea surface pCO_2 inside the eddy center is much higher than the expected values deduced from the sea surface pCO_2-SST relationship at OUT-stations without the influence of eddies

(Figs. 3.3A and 3.8A). Thus, cyclonic eddies are less of a sink in both cases. This is to say that the net effect of cyclonic eddies is a source of CO_2 to the atmosphere if we set outside-eddy region as CO_2 neutral area.

Section 3.3 Seasonal variation of CO_2 air-sea exchange across cyclonic eddies in the lee of Hawaii

Before we start to discuss further the influence of heat balance on CO_2 air-sea exchange across cyclonic eddies in the lee of main Hawaiian Islands, a brief summary of sea surface pCO_2-SST relationship without the existence of eddy in January 2005 (E-Flux II cruise) is provided first. Similar to other E-Flux cruises, underway SST and pCO_2 data were collected along all transects and at process stations (Table 2.2; Fig. 2.5; Fig. 3.10). As we mentioned in Chapter 2, for E-Flux II, no eddy was detected at IN-stations. This view is actually supported by the observed consistent pCO_2-SST relationship among three groups of data collected from different geographical locations (Fig. 3.10). However, there are small parts of pCO_2 with lower temperature show a negative relationship with SST for the IN-stations and transects (see data in circle in Fig. 3.10), which implied the occurrence of sub-mesoscale processes due to intrusion of colder subsurface water with higher pCO_2. Because of this reason, a regression between SST and pCO_2 was only applied to OUT-station data (Fig. 3.10). A positive linear SST-pCO_2 relationship between the natural logarithms of sea surface pCO_2 and SST is obtained:

$$\ln pCO_2 = 0.0426 * SST + 4.7604 \qquad (3.10)$$

($n = 2006$, $r^2 = 0.86$, $p<0.0001$, root mean square error (RMSE) = 0.0029)

The calculated slope, i.e., temperature factor ($\partial \ln pCO_2/\partial T$), is 0.0426 $ºC^{-1}$. This is essentially the same as isochemical seawater determined by Takahashi et al. (1993) for a much larger database and temperature range (0.0423 $°C^{-1}$ between 2-28°C), suggesting that temperature is the

controlling factor on sea surface pCO_2 at OUT-stations. Thus, pCO_2 at OUT-stations (OUT-pCO_2) during all three E-Flux cruises were controlled by thermodynamic effect (Temperature control: The slopes ($\partial \ln pCO_2/\partial T$) for E-Flux I - III are 0.0394, 0.0426, and 0.0408 $^oC^{-1}$, respectively).

The average wind speed from the meteorological data on NDBC buoy 51003 (location: 19.16°N and 160.74°W) was 5.8 $m \cdot s^{-1}$ (adjusted to 10 m height) in January 2005. Subsequently, CO_2 fluxes were calculated (Table 3.5). By using W-92's equation (Wanninkhof, 1992), the average sea-to-air CO_2 fluxes is -2.5 (± 1.4) mmol C m^{-2} day^{-1} (see values in circle, Table 3.5). Thus, when there was no eddy detected during E-Flux II, the entire E-Flux field area served as a CO_2 sink with a similar quantity comparing to OUT-stations in E-Flux III (also see Table 3.2). This is also clear when we observed similar average sea surface pCO_2 at OUT-stations between E-Flux II and III (Table 3.6). Please note that SST during E-Flux II and III is similar, although there was a slight cooling from E-Flux II to III (Table 3.6).

When we compare SST and pCO_2 data during all three E-Flux cruises (also including those at IN-stations, Table 3.6), it is clear that the pattern of pCO_2 variation follows the meteorological temperature change for OUT-stations. Such a temporal change in SST and pCO_2 is also consistent with the seasonal variation at Station Aloha where SST and pCO_2 reach a minimum in winter (January to March) and a maximum in fall (August to November) (Dore et al., 2003; Keeling et al., 2004). This seasonal temperature dynamics determines the magnitude of SST difference between eddy center (e.g., IN-stations) and outside-eddy ocean area, which is 3.2 ^oC for Cyclone Opal and 5.4^oC for Noah, respectively. Normally, we will expect this difference is maximal in summer and minimal in winter. Thus, seasonal temperature dynamics as well as

the age or evolution status of an eddy will both affect the extent of surface warming and subsequently, the extent of increase in sea surface pCO_2 within the eddy center.

We can use calculated pCO_2 data from DIC and TAlk in Table 3.1 and 3.3 instead of measured values for further analysis. If we compare the calculated sea surface pCO_2 at the eddy center (IN-stations) for both Cyclones Opal and Noah, the calculated pCO_2 values with expected temperature ($T_{IN(exp)}$) and DIC ($DIC_{IN(exp)}$) are similar (355.4±10.0 µatm for Cyclone Opal and 357.3±11.2 µatm for Cyclone Noah). However, the warming-caused SST increase for Cyclone Opal and Noah were averaged 0.9 and 3.4ºC, respectively. Correspondingly, these resulted in the increase in pCO_2 ~14 and ~51 µatm, respectively. This difference should contribute to the much lower pCO_2 values from observed temperature ($T_{IN(obs)}$) and DIC ($DIC_{IN(obs)}$) for Cyclone Opal (351.2±15.9 µatm) than that for Cyclone Noah (367.5±12.4 µatm). Since the mixing already covered vertical upwelling, the higher pCO_2 value in Cyclone Noah could also be derived from air-sea gas exchange and biological activity, besides the thermodynamic effect (difference caused by temperature). However, for Cyclone Noah, CO_2 degassing and biological uptake both decreased pCO_2 by ~13.8 and ~27.2 µatm, respectively. For Cyclone Opal, biological uptake decreased pCO_2 by ~ 20.8 µatm, while contribution from air-sea gas exchange is negligible (~ 2.6 µatm increase).

From the above analysis, it is more precisely to say that the magnitude of potential increase in SST within the eddy core as well as the age or evolution status of an eddy are both important to determine if a cyclonic eddy area is a CO_2 sink or source. Such a magnitude is defined as the difference between the initial SST within the eddy core (when eddy core was just formed) and SST at OUT-stations. At least for the cases of Cyclones Opal and Noah, the initial SST within the eddy core did not change much. Thus, the magnitude of potential increase in SST

within the eddy core is essentially controlled by seasonal variation in meteorological temperature as well as the age or evolution status of an eddy.

Our findings help improve the accuracy of global climatological pCO_2 distributions by assessing the role of mesoscale eddies (Robinson, 1983). By comparison of sea surface pCO_2 within the eddy core to that at OUT-stations, it is evident that sea surface pCO_2 and DIC at the eddy center is much higher than surface waters in areas outside the eddy, e.g., OUT-stations. This implies that although cyclonic eddies substantially enhance primary production (supported by significant biological uptake of sea surface pCO_2) and flourishing the ecosystem in the otherwise oligotrophic waters, their net impact on the carbon cycling and sea surface CO_2 exchange with the atmosphere is not necessarily carbon sequestration. Instead, they actually enhance the net CO_2 release to the atmosphere in the Subtropical Ocean. We conclude that this is mostly due to the cancellation of two competing mechanisms: vertical upwelling and biological uptake. If we neglect the CO_2 variability due to mesoscale eddies and apply a general sea surface pCO_2-SST equation from oligotrophic waters to interpolate sea surface pCO_2 inside the eddy, significant bias in the estimation of regional CO_2 air-sea flux is expected, which is supported by the results from Cyclone Opal and Noah. This is consistent with results from the Sargasso Sea near Bermuda where the variability of CO_2 fluxes was reduced from 30% to within 10% when more frequent pCO_2 measurements were implemented (Bates et al., 1998).

Based on the discussion above, we come up with two major conclusions: (1) Overall, cyclonic eddies enhance net CO_2 release to the atmosphere. (2) The magnitude of this net CO_2 release is positively correlated to the age or evolution status of an eddy as well as the magnitude of potential increase in SST within the eddy center, which is determined by the seasonal heat budget in the mixed layer. This magnitude generally reaches its maximum in summer and

minimum in winter. We suggest that other types of eddies in various stages of their life cycle and also in terms of different seasons need to be further evaluated for their pCO_2-SST relationships and CO_2 air-sea exchange in order to fully understand their impact on global CO_2 exchange processes.

Table 3.1 Calculated sea surface pCO_2 of different water masses for Cyclone Opal. The sea surface pCO_2 data in Fig. 3.3B were calculated from DIC, TAlk and corresponding salinities and temperatures of different water masses and they are listed in the table below. By using a salt-budget approach which will be explained in Section 4.2 (Chen et al., resubmitted), the average initial surface water DIC and temperature at six IN-stations can be estimated as a result of mixing of the original surface water and deep water with salinity maximum (expected DIC ($DIC_{IN(exp)}$) and expected temperature ($T_{IN(exp)}$), respectively). The data of the initial surface water and deep water are the averages of the three OUT-stations. The expected pCO_2 of this mixed water mass, calculated from DIC and TAlk, is 355.4±10.0 µatm. TAlk showed minor changes in the surface waters and average values of 2300 µmol kg^{-1} were used in the calculation of pCO_2. We deduce that the mixed water mass was warmed from expected temperature ($T_{IN(exp)}$ = 22.938±0.281 °C) to observed temperature ($T_{IN(obs)}$ = 23.864±0.192 °C). Warming caused the pCO_2 to increase to 369.4±10.7 µatm. By using measured gas fluxes inside the eddy (in Table 3.4) and a Revelle factor of 8.5 for low latitudes, the variation in pCO_2 due to gas exchange can be estimated (Lefevre et al., 1994). The expected pCO_2 of the mixed water mass is 372±10.9 µatm after a gas exchange correction (absorbance of CO_2 from the atmosphere). The average sea surface pCO_2 calculated from measured DIC and TAlk at IN-stations is 351.1±15.9 µatm.

Water source	Salinity	Temperature(°C)	DIC (µmol·kg^{-1})	pCO_2 (µatm)
Surface water at OUT stations	**34.8760±0.0548**	**24.926±0.225**	**1958.3±3.1**	**338.6±14.7**
Deep water with salinity maximum at OUT stations	**35.1219±0.0089**	**21.738±0.179**	**2019.4±8.2**	**397.3±16.7**
Surface water at IN stations with T_{exp} and DIC_{exp}	**35.0293±0.0061**	**22.938±0.281**	**1996.3±5.0**	**355.4±10.0**
Surface water at IN stations with T_{obs} and DIC_{exp}	**35.0293±0.0061**	**23.864±0.192**	**1996.3±5.0**	**369.4±10.7**
Surface water at IN stations with T_{obs} and DIC_{exp} after air-sea exchange correction	**35.0293±0.0061**	**23.864±0.192**	**1996.3±5.0**	**372.0±10.9**
Surface water at IN stations with T_{obs} and DIC_{obs}	**35.0293±0.0061**	**23.864±0.192**	**1982.7±5.2**	**351.2±15.9**

Table 3.2 Sea-to-air CO_2 fluxes in the lee of Hawaii during E-Flux III eddy cruise (Longitude range: -158.1646 ~ -156.1218°W; Latitude range: 18.8612 ~ 20.8004°N). Please note that circles with red color are used to label the fluxes for summarizing the regional CO_2 sea-to-air fluxes.

Whole area	CO_2 Flux ($mmolC \cdot m^{-2} \cdot d^{-1}$) LM-86[1)]	CO_2 Flux ($mmolC \cdot m^{-2} \cdot d^{-1}$) W-92[2)]	CO_2 Flux ($mmolC \cdot m^{-2} \cdot d^{-1}$) W-99[3)]	CO_2 Flux ($mmolC \cdot m^{-2} \cdot d^{-1}$) NG2000a[4)]	CO_2 Flux ($mmolC \cdot m^{-2} \cdot d^{-1}$) NG2000b[5)]	CO_2 Flux ($mmolC \cdot m^{-2} \cdot d^{-1}$) MG2001[6)]
Flux estimated from time-averaged underway pCO_2 and wind speed	-1.3 (0.8)	-2.5 (1.7)	-2.1 (1.5)	-1.6 (1.0)	-1.5 (0.9)	-1.6 (1.1)
Average flux with wind data from NDBC buoy station 51002[7)]	-1.6 (0.9)	-3.1 (1.9)	-3.0 (2.1)	-2.0 (1.6)	-1.8 (1.0)	-2.0 (1.5)
Average flux with wind data from NDBC buoy51003[8)]	-1.3 (0.8)	-2.6 (1.7)	-2.3 (1.7)	-1.7 (1.5)	-1.6 (0.9)	-1.7 (1.1)
Inside eddy	CO_2 Flux ($mmolC \cdot m^{-2} \cdot d^{-1}$) LM-86[1)]	CO_2 Flux ($mmolC \cdot m^{-2} \cdot d^{-1}$) W-92[2)]	CO_2 Flux ($mmolC \cdot m^{-2} \cdot d^{-1}$) W-99[3)]	CO_2 Flux ($mmolC \cdot m^{-2} \cdot d^{-1}$) NG2000a[4)]	CO_2 Flux ($mmolC \cdot m^{-2} \cdot d^{-1}$) NG2000b[5)]	CO_2 Flux ($mmolC \cdot m^{-2} \cdot d^{-1}$) MG2001[6)]
Flux estimated from time-averaged underway pCO_2 and wind data	-1.1 (0.7)	-2.2 (1.5)	-1.9 (1.4)	-1.5 (0.9)	-1.3 (0.6)	-1.4 (0.8)
Average flux with wind data from NDBC buoy station 51002[7)]	-1.4 (0.8)	-2.8 (1.7)	-2.7 (1.8)	-1.8 (1.1)	-1.6 (1.1)	-1.8 (1.1)
Average flux with wind data from NDBC buoy51003[8)]	-1.2 (0.7)	-2.4 (1.6)	-2.1 (1.4)	-1.6 (0.8)	-1.4 (0.7)	-1.5 (0.9)
Outside eddy	CO_2 Flux ($mmolC \cdot m^{-2} \cdot d^{-1}$) LM-86[1)]	CO_2 Flux ($mmolC \cdot m^{-2} \cdot d^{-1}$) W-92[2)]	CO_2 Flux ($mmolC \cdot m^{-2} \cdot d^{-1}$) W-99[3)]	CO_2 Flux ($mmolC \cdot m^{-2} \cdot d^{-1}$) NG2000a[4)]	CO_2 Flux ($mmolC \cdot m^{-2} \cdot d^{-1}$) NG2000b[5)]	CO_2 Flux ($mmolC \cdot m^{-2} \cdot d^{-1}$) MG2001[6)]
Flux estimated from time-averaged underway pCO_2 and wind data	-1.4 (0.8)	-2.7 (1.9)	-2.4 (1.7)	-1.8 (1.2)	-1.6 (1.0)	-1.7 (1.1)
Average flux with wind data from NDBC buoy station 51002[7)]	-1.7 (1.0)	-3.4 (2.1)	-3.3 (2.3)	-2.2 (1.4)	-2.0 (1.3)	-2.2 (1.3)
Average flux with wind data from NDBC buoy51003[8)]	-1.5 (0.9)	-2.9 (1.8)	-2.6 (1.9)	-1.9 (1.2)	-1.7 (0.9)	-1.8 (1.0)

1) Liss and Merlivat (1986) is denoted as LM-86. Negative flux indicates a direction from air to ocean.

2) Wanninkhof (1992) is denoted as W-92.

3) Wanninkhof and McGillis (1999) is denoted as W-99.

4) Nightingale et al. (2000a) is denoted as NG2000a.

5) Nightingale et al. (2000b) is denoted as NG2000b.

6) McGillis et al. (2001) is denoted as MG2001.

7) Monthly average wind speed data in March 2005. Buoy station is located at 17.14°N and 157.79°W.

8) Monthly average wind speed data in March 2005. Buoy station is located at 19.16°N and 160.74°W.

Table 3.3 Calculated sea surface pCO_2 of different water masses for Cyclone Noah. The sea surface pCO_2 data in Fig. 3.8B were calculated from DIC, TAlk and corresponding salinities and temperatures of different water masses and they are listed in the table below. By using a salt-budget approach which will be explained in Section 4.2 (Chen et al., resubmitted), the average initial surface water DIC and temperature at two IN-stations (IN1and IN2) can be estimated as a result of mixing of the original surface water and deep water with salinity maximum (expected DIC ($DIC_{IN(exp)}$) and expected temperature ($T_{IN(exp)}$), respectively). The data of the initial surface water and deep water are the averages of the three OUT-stations. The expected pCO_2 of this mixed water mass, calculated from DIC and TAlk, is 357.3±11.2 μatm. TAlk showed minor changes in the surface waters and the average values of 2303 μmol kg^{-1} were used in the calculation of pCO_2. We deduced that the mixed water mass was warmed from expected temperature ($T_{IN(exp)}$ = 23.527±0.445 °C) to observed temperature ($T_{IN(obs)}$ = 26.901±0.127 °C). Warming caused the pCO_2 to increase to 308.5±10.6 μatm. By using measured gas fluxes inside the eddy (in Table 3.4) and a Revelle factor of 8.5 for low latitudes, the variation in pCO_2 due to gas exchange can be estimated (Lefevre et al., 1994). The expected pCO_2 of the mixed water mass is 394.7±12.8 μatm after a gas exchange correction (degassing of CO_2 to the atmosphere). The average sea surface pCO_2 calculated from measured DIC and TAlk at IN-stations is 367.5±12.4 μatm.

Water source	Salinity	Temperature(°C)	DIC (μmol·kg^{-1})	pCO_2 (μatm)
Surface water at OUT stations	**34.814±0.015**	**27.004±0.111**	**1953.0±5.1**	**347.2±14.1**
Deep water with salinity maximum at OUT stations	**35.130±0.011**	**21.623±0.414**	**2020.5±5.0**	**380.3±17.3**
Surface water at IN stations with T_{exp} and DIC_{exp}	**35.007±0.011**	**23.527±0.445**	**1995.6±2.0**	**357.3±11.2**
Surface water at IN stations with T_{obs} and DIC_{exp}	**35.007±0.011**	**26.901±0.127**	**1995.6±2.0**	**408.5±10.6**
Surface water at IN stations with T_{obs} and DIC_{exp} after air-sea exchange correction	**35.007±0.011**	**26.901±0.127**	**1995.6±2.0**	**394.7±12.8**
Surface water at IN stations with T_{obs} and DIC_{obs}	**35.007±0.011**	**26.901±0.127**	**1972.6±5.2**	**367.5±12.4**

Table 3.4 Sea-to-air CO_2 fluxes in the lee of Hawaii during E-Flux I eddy cruise (Longitude range: -158 ~ -156°W; Latitude range: 18.5 ~ 21°N). Please note that square with red color is used to label the flux for summarizing the regional CO_2 sea-to-air fluxes.

IN1-IN2	IN3-IN4	Transects	Outside eddy	Whole area	References
CO_2 air-sea Flux[a)] (mmol C·m^{-2}·d^{-1})					
0.19 (0.25)	-0.26 (0.16)	-0.08 (0.18)	-0.27 (0.17)	-0.23 (0.19)	Liss and Merlivat (1986)
0.37 (0.48)	-0.51 (0.29)	-0.16 (0.35)	-0.53 (0.30)	-0.44 (0.36)	Wanninkhof (1992)
0.32 (0.43)	-0.43 (0.32)	-0.14 (0.31)	-0.46 (0.33)	-0.38 (0.35)	Wanninkhof and McGillis (1999)
0.25 (0.33)	-0.34 (0.24)	-0.11 (0.24)	-0.35 (0.25)	-0.29 (0.27)	Nightingale et al. (2000a)
0.23 (0.29)	-0.31 (0.19)	-0.10 (0.21)	-0.31 (0.19)	-0.27 (0.23)	Nightingale et al. (2000b)
0.24 (0.31)	-0.32 (0.23)	-0.10 (0.23)	-0.34 (0.22)	-0.28 (0.25)	McGillis et al. (2001)

[a)] **Monthly average wind speed data are from NDBC Buoy 51003 in March 2005. Buoy station is located at 19.16°N and 160.74°W.**

Table 3.5 Sea-to-air CO_2 fluxes in the lee of Hawaii during E-Flux II cruise (Longitude range: -158 ~ -156°W; Latitude range: 18.5 ~ 21°N). Please note that circle with red color is used to label the flux for summarizing the regional CO_2 sea-to-air fluxes.

CO_2 air-sea Flux[a)] (mmol C m^{-2} d^{-1})	**References**
-1.2 (0.6)	**Liss and Merlivat (1986)**
-2.5 (1.4)	**Wanninkhof (1992)**
-2.0 (1.5)	**Wanninkhof and McGillis (1999)**
-1.7 (1.2)	**Nightingale et al. (2000a)**
-1.5 (0.9)	**Nightingale et al. (2000b)**
-1.6 (1.0)	**McGillis et al. (2001)**

a) Monthly average wind speed data are from NDBC Buoy 51003 in March 2005. Buoy station is located at 19.16°N and 160.74°W.

Table 3.6 Average sea surface pCO_2 and SST during E-Flux I – III at OUT-stations as well as those at the eddy center of Cyclone Noah (E-Flux I) and Opal (E-Flux III). Also shown is atmospheric pCO_2 value during three E-Flux cruises.

		E-Flux I	E-Flux II	E-Flux III
OUT (Outside eddy)	SST (ºC)	27.04±0.23	25.36±0.20	25.11±0.41
	$p\,CO_2$ (µatm)	360.8±1.9	343.9±3.6	347.2±6.4
IN (Eddy center)	SST (ºC)	26.97±0.20	N/A	24.01±0.23
	$p\,CO_2$ (µatm)	368.1±3.7	N/A	351.2±5.4
Atmospheric $p\,CO_2$ (µatm)		365.1	367.5	369.4

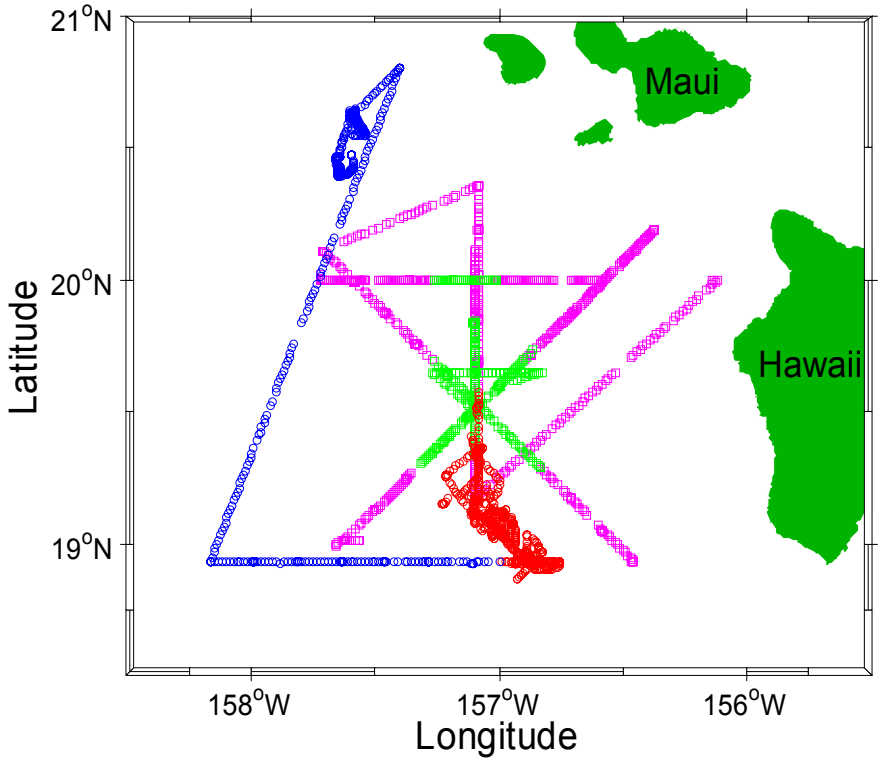

Fig. 3.1 Ship track during the E-Flux III, March 2005 cruise. The cruise track is divided into four groups according to their spatial location relative to the eddy. The initial sampling pattern consisted of several transects across the eddy. Temperature was used to distinguish Transects_In (<24.5°C and negative pCO_2-SST, green color) from Transects_Out stations (>24.5°C and positive pCO_2-SST, dark pink color). After the completion of transects, a series of IN-stations at the eddy core (as defined by temperature minima) were conducted and is labeled in red color. As the eddy was moving, the process stations did not match the center of the Transects_In. At the end of the cruise, the ship left Cyclone Opal, a series of control process stations were conducted well outside the eddy flow field (OUT-stations). This part is labeled in blue color.

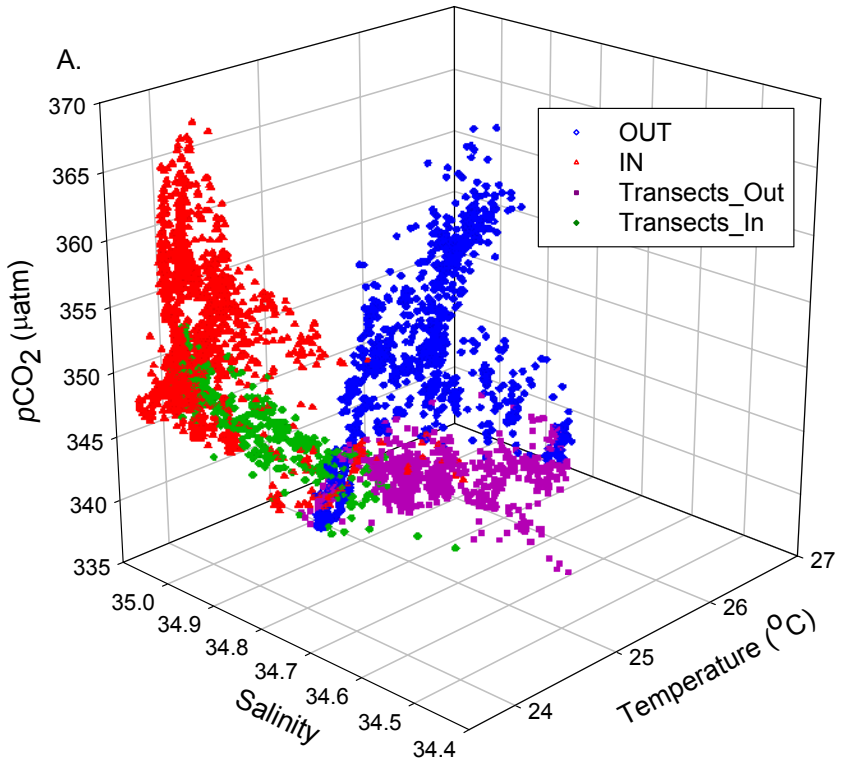

Fig. 3.2 Relationship of sea surface pCO_2 to SST and salinity in E-Flux III. Data points with four different colors follow the ship track in Fig. 2: 'Transects_Out' with dark pink squares, 'Transects_In' with green diamonds, 'Out' with blue diamonds, and 'In' with red triangles. Legends in Figs. 4 and 5 are the same and their meaning is described in Fig. 2. The pCO_2 data in Fig. 3 and 4 are the same. The large open circle in the figure represents an average pCO_2 value if the general positive correlation (Group-I line) is used to predict the value inside the eddy.

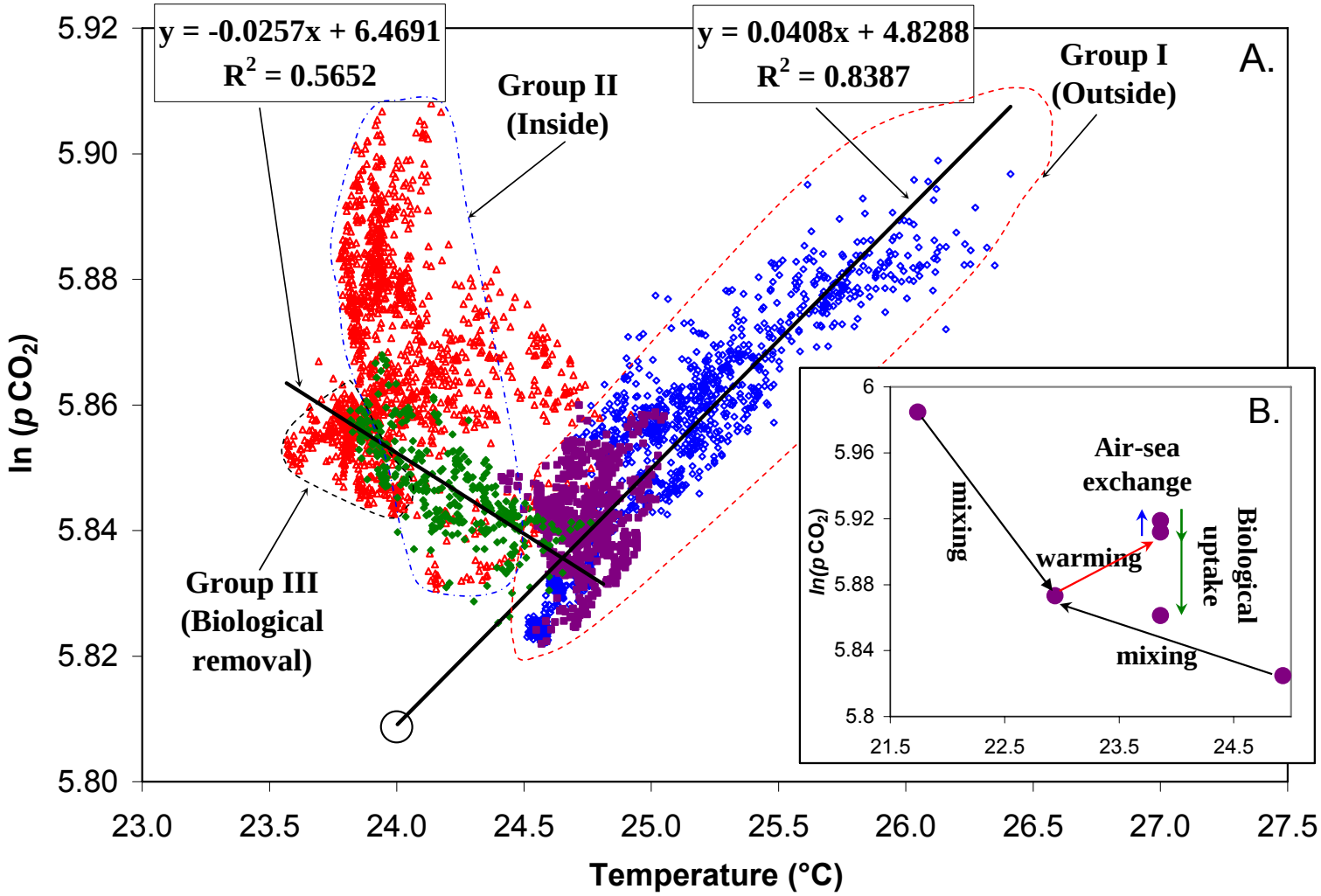

Fig. 3.3 Sea surface pCO_2 and SST relationships. (A) Relationship between sea surface pCO_2 (natural logarithms) and SST in E-Flux III; (B) Sea surface pCO_2 of different water masses: diagram of different processes affecting pCO_2 (please note that air ln (pCO_2) = 5.911).

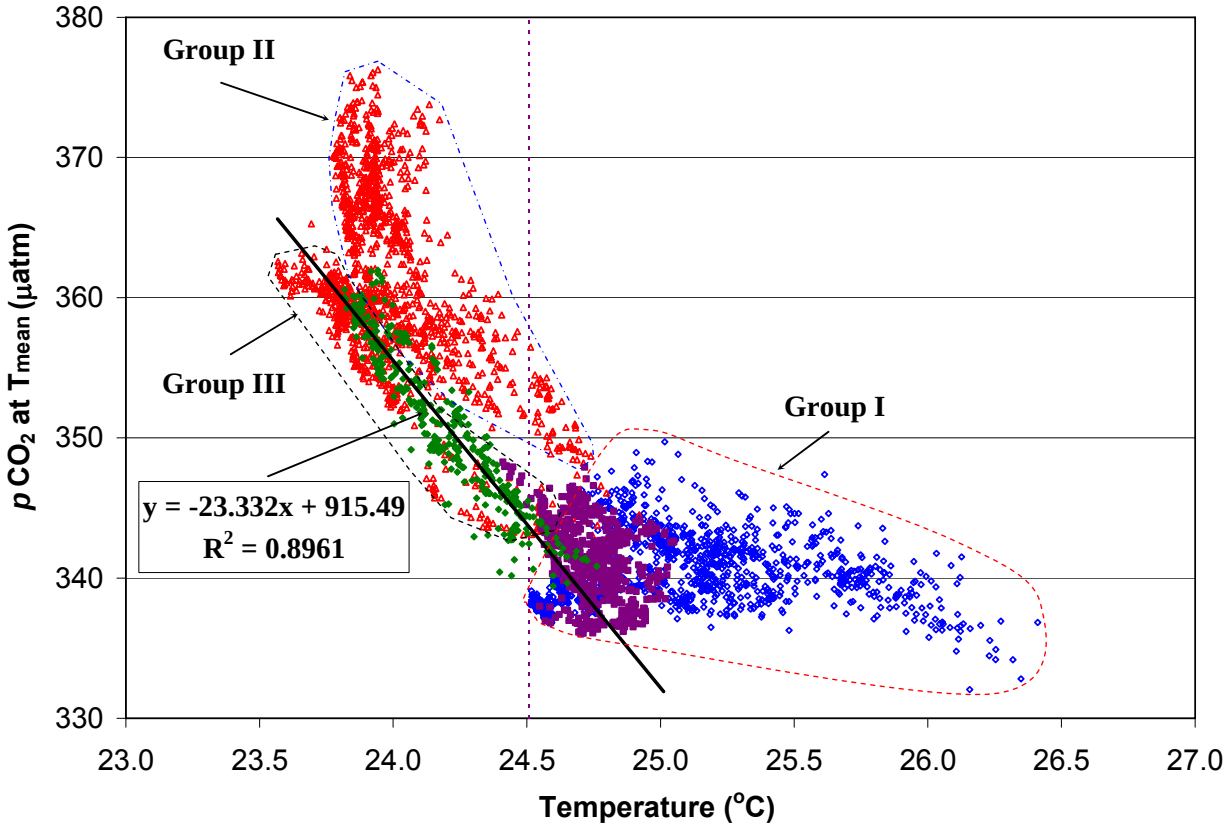

Fig. 3.4 Relationship between temperature-normalized pCO_2 at temperature of 24.51°C and SST (dashed line is at temperature 24.51°C)

A. Overall data (y=0.8954*x + 36.4748, n = 1110, r^2 = 0.895, RMSE = 1.962, p < 0.0001)

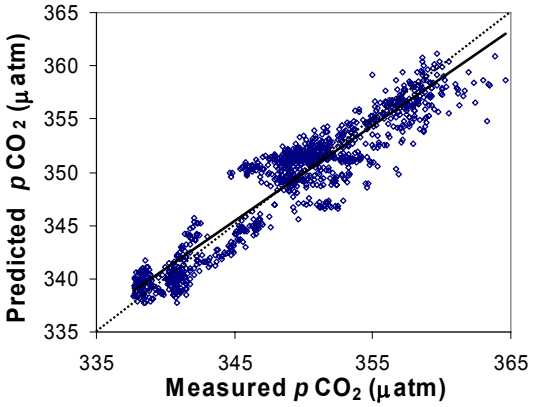

B. First half (y=0.8424*x + 54.974, n = 555, r^2 = 0.842, RMSE = 2.342, p < 0.0001)

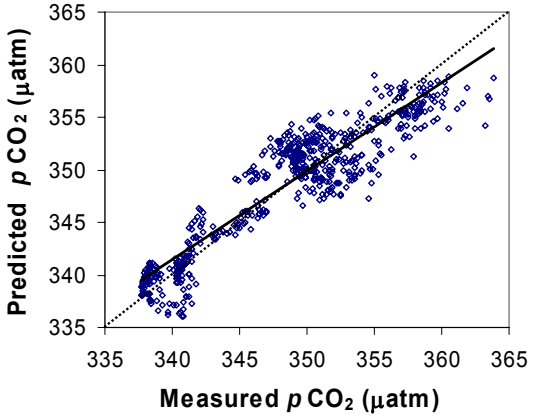

C. Second half (y=0.8424*x +55.018, n = 555, r^2 = 0.842, RMSE = 2.326, p < 0.0001)

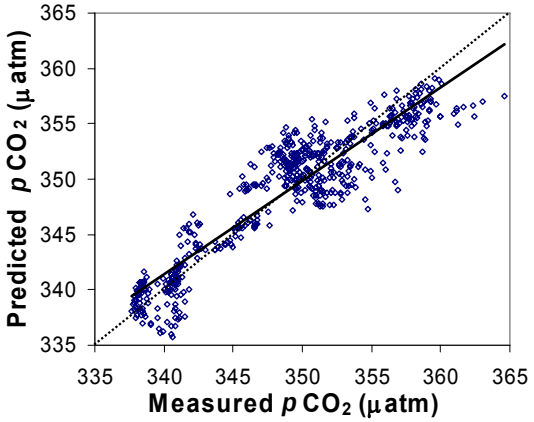

Fig. 3.5 Panel A shows all the observed versus predicted pCO_2 from outside the eddy based on principle component analysis (PCA) from in situ T, S, fluorescence, and wind speed. Panel B shows the first half data set in panel A used to derive the component loads and regression coefficients. Panel C shows the comparison when the results were applied to the second half of the data in panel A. Dotted line is 1:1 relationship.

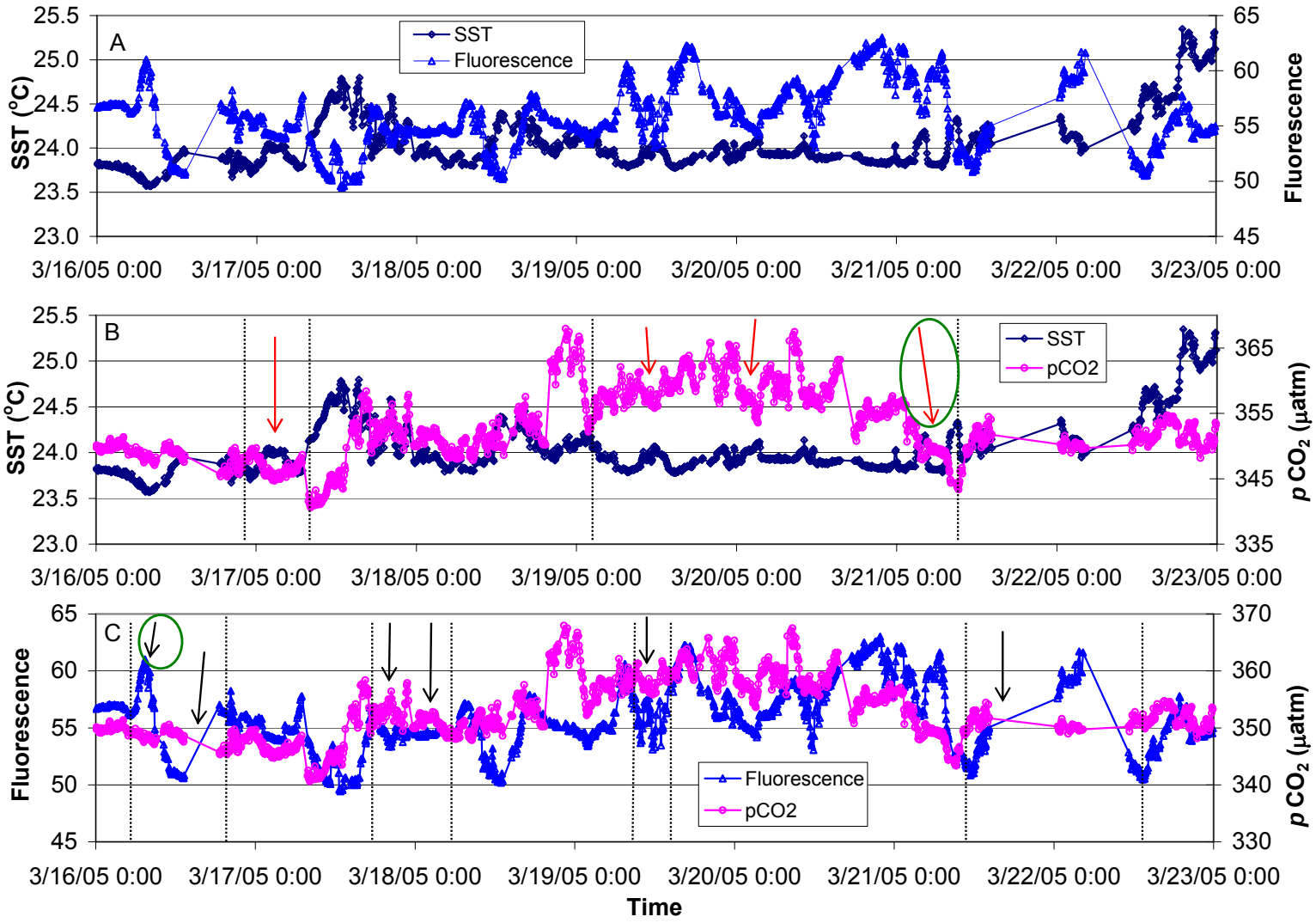

Fig. 3.6 Time-series underway data at IN-stations (center of the eddy) in E-Flux III. The figures provided time series pCO_2, SST, fluorescence and salinity data from March 16 to March 21, 2005, during which we stayed within the eddy center at IN-stations (IN1-IN6) (one day for one station). (A): SST vs. Fluorescence; (B): SST vs. pCO_2; and (C) Fluorescence vs. pCO_2.

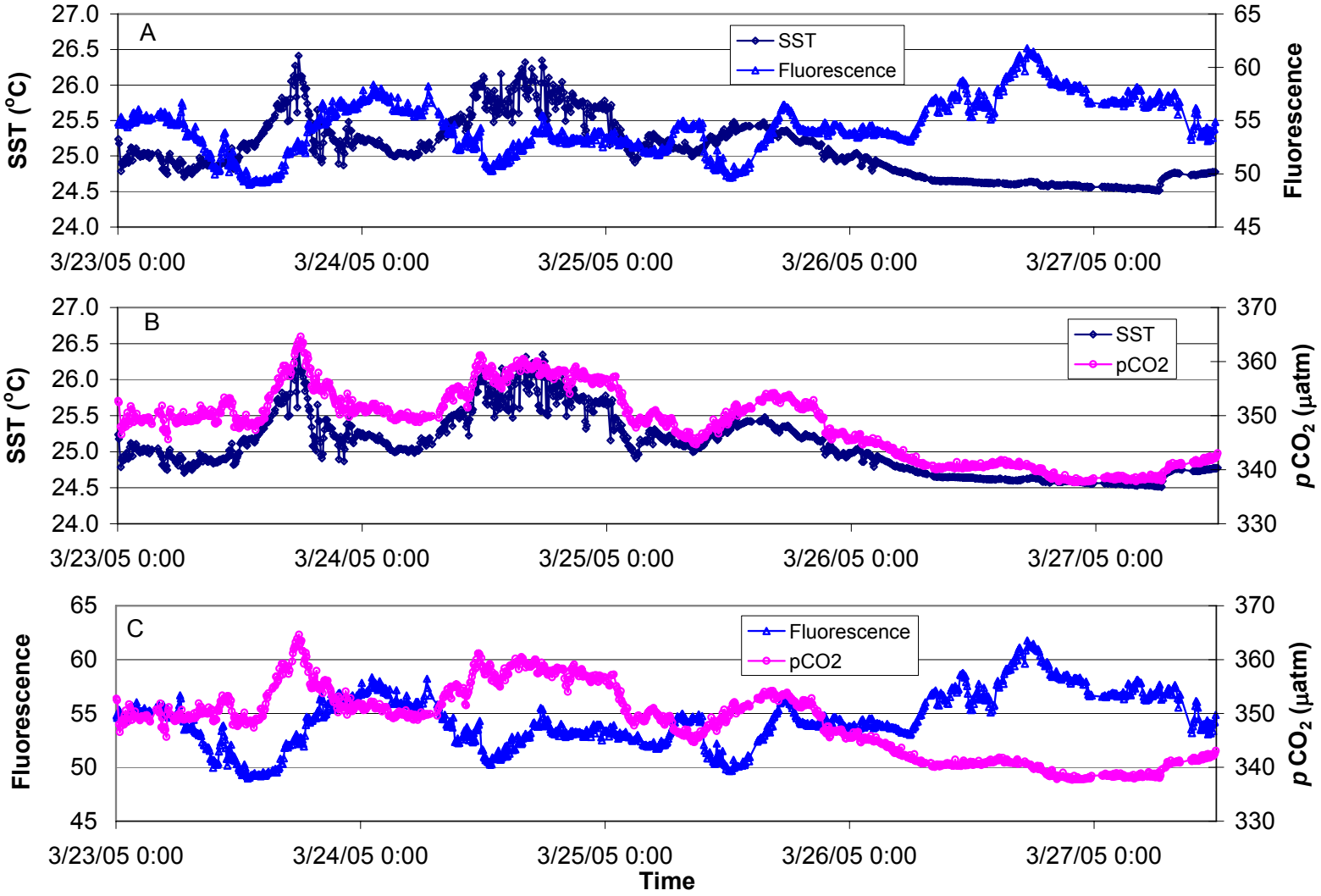

Fig. 3.7 Time-series underway data at OUT-stations (outside the eddy) in E-Flux III. The figures provided time series pCO_2, SST, fluorescence and salinity data from March 23 to March 27, 2005, during which we stayed outside the eddy at OUT-stations. (A): SST vs. Fluorescence; (B): SST vs. pCO_2; and (C) Fluorescence vs. pCO_2.

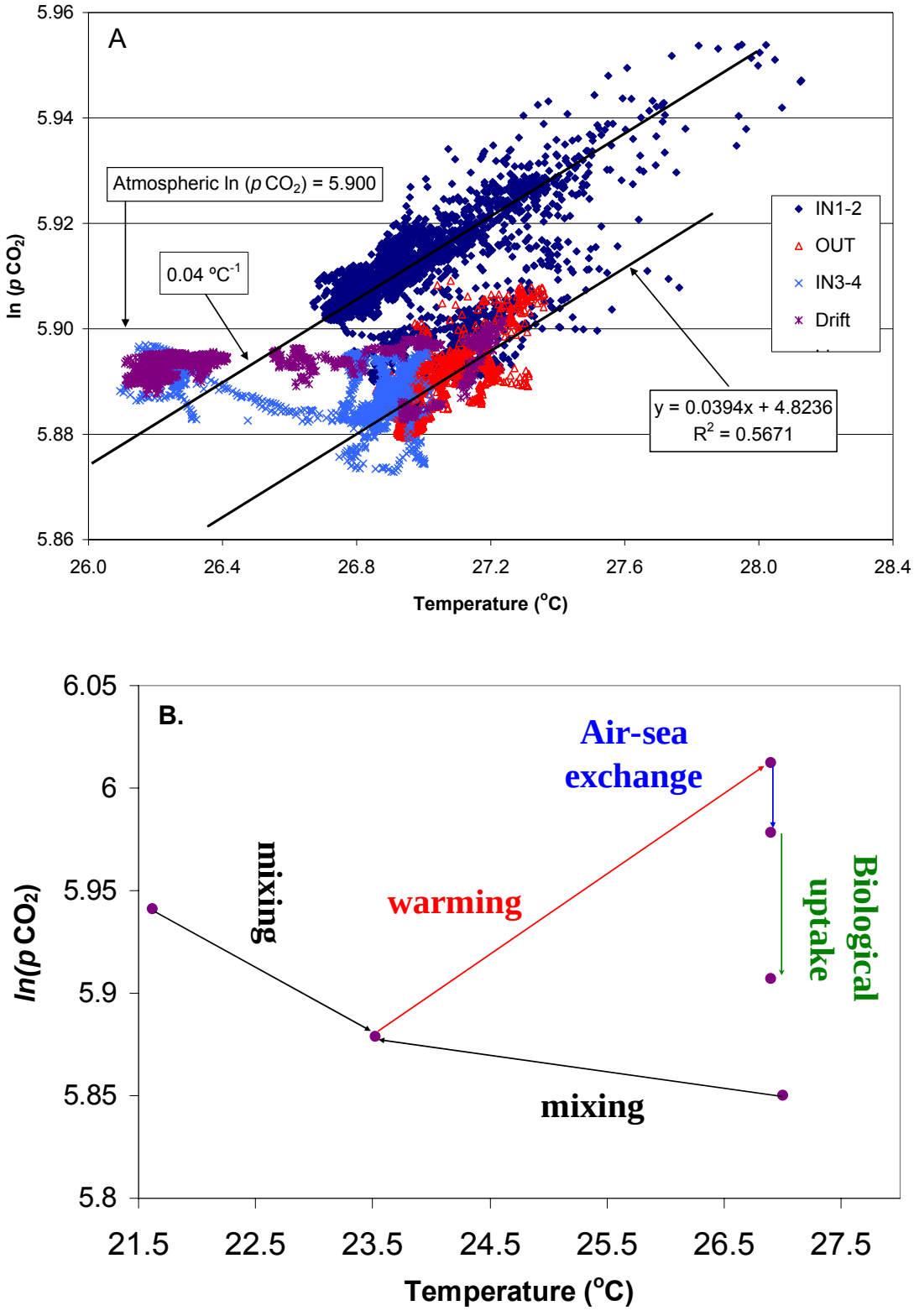

Fig. 3.8 Sea surface pCO_2 and SST relationships. (A) Relationship between sea surface pCO_2 (natural logarithms) and SST in E-Flux I; (B) Sea surface pCO_2 of different water masses: diagram of different processes affecting pCO_2 (Please note that air ln (pCO_2) = 5.900).

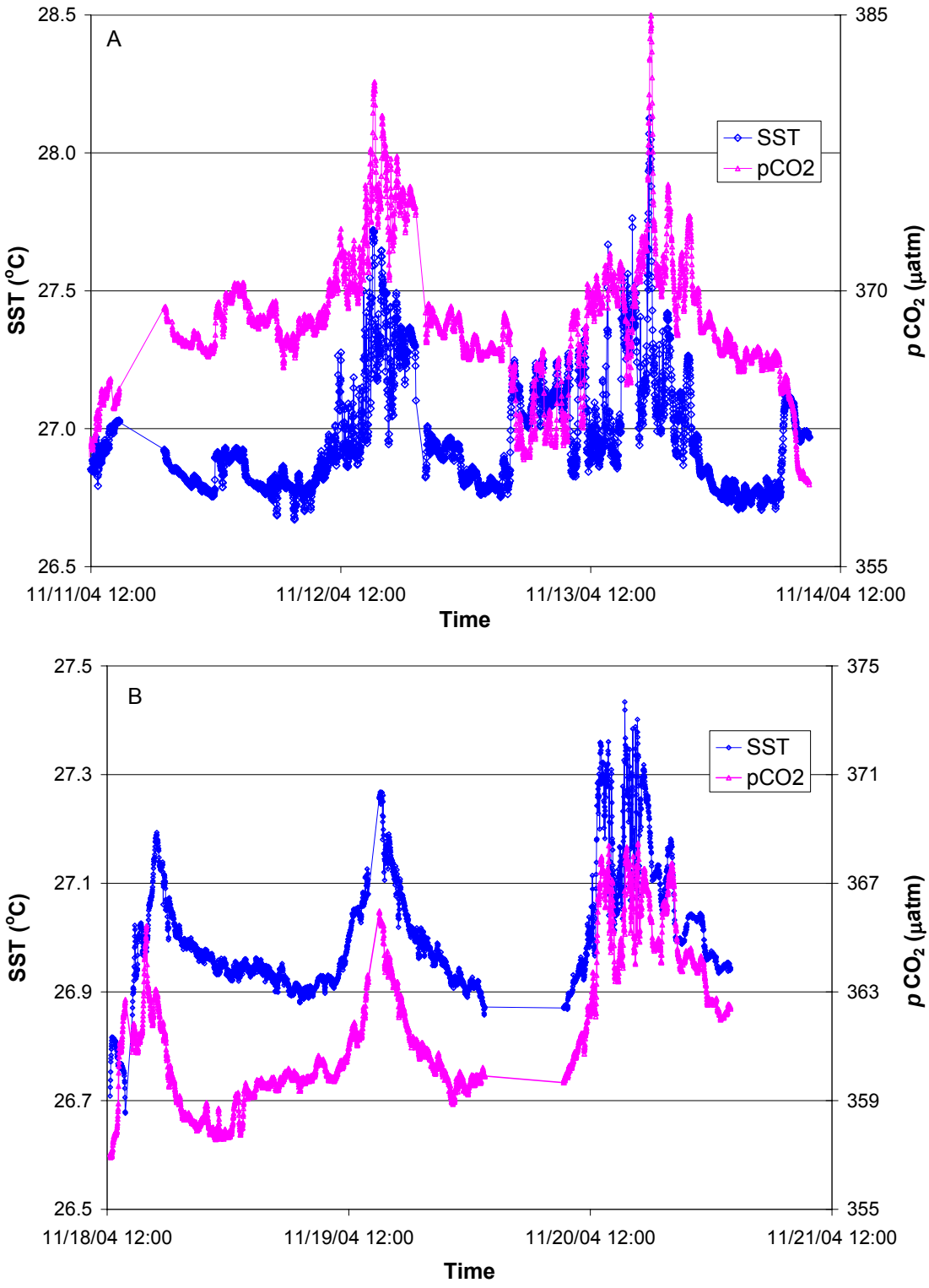

Fig. 3.9 Time-series underway pCO_2 and SST data during E-Flux I (A) IN-stations; (B) OUT-stations.

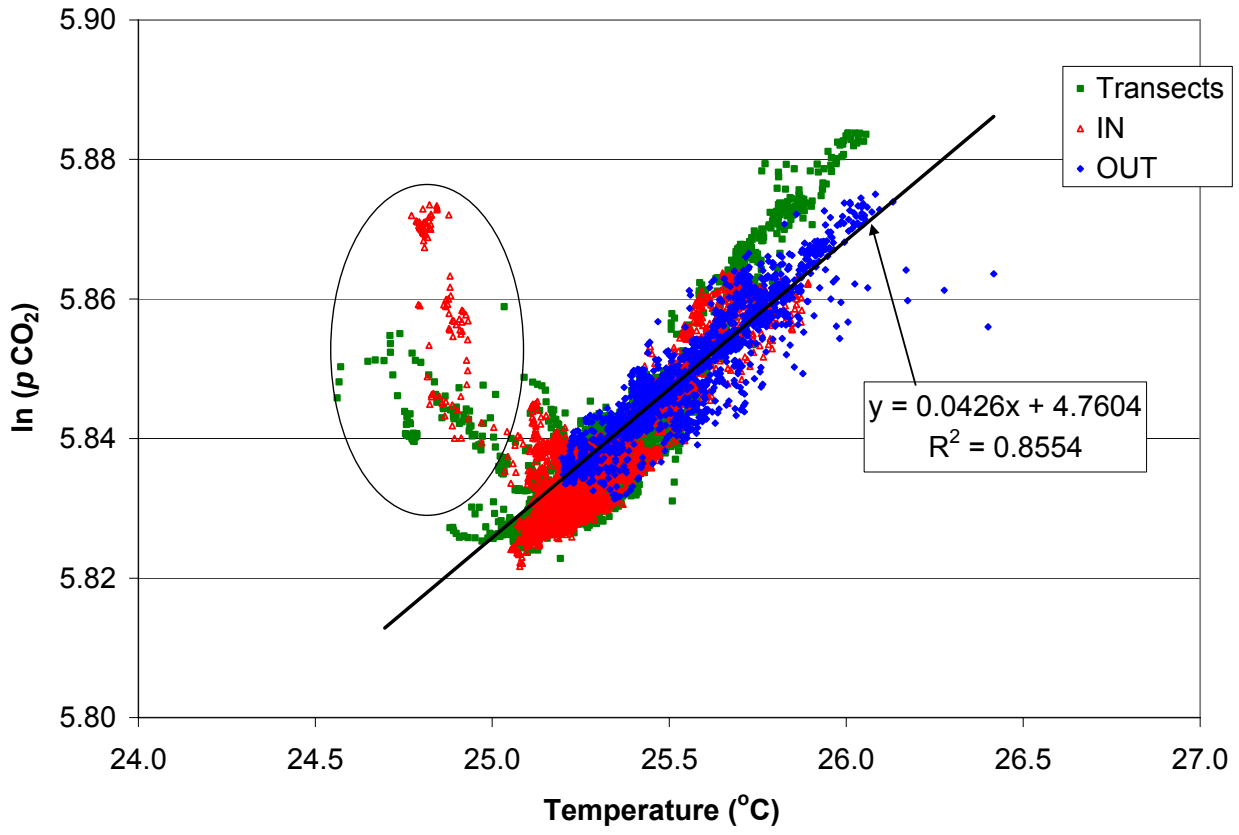

Fig. 3.10 Relationships between sea surface pCO_2 (natural logarithms) and SST during E-Flux II. Please note that for atmosphere, ln (pCO_2) = 5.907.

CHAPTER 4 THE CARBON DIOXIDE SYSTEM AND NET COMMUNITY PRODUCTION DURING MESOSCALE CYCLONIC EDDIES[2]

[2] Part of this chapter (from Section 4.1, 4.2 and 4.3) will be published soon (Chen, F., W.-J. Cai, Y. Wang, Y. M. Rii, R. R. Bidigare, C. R. Benitez-Nelson (2008), which is accepted by *Deep-Sea Research II*).

Introduction

On the basis of a long-term time series data, seasonal and long-term dynamics of the upper ocean carbon cycle was reported at the time-series station ALOHA near Hawaii, an oligotrophic subtropical ocean site (Winn et al., 1998; Keeling et al., 2004). While the long-term distinct upward trends of salinity-normalized DIC (*n*DIC) and computed oceanic pCO_2 are mainly attributed to the oceanic uptake of atmospheric CO_2, net community production (NCP) of organic carbon from a mixed layer inorganic carbon diagnostic model was inferred to be the dominant process generating the observed seasonal variability in *n*DIC (Keeling et al., 2004). This is consistent with the results from Quay and Stutsman (2003) where the DIC drawdown and simultaneous increase of $^{13}C/^{12}C$ ratio of the DIC during the warm period are primarily the result of NCP exceeding physical processes. However, as the maximum timescale resolution in their work is about 4 months, their data are insufficient to consider and may underestimate the influence of eddies, storms, and other episodic events on nutrient supply and inorganic carbon cycle in the subtropical gyre.

Within the oligotrophic subtropical ocean, basin wide geochemical estimates of NP are substantially higher than that can be explained by direct biological and physical estimates of PP and nutrient supply (Shulenberger and Reid, 1981; Jenkins and Goldman, 1985). As such, nitrogen fixation by cyanobacteria and episodic nutrient injections by mesoscale eddies and submesoscale processes, events easily missed by traditional sampling methods, have been invoked to explain the discrepancy (Falkowski et al., 1991; Capone et al., 1997; McGillicuddy and Robinson, 1997; McGillicuddy et al., 1998; Siegel et al., 1999).

Eddies are ubiquitous features throughout the oceans, with observations ranging from the Gulf of Alaska (Crawford and Whitney, 1999) to the Arabian Sea (Dickey et al., 1998; Honjo et

al., 1999; Fischer et al., 2002). Although few in number, studies of eddy biogeochemistry have shown that eddy induced local upwelling of new nutrients (e.g., nitrogen) into the euphotic zone, increases PP and NCP, influences plankton community structure, and enhances particle export to the mesopelagic (Falkowski et al., 1991; Olaizola et al., 1993; Allen et al., 1996; Anderson et al., 1996; McGillicuddy et al., 1998; Siegel et al., 1999; Seki et al., 2001; Bidigare et al., 2003; McGillicuddy et al., 2003; Vaillancourt et al., 2003; Benitez-Nelson et al., 2007; McGillicuddy et al., 2007). Yet, the global biogeochemical significance of eddies remains enigmatic and controversial (e.g., Oschlies and Garcon, 1998; McGillicuddy et al., 1998; Oschlies, 2002). Current estimates suggest that 10 to 50% of global PP is due to eddy-induced nutrient fluxes (Falkowski et al., 1991; McGillicuddy et al., 1998; Oschlies and Garcon, 1998; Siegel et al., 1999; Letelier et al., 2000). This wide range reflects a paucity of direct observations of the biological and biogeochemical impacts of eddies, along with difficulties in placing the existing observations into a broader context (Haury, 1984; McNeil et al., 1999; Savidge and Williams, 2001; Bidigare et al., 2003).

The overall effect of episodic eddies on inorganic carbon cycling also remains vague. Williams and Follows (1998) argued that the eddy-pumping mechanism, i.e., eddy mediated upwelling of nutrient-replete deep water into otherwise oligotrophic surface waters (Falkowski et al., 1991; McGillicuddy et al., 1998; Oschlies, 2002), does not necessarily lead to a corresponding decrease in dissolved inorganic carbon (DIC). Rather, they suggested that increased DIC consumption due to photosynthesis is balanced or even surpassed by the upwelling of DIC-rich waters from below. The biogeochemical evolution of the carbon dioxide system was examined in long-lived anticyclonic Haida eddies in the subpolar gyre of the North Pacific Ocean (Chierici et al., 2005). Dramatic seasonal changes in DIC and nutrients inside

Haida eddies (with DIC losses during spring and gains during fall) highlight the importance of sporadic events and their complicated influence on the regional oceanic inorganic carbon biogeochemistry, although Haida eddies occur in the subpolar gyre and are physically different from subtropical mesoscale eddies (e.g., formation mechanism and maintenance, scale and duration).

While mesoscale eddies do not necessarily decrease DIC, eddy-pumping events deliver nutrient-replete deep water from light-limited zone to the well-lit zone for otherwise oligotrophic surface waters and this nutrient perturbation and upward displacement of isopycnal surfaces will expect to trigger the growth of nutrient-limited phytoplankton or/and lighted-limited phytoplankton. Thus, enhanced NCP is desired over shorter timescales (Hawaiian lee eddies had spin-up periods averaging 5-20 days and lifetimes lasting 2-12 months (Patzert, 1969; Lumpkin, 1998)).

Although mesoscale eddies are rather ubiquitous in the ocean, they are still difficult to study since their ephemeral feature and they evolve too quickly in diverse geographical locations to be easily sampled (e.g., Bidigare et al., 2003; Dickey et al., 2008). In the lee of main Hawaiian Islands, island topography and prevailing northeasterly trade winds combine to generate mesoscale eddies throughout the year in the ‘Alenuihaha Channel between the islands of Maui and Hawaii. This area thus serves as an ideal natural laboratory providing excellent opportunities for examining eddy biogeochemistry at various stages of eddy development and decay (Falkowski et al., 1991; Seki et al., 2001; Bidigare et al., 2003; Vaillancourt et al., 2003). In this study, we examined NCP and inorganic carbon biogeochemistry in two first baroclinic mode cyclonic eddies, subsequently named Cyclone Noah and Opal, during three consecutive cruises of the E-`Flux Program (E-Flux I, II and III).

Section 4.1 Inorganic carbon dynamics in the lee of main Hawaiian Islands

Observation of Cyclone Opal

Hydrology and carbonate chemistry across Cyclone Opal

Vertical sections of Cyclone Opal from Transect 3 were characterized by intense uplift of isothermal, isohaline, and isopycnal surfaces in the upper 250 m across the 40 km eddy core (Figs. 4.1A-C) (Nencioli et al., 2008; Dickey et al., 2008). Differential anomalies of temperature and density were confined between 40 and 160 m depth (Nencioli et al., 2008). In contrast, salinity had a subsurface maximum within the eddy core characterized by a positive salinity differential anomaly (~0.2 psu) above a region of high negative salinity differential anomaly (about -0.4 psu) (Fig. 4.1B) (Nencioli et al., 2008).

Vertical sections of carbonate parameters (Figs. 4.1E, 4.1G, and 4.1H) and N+N (Fig. 4.1D) all showed substantial vertical displacements across the eddy center. For example, DIC concentrations of 1990 μmol kg^{-1} shoal from 130-160 m at the eddy edge to 40-60 m at the eddy center, following the σ_t = 24 kg m^{-3} isopycnal surface (Fig. 4.1C and Nencioli et al. (2008)). Hydrographic data (Figs. 4.1A-C), DIC (Fig. 4.1G), and calculated pCO_2 (Fig. 4.1H) all suggest an intrusion of cold, salty, DIC-rich deep water into the upper water that outcropped at the surface at the eddy center. In contrast, although isopleth uplift also occurred at the eddy center, no significant increase in N+N or decrease in pH in the upper 50 m was observed (Figs. 4.1D-E). The same conclusion can be derived from corresponding depth profiles of the above properties (Fig. 4.2).

The lack of a substantial concentration increase in N+N (or positive N+N anomalies) in the upper 50 m at the eddy core is likely due to the enhanced biological consumption there (see next Section). This enhanced biological production also serves to increase pH, thus, partially ameliorating the influence of uplifted low pH deep water. Finally, TAlk vertical section shows little variation in the upper 200 m as may be expected (Fig. 4.1F). Variation is within the uncertainties of the measurement, and therefore, hindered further discussion.

IN versus OUT-stations

In order to understand the biogeochemistry of Cyclone Opal, it is first necessary to describe typical water mass distributions in the North Pacific subtropical gyre. The temperature-salinity (T-S) relationships observed throughout the study are typical for the subtropical waters surrounding Hawaii, and are similar to Station ALOHA, site of the Hawaii Ocean time-series program (HOT), located 100 km due north of Oahu (Figs. 2.1, 2.6A, and 4.3A) (Sabine et al., 1995; Li et al., 2000). The water column is comprised of Subtropical Surface Water, Subtropical Salinity Maximum Water (150±30 m), and Shallow Salinity Minimum Water (320±30 m) (Wyrtki and Kilonsky, 1984; Sabine et al., 1995; Li et al., 2000). IN- and OUT-stations in E-Flux II and E-Flux III have similar T-S relationships in the upper water column (Fig. 4.3A). Depth profiles of T and S reveal how Subtropical Salinity Maximum Water was uplifted from ~150 m at OUT-stations to ~60-90 m at IN-stations at the eddy center (Fig. 4.2A-B). Mixed layer depths averaged 51±8 m at IN-stations and 95±7 m at OUT-stations, respectively. Here, we define the mixed layer depth (MLD) as the depth at which seawater temperature is 1ºC less than the temperature at 10 m, following the convention established by Benitez-Nelson et al. (2007) and Nencioli et al. (2008).

Surface water at the center of Cyclone Opal is 0.160 to 0.171 psu saltier and 1.076 to 1.817°C colder than the surrounding ocean depending on the depth of integration (Table 4.1A and Figs. 4.2A-B). Here, the concept of 'surface water' generally refers to water mass in the mixed layer, i.e., 0-50 m at the eddy center and 0-95 m in ambient waters outside the eddy. However, for the purpose of this study, in addition to the MLD, we also define two other depth horizons at the eddy center: 0-75 m (the depth of the DCML) and 0-110 m (just below the 0.1% light level). Cooler and saltier surface waters at IN-stations suggest that they have been influenced by the intrusion and mixing of deeper Subtropical Salinity Maximum Water from below (Figs. 4.2B and 4.3A, Table 4.1A). Below the salinity maximum, the linear decrease in salinity reflects the mixing between the Subtropical Salinity Maximum Water and the Shallow Salinity Minimum Water (Sabine et al., 1995).

The uplift of isopycnal surfaces at the core of Cyclone Opal results in a corollary response in hydrography and biogeochemistry relative to surrounding waters (Figs. 4.2C-F), a conclusion further supported by the close relationship between N+N concentration and density at both IN- and OUT-stations (e.g., Fig. 4.3C). These uplifted deeper waters are generally rich in nutrients and DIC, but poor in total and dissolved organic matter (Figs. 4.2C-F) (Benitez-Nelson et al., 2007). Mixed layer DIC at IN-stations averaged 1983.8±3.2 μmol kg^{-1} and *n*DIC 1986.3±3.3 μmol kg^{-1} (see Table 4.6, μM/(1.1241 kg dm^{-3} (density)) = μmol kg^{-1}). Surface water DIC at the eddy center is therefore ~27 μmol kg^{-1} higher than surrounding waters at OUT-stations (averaged 1956.8±4.4 μmol kg^{-1} over 0-75 m depth). Please note that the mixed layer at OUT-stations is much deeper (95±7 m), salinity, temperature, and DIC over 0-75 m depth is uniform and the average values over 0-75 m depth in Table 3 is used as surface water properties at OUT-stations. This difference is comparable to the seasonal variability (±15 μmol kg^{-1}) at

Station ALOHA (Keeling et al., 2004). In contrast, TOC is much lower than that at OUT-stations at every depth horizon. There is no obvious difference in DON between IN- and OUT-stations, mainly due to substantially lower DON concentration and larger relative uncertainties.

Unlike TOC and DIC, N+N concentrations within the MLD at IN-stations (Fig. 4.2D) are the same, within error, as that observed at OUT-stations and are also similar to that found from Transect 3 (see results in previous session). The lack of substantial concentration increase (or positive N+N anomalies, Nencioli et al. (2008)) in the mixed layer could be a result of rapid biological consumption immediately after the initial eddy-pumping event (Rii et al., 2008). This is further evident by the much shallower layer of available N+N and sharper nutricline at IN-stations (Fig. 4.2D and 4.3B). This conclusion is also supported by enhanced growth and production rates of the *Prochlorococcus* spp.-dominated ambient community at IN-stations, although there is little compositional or biomass response in the mixed layer (Landry et al., 2008). It is true that the eddy is not necessary to bring new nutrients into the mixed layer. However, we judge the uplift of the deep salinity maximum water with its nutrient into the mixed layer by the salinity structure and composition, not the nutrient level. Please notice that the average salinity over 0-50 m at IN-stations is 35.044±0.013, which is even higher than the average salinity at 100 m depth at OUT-stations (Fig. 4.2B, Table 4.1). It seemed likely for the intrusion of deep nutrient-rich water into the mixed layer at the beginning of Cyclone Opal.

Observation of Cyclone Noah

Hydrology and carbonate chemistry across Cyclone Noah

Vertical sections of Cyclone Noah from Transects 2-4 were characterized by moderate uplift (~50 m) of isothermal, isohaline, and isopycnal surfaces in the upper 250 m across the

semi-elliptical eddy core (Figs. 4.4A-C, Fig. 4.5A-C, and Figs. 4.6A-C) (Kuwahara et al, 2008; Dickey et al., 2008). Please note that Transect 1 is not close enough to across the eddy center and is not discussed here. Differential anomalies of temperature and density occurred between 45 and 150 m depth in the center of Cyclone Noah (Kuwahara et al., 2008). In contrast, salinity shows a positive salinity differential anomaly (> 0.15 psu) between surface and ~100 m depth above a region of negative salinity differential anomaly (~ 0.05-0.01 psu) (Figs. 4.4B, 4.5B, and 4.6B) (Kuwahara et al., 2008). Thus, although the isopycnal uplift for Cyclone Noah is less significant than Opal due to its decay phase, the vertical structure of hydrographic differential anomalies is essentially similar to each other.

Vertical sections of carbonate parameters all show moderate vertical displacements across the eddy center (Figs. 4.4-4.6). For example, DIC concentrations of 1990 μmol kg^{-1} shoal from 110-130 m at the eddy edge to 50-80 m at the eddy center (Figs. 4.4F, 4.5G, and 4.6F). Thus, hydrographic data, DIC, and calculated pCO_2 (Fig. 4.5H) all suggest an intrusion of cold, salty, and DIC-rich deep water into the upper euphotic zone. Furthermore, the distance to which DIC doming flattened horizontally for Transects 2 and 3 is much longer than that for Transect 4, which is also consistent with the semi-elliptical shape from hydrographical data (Figs. 4.4F, 4.5G, and 4.6F).

However, temperature varies much less in the mixed layer (the upper 0-30 m) across the Transects 2-4 (Figs. 4.4A, 4.5A, and 4.6A), although we can observe significant outcrops of higher salinity water from below at the surface of the eddy center (Figs. 4.4B, 4.5B, and 4.6B). This is consistent with our results in Chapter 3 that there was essentially no SST difference between the eddy core and outside-eddy area, instead the minor variation should be due to diurnal fluctuation (Fig. 3.9A-B). The same conclusion can be derived from corresponding depth

profiles of the above properties (Fig. 4.7). This clearly indicates the much longer time for surface warming due to heat balance and therefore further confirms the view that Cyclone Noah was indeed in a decay phase during sampling period.

For Cyclone Opal, we contribute the lack of increase in N+N in the upper 50 m (i.e., the mixed layer) at the eddy center to the enhanced biological consumption. This same reason and much older age of Cyclone Noah should ensure the complete consumption and cause the observed lack of increase in N+N in almost whole euphotic zone across Cyclone Noah (Fig. 4.5D; also see discussion in the next session). The same reason as Cyclone Opal, enhanced biological production also serves to increase pH and partially cancel the influence of uplifted low pH deep water (Figs. 4.4D, 4.5E, and 4.6D). Finally, TAlk vertical section shows little variation relative to its precision of measurement in the upper 200 m, and therefore, no further discussion is presented (Figs. 4.4E, 4.5F, and 4.6E).

IN versus OUT-stations

Similar to Cyclone Opal, to understand the biogeochemistry of Cyclone Noah, it is first necessary to examine the T-S relationships at both IN- and OUT-stations. The structure of T-S diagram during E-Flux I (Fig. 4.8A) is consistent with that during E-Flux II and III and similar to Station ALOHA as mentioned in the case of Cyclone Opal. The water column is comprised of Subtropical Surface Water, Subtropical Salinity Maximum Water (150±30 m), and Shallow Salinity Minimum Water (320±30 m) (Wyrtki and Kilonsky, 1984; Sabine et al., 1995; Li et al., 2000). At IN-stations, the Subtropical Salinity Maximum Water was uplifted from ~150 m at OUT-station to ~100 m at IN-stations at the eddy center (Figs. 4.7A-B), consistent with the maximal positive differential salinity anomaly and negative differential temperature anomaly at ~ 100 m observed by Kuwahara et al. (2008). Mixed layer depths are 30-50 m at IN-stations and

89±6 m at OUT-stations, respectively (Kuwahara et al., 2008; Rii et al., 2008; also see Fig. 4.7A).

Despite the similar T-S relationships between Cyclone Opal and Noah, the T-S diagram at IN-stations for Cyclone Noah deviated significantly from that at OUT-stations (Fig. 4.8A). Surface water at the center of Cyclone Noah is about 0.182-0.208 to 0.178-0.211 psu saltier in salinity than the ambient waters outside the eddy over the mixed layer depth and the integrated euphotic zone (0-110 m), respectively (Table 4.3 and Figs. 4.7B). However, the difference in temperature over the mixed layer was 0.051-0.218°C, although the difference over the euphotic zone was much larger, 1.260-1.944°C (Table 4.3 and Figs. 4.7A). Saltier surface waters at IN-stations suggest that they have been influenced by the intrusion and dominated by the deeper Subtropical Salinity Maximum Water upwelled from below (Figs. 4.7B and 4.8A, Table 4.3). Meanwhile, the significant surface water warming at the Cyclone Noah center after the original mixing is confirmed by the fact that the mixed layer temperature at IN-stations is almost the same as that at OUT-stations as we mentioned from the T-S diagram (Figs. 4.7A and 4.8A, Table 4.3A). Surface water warming suggests that this water mass has been isolated long enough to absorb significant shortwave radiation. This pattern is consistent with the disappearance of the eddy feature from SST remote sensing imagery (Fig. 2.3). If Cyclone Noah were still actively upwelling, we would expect to observe much cooler SST in addition to the observed higher salinity surface water at IN-stations.

Similar to Cyclone Opal, the uplift of isopycnal surfaces at the center of Cyclone Noah resulted in the response in hydrography and biogeochemistry relative to surrounding waters (Fig. 4.7). This is further supported by the close relationship between concentration and density isopycnals at both IN- and OUT-stations (e.g., Fig. 4.8C). For Cyclone Noah, mixed layer DIC at

IN-stations arranged from 1969.7-1983.1 μmol kg^{-1} and *n*DIC from 1969.8 to 1981.7 μmol kg^{-1}, respectively (see Table 4.9A, μM/(1.1241 kg dm^{-3} (density)) = μmol kg^{-1}). Surface water DIC at the eddy center is therefore ~14.6-29.9 μmol kg^{-1} higher than surrounding waters at OUT-stations (see Table 4.4, averaged 1955.1±5.5 μmol kg^{-1} over 0-75 m depth). The observed difference in DIC values at IN-stations of Cyclone Noah was comparable to the difference between IN- and OUT-stations of Cyclone Opal (average ~27 μmol kg^{-1}) and seasonal variability (±15 μmol kg^{-1}) at Station ALOHA (Keeling et al., 2004). Please note that the mixed layer at OUT-stations is much deeper (89±6 m). Salinity, temperature, and DIC over 0-75 m depth is relatively uniform and the average values over 0-75 m depth in Table 4.4 is used as surface water properties at OUT-stations.

With regard to nutrients, N+N at IN-stations of Cyclone Noah was depleted in most of the euphotic zone (Fig. 4.7D), while it was only depleted in the mixed layer for Cyclone Opal (Fig. 4.2D). Moderate enhancement in N+N concentration at IN-stations of Cyclone Noah can only be observed at the base of the euphotic zone (Fig. 4.7D). As we mentioned in previous Session, the lack of increase in N+N should be due to the almost complete biological consumption of the extra nutrients that uplifted into the euphotic zone during the initial eddy formation. Please note that initial nutrients injection due to eddy-caused isopycnal uplift is also evident by the much sharper nutricline at IN-stations (Figs. 4.8B). Thus, the significant surface-water warming and almost complete biological consumption on N+N in the entire euphotic zone both confirm the decay phase of Cyclone Noah during the sampling time as proposed by Kuwahara et al. (2008).

Such a decay phase is also supported by biological observation. For example, only ~20-m upward displacement of DCML was observed within the eddy core of Cyclone Noah which is

much lower than that for Cyclone Opal (~50 m upward displacement) (Rii et al., 2008). It is also reported that within the mixed layer, there is only a modest increase (~1.3-fold) in total chlorophyll a concentration and cyanobacteria still dominated at the center of Cyclone Noah, although there is a modest shift in phytoplankton community to larger size structure (nanoplankton 2-18 μm and microplankton > 18 μm) (Rii et al., 2008). Meanwhile, small eukaryotes and *Prochlorococcus spp.* occupied the DCM (Rii et al., 2008). This may indicate phytoplankton bloom have already decayed significantly by the time of sampling due to the depletion of extra nutrients pumped into the euphotic zone during the initial eddy formation.

Comparison of OUT-stations in the lee of Hawaii to Station ALOHA

Three consecutive cruises from November 2004 to March 2005 enabled us to study temporal change of DIC and other hydrographic properties at OUT-stations in the lee of Hawaii from late fall through winter seasons. From November 2004 to March 2005, surface water (0-75 m) temperature at OUT-stations decreased from 26.823±0.126ºC (E-Flux I, data not shown) to 24.627±0.016ºC (E-Flux III) (Tables 4.1 and 4.3; Fig. 4.9A). This trend is consistent with the seasonal varying level of the 14-year mean time-series data in temperature (from ~26ºC in November to ~23ºC in March) at Station ALOHA (Keeling et al., 2004). Since the lower latitude of OUT-stations, it is reasonable to observe the higher temperature at OUT-stations than that at Station ALOHA. Nonetheless, temperature profile shows that MLD was stable throughout the winter season (Fig. 4.9A). During the same period, surface water (0-75 m) salinity at OUT-stations during E-Flux I, E-Flux II, and E-Flux III was 34.826±0.013, 34.875±0.024, and 34.900±0.041, respectively (Table 4.4; Fig. 4.9B). Assuming a typical net evaporation rate of ~ 435 mm yr^{-1} between 20ºN and 30ºN in the ocean (Peixoto and Oort, 1992) and an average mixed layer depth of 90 m at OUT-stations, the net influence of evaporation would result in an

increase of ~0.06 in salinity within the upper 90 m over a 4 month period. This is consistent with the observed increase in salinity above. Lower salinities in the lee of Hawaii relative to the 14-year mean salinity at Station ALOHA, 35.038 (Keeling et al., 2004), suggest a greater intrusion of tropical surface water with lower salinity.

Average DIC and *n*DIC (salinity 35 normalized DIC) during three consecutive cruises (from November 2004 to March 2005) arranged 1952.0±5.7-1956.8±4.4 and 1959.0±5.7-1964.9±5.5 μmol kg^{-1}, respectively (Table 4.4). Consistent DIC and *n*DIC values and lack of nutrients (e.g., N+N in Fig. 4.9D) also confirm the stable characteristics of surface waters in the lee of main Hawaiian Islands during winter months with the absence of cyclonic eddies. At Station ALOHA, average *n*DIC during the same period is ~1975-1984 μmol kg^{-1} using DIC values measured in 2002 (from Keeling et al., 2004) and considering seasonal and long-term changes (DIC reached its peak in April and *n*DIC increased on average by 1.22±0.08 μmol kg^{-1} yr^{-1}, Keeling et al. (2004)). The *n*DIC at our OUT-stations is ~15-20 μmol kg^{-1} lower than that at Station ALOHA. The influence of lower DIC surface water from the South on Station ALOHA was mentioned by several studies during their horizontal advection flux estimation (Winn et al., 1994; Quay and Stutsman, 2003; Keeling et al., 2004), which is consistent with our results. A more thoroughly study on the seasonal and annual variation in DIC and other biogeochemical and hydrographical properties requires further field sampling and analysis.

Section 4.2 Description of mass balance models for NCP estimation

The hydrological characteristics and physical processes at OUT- and IN-stations are very different. OUT-stations are dominated by mixing across a stable pycnocline, whereas IN-stations are influenced by the doming of isopycnal surfaces across the eddy feature. Thus, different mass balance models are required for estimating NCP.

Mixed layer model for NCP estimation at OUT-stations

The mass balance approach used in the mixed layer outside the eddy is a classical approach in the subtropical open ocean. The mixed layer DIC budget typically incorporates the following processes: (1) air-sea gas exchange, (2) vertical diffusion from below, (3) entrainment of DIC from the thermocline during mixed layer deepening, (4) horizontal transport, and (5) net community production (Gruber et al., 1998; Lee, 2001; Quay and Stutsman, 2003; Keeling et al., 2004). Here, we apply this model to OUT-stations using the following general equation and solving for NCP:

$$\frac{dDIC_{Inventory}}{dt} = F_{air-sea} + F_{Diff} + F_{Adv} + F_{Entrain} - NCP_{DIC} \qquad (4.1)$$

where NCP is net community production in the mixed layer, $dDIC_{Inventory}/dt$ is the change in DIC inventory in the mixed layer over time, and $F_{air\text{-}sea}$ is the air to sea CO_2 flux at the surface with the direction from air to sea, which averaged 2.9±1.8 mmol C m^{-2} day^{-1} outside Cyclone Opal during E-Flux III (Chen et al., 2007) and -0.53±0.30 mmol C m^{-2} day^{-1} outside Cyclone Noah during E-Flux I, respectively. F_{Diff} for DIC is the vertical diffusive flux of DIC from below and is estimated from the vertical diffusion coefficient (K_z) and vertical gradient of DIC versus depth below the mixed layer. F_{Adv} is the DIC flux from horizontal and vertical advection and is calculated from the horizontal or vertical velocity and the DIC gradient. Advection is assumed to

be zero for OUT-stations. The uncertainty introduced by this assumption is discussed in Section 4.3 for Cyclone Opal. $F_{entrain}$ is the entrainment flux of DIC from the thermocline whenever the mixed layer deepens and is also assumed to be zero since the MLD at OUT-stations during E-Flux I (November 4-20th, 2004), E-Flux II (January 10 – 28th, 2005), and E-Flux III (March 10 – 28th, 2005) was, within error, identical (Dickey et al., 2008). All flux units are in mmol C m^{-2} day^{-1}. Steady state ($dC_{inventory}/dt = 0$) is assumed since DIC as well as salinity, N+N, TOC, and DON during E-Flux study at OUT-stations showed little variability in the upper water column (Table 4.2) (see Section 4.3). Thus, this mixed layer model is only applied to the winter season.

Similar mass balance equations can be written to estimate NCP from N+N, TOC, and DON. For example, the mass balance for "new nitrogen" (N+N) is described by the following equation (note the absence of the air-sea gas exchange term):

$$NCP_{N+N} = (F_{Diff} + F_{Adv} - \frac{d(N+N)_{Inventory}}{dt}) * (C/N)_{OM} \qquad (4.2)$$

where $d(N+N)_{Inventory}/dt$ is the change of N+N over time in the mixed layer, the Redfield ratio of carbon (C) to nitrogen (N) in organic matter ($(C/N)_{OM}$) is ~ 6.6 (Redfield, 1958).

Please note that there are no TOC and DON data for E-Flux I cruise. Thus we only discuss E-Flux III for these two methods. For mass balance equation of TOC, an additional term, F_{Export}, must be added, which represents the particulate organic carbon (POC) flux exported out of a defined layer (averaged 1.25±0.51 mmol C m^{-2} day^{-1} at 150 m at OUT-stations in E-Flux III using sediment traps and ^{234}Th derived fluxes (Benitez-Nelson et al., 2007)):

$$NCP_{TOC} = \frac{dTOC_{Inventory}}{dt} + F_{Export} - F_{Diff} - F_{Adv} \qquad (4.3)$$

where $dTOC_{Inventory}/dt$ is the change of TOC over time in the mixed layer. For TOC, suspended and sinking particles are a minor component (≤ 5%), such that it is mainly comprised of

dissolved organic carbon (DOC) (Landry et al., 2008; Mahaffey et al., 2008). Thus, the diffusive flux (F_{Diff}) can still be estimated by K_z and a vertical gradient. The DON mass balance does not include a particle flux term since we only consider the dissolved phase:

$$NCP_{DON} = (\frac{dDON_{Inventory}}{dt} - F_{Diff} - F_{Adv}) * (C/N)_{DOM} \quad (4.4)$$

where $dDON_{Inventory}/dt$ is the change of DON over time in the mixed layer. Note that DON is converted to C units using a C:N ratio for dissolved organic matter (~ 13.6, $(C/N)_{DOM}$) (Benner et al., 1992).

The vertical diffusion coefficient, K_z, was determined according to equation from Denman and Gargett (1983):

$$K_z = 0.25 * \varepsilon_d * N^{-2} \quad (4.5)$$

where ε_d denotes the rate of turbulent energy dissipation and N is the Brunt Väisälä frequency, computed from the vertical density gradient below the mixed layer (Denman and Gargett, 1983). Turbulent energy dissipation may range between 10^{-9}-10^{-7} m^2 s^{-3}, here we use $2*10^{-8}$ m^2 s^{-3} as representative of the upper ocean thermocline at times of low wind speeds (Gruber et al., 1998; Quay and Stutsman, 2003). This value was applied by Gruber et al. (1998) for the seasonal inorganic carbon budget at the BATS site in the northwestern Sargasso Sea and was also used to determine K_z between 1994 – 1999 at Station ALOHA by Quay and Stutsman (2003). Using equation (4.5), we calculated the K_z of 0.3-0.5 (or 0.42 ± 0.05) cm^2 s^{-1} for the OUT stations during E-Flux III and 0.2-0.3 (or 0.26 ± 0.06) cm^2 s^{-1} for the OUT stations during E-Flux I, which is within the range of that determined at Station ALOHA, where K_z ranged from >1 cm^2 s^{-1} during the winter to a minimum of ~ 0.2 cm^2 s^{-1} in late summer (Quay and Stutsman, 2003). We should note that uncertainties in the K_z are typically ±100 % or greater (Quay and Stutsman, 2003).

Two end-member mixing model for eddy-induced NCP at IN-station

Due to the uplift of deep Subtropical Salinity Maximum Water at IN-stations (Fig. 4.2B and Fig. 4.7B), our assumptions of steady state and no vertical advection used in the mixed layer model for the OUT-stations (see previous Session) are likely invalid. As such, a mass balance approach based on a two end-member mixing model is used to determine the average NCP rate over the time period between Cyclone Opal's formation and sample collection. Due to sampling constraints, we have no direct measurement of nutrient and other biogeochemical parameters at the time of eddy formation. We would expect that by the time of sampling, a significant fraction of the nutrients and DIC upwelled into surface waters had already been consumed and organic matter accumulated due to biological activity. Thus, an estimate of the initial conditions following isopycnal uplift is necessary to determine the magnitude of biologically active components consumed or produced by the biological community.

We emphasize that it is not appropriate to make direct comparisons of chemical constituents between IN- and OUT-stations since OUT-stations do not represent the initial conditions at the eddy center, i.e., the chemical composition of the water immediately following uplift, but prior to the start of biological activity. The fact that cooler and saltier surface water at IN-stations is located near the T-S line between the two water masses, the Subtropical Surface Water and Subtropical Salinity Maximum Water (Fig. 4.3A), suggests that the surface water in the center of the eddy can be interpreted as a mixture of two end members. This assumption is further supported by the fact that a portion of Cyclone Opal, about 50 km in diameter and up to 70 m deep located at the eddy center, is isolated from the surrounding waters (well within the solid body rotation) (Nencioli et al., 2008). Such as a solid body rotation was also observed for

Cyclone Noah with a smaller diameter (no larger than 20 km) and up to ~75 m during E-Flux I (Kuwahara et al., 2008).

Use of a two end-member mixing strategy is not unique. The theory of two end-member mixing and its use in estuarine mixing is discussed in detail by Officer (1980) (Officer, 1980). Although specific physical mechanisms are not explicitly described during two end-member mixing, net results of open ocean vertical advection and mixing are quantitatively incorporated by using a salt budget. Li et al. (2000) applied this method to water column remineralization at Station ALOHA and similar models based on salt budget have been applied to a range of upwelling regimes, e.g., Costa Rica Dome in the Eastern Tropical Pacific Ocean, Peru current, NW Africa, and the SW Africa upwelling systems (Broenkow, 1965; Minas et al., 1986).

In applying the two end-member mixing model, we choose salinity as the conservative tracer. It should be noted that temperature is not strictly conservative in the upper ocean due to heat exchange and for example, there are changes in overall heat content between E-Flux II and E-Flux III OUT-stations that cannot be explained by air-sea interaction (Fig. 4.2A). During our cruises, SST at OUT-stations cooled by ~1.7ºC from mid November (E-Flux I) to late January (E-Flux II) and ~0.5ºC from late January to mid March (OUT-stations during E-Flux III) (Fig.4.2A and 4.9A, see Section 4.1). The concave upward shape of the T-S diagram in the upper water column, on the other hand, indicates warming of the eddy surface water for Cyclone Opal during E-Flux III (Fig. 4.3A). Surface warming at the center of Cyclone Noah was even more significant during E-Flux I (Fig. 4.8A). Salinity, however, remained relatively constant from January to March at OUT-stations (Fig. 4.2B). We thus assume that there is no change in salinity and DIC outside the eddy during study period. We will discuss the uncertainties introduced by this simplification in Section 4.3.

Here, it is assumed that the surface water within the core of Cyclone Opal (with salinity S_{IN}) is a mixture of the deep Subtropical Salinity Maximum Water (with salinity S_d) and the original surface water, i.e., surface water at OUT-stations (with salinity S_{OUT}). The fraction of each water type in the mixture is a direct function of salinity. Therefore a salt budget model can be formulated as:

$$S_{IN} = f * S_d + (1 - f) * S_{OUT} \tag{4.6}$$

with $$f = (S_{IN} - S_{OUT}) / (S_d - S_{OUT})$$

and $$1 - f = (S_d - S_{IN}) / (S_d - S_{OUT}) \tag{4.7}$$

where f is the fraction of deep salinity maximum water and (1-f) is the fraction of the original surface waters. To convert this fraction to volume, we use:

$$S_{IN} * V_T = V_d * S_d + V_s * S_{OUT} \tag{4.8}$$

where V_T is the total volume, $V_d = V_T * f$, the volume of deep water in the mixture, and $V_s = V_T * (1-f)$, the volume of surface water in the mixture (Fig. 4.10).

Thus, the expected DIC concentration ($DIC_{IN(exp)}$) in the center of the eddy due to two end-member mixing in the absence of biological process can be determined as:

$$DIC_{IN(\exp)} = (V_d * DIC_d + V_s * DIC_{OUT}) / V_T \tag{4.9}$$

or,

$$\begin{aligned} DIC_{IN(\exp)} &= f * DIC_d + (1 - f) * DIC_{OUT} \\ &= DIC_d * \frac{(S_{IN} - S_{OUT})}{(S_d - S_{OUT})} + DIC_{OUT} * \frac{(S_d - S_{IN})}{(S_d - S_{OUT})} \end{aligned} \tag{4.10}$$

where the subscripts of DIC_{OUT} and DIC_d describe the concentrations of DIC measured in OUT-station surface water with salinity S_{IN} and in deep salinity maximum water with salinity S_d, respectively (also see explanation to equation (4.7)). Similarly, the expected concentrations of

other desired biogeochemical parameters, such as N+N, TOC, and DON, in the IN-station surface waters can also be calculated as a function of salinity.

Let us now examine the meaning of $DIC_{IN(exp)}$ further. The change in DIC inventory in a surface layer can be represented by the following mass balance equation:

$$\frac{dDIC_{Inventory}}{dt} = \sum DIC_{Input} - \sum DIC_{Output} + F_{air-sea} - NCP_{DIC} \qquad (4.11)$$

where DIC_{input} and DIC_{output} are the total input rate and output rate of DIC, respectively. $F_{air\text{-}sea}$ is the average flux of CO_2 air-sea exchange at the eddy center. During E-Flux III, this flux was estimated to be 2.4 (±1.8) mmol C m^{-2} day^{-1} (with the direction from air to sea) (Chen et al., 2007). During E-Flux I, this flux was estimated to be 0.37 (±0.48) mmol C m^{-2} day^{-1} (with the direction from air to sea) (see Section 3.2). Applying the same conceptual salt budget model to DIC (Fig. 4.10), we have

$$\frac{dDIC_{Inventory}}{dt} = V_T * (DIC_{IN(obs)} - DIC_{OUT}) * \frac{H}{V_T * T} \qquad (4.12)$$

and

$$\sum DIC_{Input} - \sum DIC_{Output} = V_d * (DIC_d - DIC_{OUT}) * \frac{H}{V_T * T} \qquad (4.13)$$

where H is the height of the relevant surface water column in the center of the eddy, and T is the elapsed time, e.g., time period between Cyclone Opal's formation and sample collection, approximately 35 days (average ~ 5 weeks) and ~90 days for Cyclone Noah (Dickey et al., 2008). $DIC_{IN(obs)}$ is the observed (i.e., measured) average DIC in IN-station surface water column, By dividing all DIC inventory terms with area (H/V_T) and time (T), the unit for NCP becomes mmol C m^{-2} d^{-1}. This is the unit for all the fluxes and inventory change terms in this chapter.

Inserting equations (4.12) and (4.13) into equation (4.11), we obtain:

$$NCP_{DIC} = \sum DIC_{Input} - \sum DIC_{Output} - \frac{dDIC_{Inventory}}{dt} + F_{air-sea}$$

$$= \left\{V_d * (DIC_d - DIC_{OUT}) - V_T * (DIC_{IN(obs)} - DIC_{OUT})\right\} * \frac{H}{V_T * T} + F_{air-sea}$$

$$= \left\{V_d * DIC_d + (V_T - V_d) * DIC_{OUT} - V_T * DIC_{IN(obs)}\right\} * \frac{H}{V_T * T} + F_{air-sea}$$

$$= \left\{\left[V_d * DIC_d + V_s * DIC_{OUT}\right]/V_T - DIC_{IN(obs)}\right\} * \frac{H}{T} + F_{air-sea}$$

By comparing with equation (4.9), we have

$$NCP_{DIC} = (DIC_{IN(\exp)} - DIC_{IN(obs)}) * \frac{H}{T} + F_{air-sea} \qquad (4.14)$$

Hence, the difference (ΔDIC) between the expected DIC at IN-stations, $DIC_{IN(exp)}$, and that actually measured, $DIC_{IN(obs)}$, once corrected for air-sea gas exchange of CO_2, results in the average rate of net biological uptake over the time period since eddy formation.

This approach was also applied to N+N, TOC and DON data to derive NCP. The equations are as follows:

$$NCP_{N+N} = ((N+N)_{IN(\exp)} - (N+N)_{IN(obs)}) * \frac{H}{T} * (C/N)_{OM} \qquad (4.15)$$

$$NCP_{TOC} = (TOC_{IN(obs)} - TOC_{IN(\exp)}) * \frac{H}{T} + F_{Export} \qquad (4.16)$$

$$NCP_{DON} = ((DON)_{IN(obs)} - (DON)_{IN(\exp)}) * \frac{H}{T} * (C/N)_{DOM} \qquad (4.17)$$

where all the subscripts above have the same meaning as those in equation (4.14). For the N+N model, there is no air-sea exchange and nitrogen is converted to carbon assuming a C/N Redfield ratio of 6.6 (Redfield, 1958).

Again, please note that there are no TOC and DON data for E-Flux I cruise. Thus we only discuss E-Flux III for these two methods. For TOC, we must add an additional term, the POC export flux (F_{Export}) at the base of the defined water column (Williams, 1993). This flux was

estimated for the eddy core using the average of the sediment trap and ^{234}Th derived fluxes by Benitez-Nelson et al. (2007). For DON, N is converted into C assuming a much higher C/N ratio of 13.6 in dissolved organic matter (Benner et al., 1992). Please note that NCP from the DON mass balance does not include particle export at the bottom of the euphotic zone.

One caveat which we have yet to consider in the NCP determination based on DIC mass balance is possible carbonate removal due to biogenic calcium carbonate formation ($CaCO_3$ precipitation). There was no evidence of any significant growth of these types of organisms within Cyclone Opal and Noah (Brown et al., 2008; Landry et al., 2008; Rii et al., 2008). This was further supported by calculating a salt budget for dissolved calcium during E-Flux III (data not shown) that indicated little to no difference between observed and expected calcium concentrations (only available for E-Flux III), ~ 0.02 mmol·kg^{-1}, well within the measurement error, and only minor changes in TAlk between surface water and depth (Fig. 4.1F, 4.4E, 4.5F, and 4.6E). We should also note that we did not include data from station IN1 in E-Flux III for further discussion (Table 4.7). As we mentioned in Chapter 2, cast 49 at station IN1 was determined to be outside of the eddy core using ADCP data.

Section 4.3 NCP in Cyclone Opal

NCP at OUT-stations

The average NCP and other net flux terms at three OUT-stations were estimated from the mass balances of DIC, N+N, TOC, and DON by using the mixed layer model described in Section 4.2. Assuming negligible entrainment and horizontal advection and steady state (i.e., negligible time rate of change), mixed layer NCP estimates from these mass balances are 5.63±1.88, 0.84±0.16, 1.89±0.51, and 0.78±0.35 mmol C m^{-2} d^{-1}, respectively (Table 4.5). Significant uncertainties may be introduced to the individual flux terms due to our model

assumptions. For example, horizontal advection was ignored. In order to assess the magnitude of the horizontal advection term, we use DIC data collected during E-Flux II, across a southeast to northwest transect (Transect 6, Table 2.2 and Fig. 2.5) that included a region close in proximity to the OUT-stations (roughly the same location for E-Flux II and III). Transect 6 showed a northwestward *n*DIC gradient of 0.01±0.02 mmol C m^{-3} km^{-1}. Assuming a net horizontal velocity of ~ 2 cm s^{-1} (Quay and Stutsman, 2003) results in a horizontal flux term of 1.64±3.30 mmol C m^{-2} d^{-1} which is about 30% of our initial estimate of NCP (Table 4.5). No similar measurements were conducted for TOC and DON. We should mention that for N+N, since it is always depleted in the mixed layer, likely has limited concentration gradients and thus significant horizontal advection is not expected.

The temporal stability of the biogeochemical properties in the absence of an eddy (OUT-stations) can be assessed by comparing the average DIC, salinity, N+N, TOC, and DON between E-Flux II and III cruises (Table 4.2). Since no mesoscale eddies were observed during E-Flux II (Dickey et al., 2008), all station data from this cruise, including stations collected in the eddy generation region, were compared to the data at E-Flux III OUT-stations. Overall, there are a ≤ 0.03 increase in salinity and ≤ 5 μmol kg^{-1} increase in DIC in the mixed layer between E-Flux II and III. This increase is within the uncertainties of our measurement (Table 4.2). Furthermore, average *n*DIC values over the upper 0-75 m (well within the mixed layer) during E-Flux II and E-Flux III are also the same within error (1959.0±5.8 and 1962.4±4.5 μmol kg^{-1}, respectively, calculated from the data in Table 4.1 and 4.2). These results suggest that surface waters without the influence of eddies in the lee of Hawaiian Islands are quite stable within the winter season, which further justified our choice of E-Flux III OUT-stations as truly representative of the background, non-eddy impacted biogeochemistry of Hawaiian lee waters during E-Flux III. In

order to assess the temporal impact on NCP budgets, we used an elapse time between the two cruises as ~ 2 months, and applied a small NCP correction factor (see Table 4.5).

After the adjustments of spatial and temporal change, NCP from the mass balance of DIC decreases from 5.63±1.88 to 4.49±8.39 and mmol C m^{-2} d^{-1}. TOC derived NCP, however, increases from 2.44±1.00 to 3.37±1.11 mmol C m^{-2} d^{-1}. Combined, the revised TOC and DIC estimates and the initial NCP estimates derived from N+N and DON result in an average NCP of 2.37±4.24 mmol C m^{-2} d^{-1} at OUT-stations (Table 4.5).

We did not conduct similar estimates for N+N and DON because mixed layer N+N was depleted in both cruises and DON data was more complicated due to change in composition, for example, preferential loss of nitrogen during organic matter degradation (Benner et al., 1992). In addition, the results for N+N and DON must be converted to C by using C/N ratios (6.6 for N+N and 13.6 for DON), amplifying the errors significantly.

NCP at IN-stations

NCP calculations and the associated errors

To estimate NCP at IN-stations, we first applied the two end-member mixing model (described in Section 4.2) to calculate the expected concentrations of DIC, N+N, TOC, and DON over three different depth horizons (0-50 m (surface to the average MLD), 0-75 m (surface to DCML), and 0-110 m (the average euphotic zone)). In the mixed layer, uniform concentrations enable a simple mass balance of inputs and outputs. For the other two depth horizons above (0-75 m and 0-110 m), however, non-uniform hydrographic and biogeochemical distributions complicate the calculation as different processes may affect distributions depending on their position in the water column. Nonetheless, we argue that a one-box, two end-member mixing model is still valid for determining the average and total NCP over a given depth horizon as long

as the mixing components of a specific biogeochemical quantity are constrained using a salt budget. While this is likely true for the mixed layer and the 0-75 m depth horizon given the physics of Cyclone Opal (e.g., Nencioli et al., 2008), the 0-110 m depth integration at IN-stations should be viewed with caution as it includes the depth to which Subtropical Salinity Maximum Water extends (Nencioli et al., 2008).

Observed average concentrations at IN-stations, OUT-stations, and in the deep Subtropical Salinity Maximum Water are given in Table 4.6. These data, as well as the salinity data in Table 4.1, are used to calculate the expected IN-station concentrations and the fraction of the Subtropical Salinity Maximum Water within the desired depth horizons. Results (i.e., expected concentrations) are also presented in Table 4.6.

Using the two end-member mixing model described in Section 4.2, we determined average NCPs with uncertainty over three depth horizons. Specifics of the calculation of $DIC_{IN(exp)}$ in the mixed layer are given below as an example. According to equation (4.10), we first must determine the DIC concentration and salinity in the deep salinity maximum water, i.e., DIC_d and S_d, which are 2068.0±3.3 μM (converted from μmol kg^{-1}) and 35.122±0.009, respectively (Table 4.1 and 4.6). DIC_{OUT} and S_{OUT} are 2002.9±3.3 μM and 34.882±0.030, respectively, while S_{IN} is 35.044±0.013. Thus, $DIC_{IN(exp)}$ is calculated to be 2046.9±4.1 μM.

Before we start to discuss further results by using salt budget, we need to justify the appropriateness of using two end-member mixing model since one would argue that the same value for f ratio and expected values (e.g., $DIC_{IN(exp)}$) in Table 4.6 should be able to be derived if this two end-member mixing model is appropriate. However, inconsistency is observed that the expected temperature (T_{exp}) is 22.71ºC, which is ~1ºC colder than measured 23.65ºC (Table 4.1). Please recall that initial eddy formation occurred probably in early February (right after E-Flux

II) when surface water temperature at OUT-stations was much higher than that during E-Flux III (Fig. 4.2A and 4.9A, Table 4.1). In Section 4.1 and this Section, salinity and DIC values at OUT-stations between E-Flux II at the end of January and E-Flux III in March were compared and their values show minor variation (a $\leq$ 0.03 increase in salinity and $\leq$ 5 μmol kg^{-1} increase in DIC in the mixed layer between E-Flux II and III). However, in order to explore the effectiveness of this two end-member mixing model more convincingly, we can use the OUT-station data during E-Flux II (Table 4.2) to calculate the expected values. Let us still use the depth interval over 0-50 m as example. Now using the same estimate for S_{in}, but the estimates of S_{out} (=34.858±0.030), S_d (=35.131±0.010), DIC_d (=2073.9±4.9 μM) and DIC_{out} (=1997.3±5.2 μM) are from E-Flux II cruise (Table 4.2). We got f = 68.1% and DIC_{exp} = 2049.6 μM over 0-50 m depth. This is consistent with the results in Table 4.6, where f = 67.6% and DIC_{exp} = 2046.9 μM. Thus, we are confident to simply use E-Flux III salinity and DIC data for the mass balance calculation here.

In contrast, mixed-layer surface waters at OUT-stations in E-Flux III were considerably cooler, ~0.5ºC, relative to the sampled stations in E-Flux II (Fig. 3A). On the other hand, the temperature of deep salinity maximum water mass in E-Flux II was also slightly higher when compared to that in E-Flux III (22.308±0.369 ºC for E-Flux II (Table 4.1B) and 21.738±0.179 ºC for E-Flux III (Table 4.1A), respectively). If one considers this higher initial surface temperature and higher initial deep water temperature, the resulting expected IN-station temperature over 0-50 m (23.25ºC) is substantially higher than previously estimated 22.71ºC by using the E-Flux III data, and much closer to the measured value (23.65ºC). The reason of the difference, ~0.4ºC (instead of 1ºC in the previous estimate), is unclear. But the uncertainties and sea surface heat exchange should at least partially contribute to this difference. The analysis above suggests that salinity is more conservative and thus more appropriate to be used as end members in the

proposed twp end-member mixing model, although theoretically, salinity and temperature should be able to access the similar results.

The error (1 SD uncertainty) of $DIC_{IN(exp)}$ depends on the errors in all the terms in equation (4.10). Sensitivity analyses suggest that changes of 1 SD uncertainty in the individual terms in equation (4.10) resulted in a $DIC_{IN(exp)}$ range of 1.1 to 3.5 μM. If the individual error terms are independent, an accumulated error of ±5.2 μM is estimated. This results in an average difference between $DIC_{IN(exp)}$ and $DIC_{IN(obs)}$ (ΔDIC) of 15.3±5.2 μM (Fig. 4.11). Thus, although the error is large, the ΔDIC is still significant. Using this calculated change in DIC and the error in $F_{air\text{-}sea}$ in equation (4.14), we determined a NCP_{DIC} of 24.3±9.5 mmol C m^{-2} d^{-1} for the mixed layer (Table 4.7A). We should mention that the NCP estimates here do not include the errors in terms of H and T in equation (4.14). The same strategy was used to determine differences between other observed and expected values (ΔDIC, Δ(N+N), ΔTOC, and ΔDON over different depth horizons) and NCP from equations (4.14) to (4.17) (Fig. 4.11 and Table 4.7). Please note that the concentrations of Δ(N+N) and ΔDON were converted to carbon based unit by using different C/N ratios (Redfield C/N ratio (6.6) and C/N ratio for dissolved organic matter (13.6), respectively).

Overall, the average differences between observed and expected values of the various biogeochemical constituents (ΔDIC, Δ(N+N), ΔTOC, and ΔDON) decreased with increasing integration depths from 0-50 m to 0-110 m, especially from 0-75 m to 0-110 m. This trend suggests that the depletion of DIC and N+N and the accumulation of TOC and DON occurred mostly in the upper euphotic zone (above the DCML). From equations (4.14) to (4.17) in Section 4.2, differences between expected and observed concentrations (ΔDIC, Δ(N+N), ΔTOC, and ΔDON) are critical for the NCP estimation. If these differences are significantly different from

zero, we will expect the significant positive NCP. For example, from the calculated average ΔDIC above, the corresponding NCP_{DIC} (24.3±9.5 mmol C $m^{-2}\cdot d^{-1}$, Table 4.7A) in the mixed layer is also significant.

Among these four biogeochemical parameters, the ΔDON has the greatest uncertainties over all the depth horizons. A major reason is that the decrease in DON with depth is relatively small and varies widely (Fig. 4.2F, Table 4.2). For the other three parameters, the differences between observed and expected values within the 0-50 m and 0-75 m depth horizons are much larger than the calculated uncertainties. Over the 0-110 m depth horizon, however, smaller differences between observed and expected values resulted in significant relative errors (Fig. 4.11). Thus, the relative errors on the NCP calculation also increase with increasing depth integration (Table 4.7A-C). Please note that there is no substantial decrease in NCP estimates when integrated to deeper depths (0-110 m) as smaller values of ΔDIC, Δ(N+N), ΔTOC, and ΔDON are multiplied by a larger depth interval to obtain depth-integrated NCP.

NCP at individual IN-stations was determined over the three depth horizons (0-50 m, 0-75 m, and 0-110 m) in order to assess the temporal variability and stability of estimates (Table 4.7A-C). Results suggest that NCP calculated by using N+N and TOC is substantially less variable than that by using DIC. This likely reflects the fact that the difference between observed and expected DIC values is small relative to their background concentrations and associated uncertainties, especially with the increase of depth horizon. For example, ΔDIC over the 0-110 m depth horizon is 3.3±4.9 μM. It is therefore difficult to distinguish the biological change in the DIC signal above the large background of DIC (Table 4.6). This problem is further confounded by the small salinity difference between surface and deep waters (Table 4.1). For example, sensitivity analyses suggest that a change of 0.01 in IN-station salinity (S_{IN}) or a 4 μM change in

IN-station DIC ($DIC_{IN(obs)}$) over the upper 0-110 m results in a significant difference in the estimated NCP of ~ 100%. In contrast, the same change in S_{IN} only causes ~ 20-30% change in estimated NCP from N+N and TOC. Nevertheless, the in depth error analysis provided above, as well as the consistency in results using the various biogeochemical parameters, suggests that the NCP determined at the IN-stations reflects the general trend of enhanced NCP in the center of Cyclone Opal, especially within the mixed layer (0-50 m) and DCML (0-75 m) (Tables 4.7A-C).

We should mention that evaporation and precipitation were also not explicitly included in the above calculations. Assuming a typical net evaporation rate of 435 mm yr^{-1} between 20ºN and 30ºN in the ocean (Peixoto and Oort, 1992) and an average mixed layer depth of 50 m at IN-stations, the net influence of evaporation would result in an increase of 0.025 in salinity over the upper 50 m over a 1 month period. This is comparable to the observed increase in salinity between E-Flux II and E-Flux III OUT-stations (Table 4.6). Applying this salinity adjustment to the IN and OUT stations in equation (4.7), the f value would be reduced by 8% to 60%. When this is applied to equation (4.10), however, DIC_{OUT} should equally be reduced to a lower pre-evaporation value. The resulting $DIC_{IN(exp)}$ would be 4.7 μM lower. However, for an appropriate comparison with the $DIC_{IN(obs)}$, this initial $DIC_{IN(exp)}$ should also be subjected to evaporative concentration. Thus the final $DIC_{IN(exp)}$ is only 3.2 μM lower than the earlier calculation which is significant, implying a 20% overestimation of our DIC-based NCP, but is still within the overall uncertainty due to other terms estimated earlier (±5.2 μM). The above exercise is equivalent to the use of E-Flux II as the initial surface water end-member that has lower salinity and DIC values.

We should also mention that at station IN0, the average salinity over 0-110 m interval is a bit lower than the average salinity over 0-100 m when comparing the average salinity from

different depth intervals. This implies that at 100-110 m depth interval, water mass with lower salinity below the Subtropical Salinity Maximum Water may already intrude into the bottom of the euphotic zone. However, our salt-budget approach to estimate NCP does not expect this situation. The larger negative value of NCP_{DIC} in 100-110 m should be due to this intrusion of deeper water mass with much higher DIC/salinity ratio than the water mass above it.

Vertical distribution of NCP

In the center of Cyclone Opal, higher carbon export is expected due to enhanced NCP and a shift in community structure from small pico-phytoplankton to large diatoms (Rii et al., 2008). The average NCPs (averaged from the mass balances of DIC, N+N, TOC, and DON) over the three depth horizons are 14.2 ± 9.2 (0-50 m), 18.5 ± 10.7 (0-75 m); and 14.1 ± 10.6 mmol C m^{-2} d^{-1} (0-110 m), respectively (Table 4.7). These values are significantly higher than the average NCP at OUT-stations in the mixed layer (~ 0-95 m), 2.37±4.24 mmol C m^{-2} d^{-1}. However, less than 15% of the average NCP in the euphotic zone was exported as POC below 150 m (1.8±0.9 mmol C m^{-2} d^{-1}, Benitez-Nelson et al. (2007)). The rest of the organic carbon production must either accumulate in the upper water column (0-110 m) as DOC or exported laterally. Contemporaneous measurements of suspended particulate C and particulate N indicate that TOC is mainly comprised of DOC (Landry et al., 2008; Mahaffey et al., 2008). Using the two end-member salt budget approach (see Section 4.2), average observed TOC (66.0±2.0 μM) is 5.5 μM higher than the expected value (60.5±3.6 μM) over the upper 110 m (Table 4.6). Such a difference is equivalent, within error, to our average NCP estimates, suggesting that enhanced NCP was stored in the upper water column as DOC.

To better understand the NCP throughout the water column, we plotted NCP over several different depth intervals (Fig. 4.12). Please note that the NCP within the 50-75 m depth interval

is actually the difference between the NCP over 0-75 m and that over 0-50 m. The same strategy is used to obtain NCP over the 75-110 m interval. Most of the NCP took place within the mixed layer (over 0-50 m depth horizon, Fig. 4.12). This is supported by the positive dissolved oxygen anomaly in the shallow euphotic zone of the eddy center (Nencioli et al., 2008). We should mention that no dissolved oxygen (DO) data from bottle sample were available for calibration. However, the intercomparison can still be done by using individual profiles (Nencioli et al., 2008).

In general, the upper two layers (0-50 m and 50-75 m) maintained a positive NCP. The positive NCP within the mixed layer is consistent with modest increases in *Prochlorococcus* spp. and diatom abundance as well as the growth rates of *Prochlorococcus* spp. and other small phytoplankton, such as prymnesiophytes and pelagophytes (Landry et al., 2008; Rii et al., 2008). Positive NCP rates from 50 to 75 m is coincident with increased biomass and a shift in community structure from *Prochlorococcus* spp. to large (>20 μm) diatoms (Landry et al., 2008). Above the DCML, in the upper 50-60 m, the diatom community was comprised of physiologically unhealthy diatoms with significantly depressed growth rates and proportionately greater grazing losses relative to the mixed layer and the DCML (Landry et al., 2008). Such an elevated biomass of diatoms between 50 m and the DCML confirms the intrusion of the deep nutrient-rich water and enhanced biological production after the initial isopycnal uplift of Cyclone Opal. It is further consistent with the positive NCP from 50 to 75 m, although there was no obvious growth rate enhancement due to Si limitation at the time of sample collection (Rii et al., 2008).

In contrast, the lower layer (75-110 m) had close to zero NCP. While diatom biomass and growth rates were still significant, large (>50 μm) ciliates and dinoflagellates, the most likely

protistan grazers of diatoms, were also ~ 3 times higher than ambient biomass levels (Brown et al., 2008). These consumers capture and process their food as individual prey items and produce individual empty frustules as a by-product of grazing (Jacobson and Anderson, 1996; Jeong et al., 2004; Landry et al., 2008). As such, they tend to produce smaller suspended particles and dissolved organic matter rather than large organically dense fecal pellets. These are consistent with the higher rates of remineralization implied below the DCML using $^{234}Th/^{238}U$ disequilibria and lower rates of particle export (Maiti et al., 2008; Rii et al., 2008). Nonetheless, NCP may still be underestimated within 75-110 m. As mentioned in Section 4.2, there is solid body rotation down to ~ 70 m at the eddy center, essentially isolating this water mass from the surrounding waters. Below 70 m, mixing along isopycnal surfaces may have occurred allowing the horizontal intrusion of deep nutrient-rich water at the eddy center. Thus the age of water mass within the lower layer (75-110 m) may have been much younger than the assumed elapse time, which is ~ 35 days (Dickey et al., 2008; Nencioli et al., 2008).

NCP from TOC mass balance is likely a conservative estimate (equation 4.16; Tables 4.7A-C; Fig. 4.12) in that we applied the carbon export flux at 150 m to shallower depth intervals (0-50 m, 0-75 m, and 0-110 m). However, we would expect higher carbon export fluxes at shallower depths since carbon export fluxes generally decrease with depth (Cochran et al., 1993; Amiel et al., 2002). Please note that NCP estimated from TOC mass balance in the lower layers (75-110 m) shows small positive values at IN-stations (IN2: Fig. 4.11C, IN5: Fig. 4.11F, IN6: Fig. 4.11G, IN7: Fig. 4.11H, and the average NCP in Fig. 4.11A). Such an uncoupled spatial distribution between NCP_{DIC} and NCP_{TOC} may reflect the fact that positive NCP_{TOC} in the lower euphotic zone may be due to the accumulation of dissolve organic carbon from grazing and heterotrophic activities in the lower euphotic zone, whereas most new-photosynthesized organic

carbon is produced in the upper euphotic zone since most photosynthesis occurs and DIC removal mainly takes place there.

NCP values for N+N and DON may be underestimated since there are other fluxes which were not considered in our model. For example, the N_2 fixation, which was not included in our model, is an important pathway for the subtropical ecosystem to sustain. In the cases of TOC and DON, things may be further complicated by changes in composition, as refractory organic C and N should not contribute to NCP. Our observed TOC and DON data, unfortunately, do not give us such information. Besides, preferential loss of nitrogen during degradation and remineralization of organic matter may bring substantial uncertainties to DON data as well (Fig. 4.2F).

Section 4.4 NCP in Cyclone Noah

NCP at OUT-stations

The average NCP and other net flux terms at three OUT-stations during E-Flux I were estimated from the mass balances of DIC and N+N by using the mixed layer model described in Section 4.2. Please note that samples for TOC and DON analysis were not collected in this cruise. Assuming negligible entrainment and horizontal advection and steady state (i.e., no time rate of change), mixed layer NCP estimates from DIC and N+N are 3.18±0.47 and 1.34±0.31 mmol C m^{-2} d^{-1}, respectively (Table 4.8). As discussed in Section 4.3, significant uncertainties may be introduced to the individual flux terms due to mixed-layer model assumptions. For example, based on the DIC results in E-Flux II, horizontal advection is up to 36% of the corrected NCP estimation (Table 4.5). For N+N, as it is always depleted in the mixed layer, large gradients and horizontal advection are not expected. Unfortunately, similar justification of

horizontal advection and temporal variation is not available for E-Flux I due to the limitation of cruise opportunity.

Average NCP estimate from DIC and N+N was 2.26±0.56 mmol C m^{-2} d^{-1} at OUT-stations during E-Flux I (Table 4.8), which is essentially the same as the OUT-station NCP during E-Flux III (2.37±4.24 mmol C m^{-2} d^{-1}) (Table 4.5). In comparison, NCP at Station ALOHA, approximately 300 km north of our study area, ranges from 4.1±0.8 to 7.4±4.7 mmol C m^{-2} d^{-1} over the mixed layer or euphotic zone (as summarized by Keeling et al. (2004)). Please note that NCP within the mixed layer is roughly 80% of NCP over the entire euphotic zone at Station ALOHA (Keeling et al., 2004). Our lower results appear reasonable given that the NCP estimates here are during the winter season (Quay and Stutsman, 2003; Keeling et al., 2004).

NCP at IN-stations

NCP calculations and associated errors

Similar to Cyclone Opal in Section 4.3, to estimate NCP at IN-stations, we first applied the two end-member mixing model (see Section 4.2) to calculate the expected concentrations of DIC and N+N over two different depth horizons (0-MLD and 0-110 m (the average euphotic zone)). Again, a one-box, two end-member mixing model is valid for determining the average and total NCP over a given depth horizon as long as the mixing components of a specific biogeochemical quantity are constrained using a salt budget. The 0-110 m depth integration at IN-stations should be viewed with caution as it includes the depth to which Subtropical Salinity Maximum Water extends (Kuwahara et al., 2008; Nencioli et al., 2008).

Observed average concentrations at IN-stations, OUT-stations, and in the deep Subtropical Salinity Maximum Water are given in Table 4.9. These data, as well as the salinity data in Table 4.3, are used to calculate the expected IN-station concentrations and the fraction of

the Subtropical Salinity Maximum Water within the desired depth horizons. Results (expected concentrations) are also presented in Table 4.9.

Unlike Cyclone Opal where there was an intense uplift of DCML with substantial increase in chlorophyll concentrations and shift in community structure, here for Cyclone Noah, the uplift of DCML is much less and only a moderate increase in chlorophyll concentrations occurred. Here three stations were considered within the eddy core of Cyclone Noah, i.e., IN-stations. Their related calculation and NCP values are provided with uncertainties over two different depth horizons by using the same end-member mixing model described in Section 4.2 (Table 4.9 and 4.10). An example for specifics of the calculation was already described in Section 4.3 ($DIC_{IN(exp)}$ in the mixed layer). Thus, we do not present the detail analysis here. Instead, we will directly present the analytical results and we still use DIC results in the mixed layer as example. According to equation (4.10), accumulated errors of $DIC_{IN(exp)}$ in the mixed layer range between 8.9 and 12.2 μM (Table 4.9A). Although the errors are large, the ΔDICs are still significant in the mixed layer (Fig 4.13A). Using these calculated change in DIC and the error in $F_{air\text{-}sea}$ in equation (4.14), we determined the values of NCP_{DIC} from 7.4±3.3 to 10.1±3.9 mmol C m^{-2} d^{-1} for the mixed layer by assuming ~90 days as the age of Cyclone Noah (Table 4.10A). We should mention again that the NCP estimates here do not include the errors in terms of H and T in equation (4.14). The same strategy was used to determine differences between other observed and expected values (ΔDIC and Δ(N+N) over two different depth horizons) and NCP from equations (4.14) to (4.17) (Fig. 4.13 and Table 4.10).

Similar to Cyclone Opal, the differences between observed and expected values of the two biogeochemical constituents (ΔDIC and Δ(N+N)) decreased with increasing integration depths (Figs. 4.13A-B). Over the 0-110 m depth horizon, smaller differences of ΔDIC and

Δ(N+N) resulted in significant relative errors (Fig. 4.13A-B). Thus, the relative errors on the NCP calculation also increase with increasing depth horizon (Table 10A-B). NCP calculated by using N+N is substantially less variable than that by using DIC, especially for the 0-110 m case (Table 4.10B). The above trend is generally consistent with the conclusion from Cyclone Opal. The effectiveness of the two end-member mixing model is confirmed by this case study as well.

The uncertainty of NCP caused by evaporation and precipitation, especially NCP_{DIC}, should be carefully evaluated for Cyclone Noah since the much longer elapsed time after its formation (assuming 3 months) and therefore more evaporation would be expected. If we just use this elapsed time and net evaporation rate of 435 mm yr^{-1} between 20ºN and 30ºN in the ocean by Peixoto and Oort (1992), the influence of evaporation/precipitation on NCP estimates is significant, decreasing the NCP values in Table 4.10 by at least 60%. However, a closer examination of GOES SST image in the lee of Hawaii area about one and a half months before sampling time shows that Cyclone SST feature was relaxed during the late September (Fig. 4.14), and started to re-intensify its surface feature in the GOES SST image for September 28-29th, 2004. These phenomena make us believe that active isopycnal uplift may occur during the time period between the end of September and the beginning of October. Thus the time for our collected samples during E-Flux I to experience the evaporation/precipitation should be about one month or more (similar to Cyclone Opal) and much shorter than the age of Cyclone Noah. Thereafter, the corrected NCP results are presented in Table 4.11. Comparing to each other, our NCP results in Table 4.10 are still reasonable without considering the effect of evaporation/precipitation, although this may overestimate the NCP_{DIC} by 20-30%. For NCP_{N+N} estimates, the effect is within ~10% since N+N was depleted at OUT-stations and minor

variation in salinity does not affect $N+N_{IN(exp)}$ much. For purpose of consistency, we will use the results from Table 4.10 for further comparison.

On the other hand, more uncertainties for NCP estimation emerge for this case. As we already mentioned, NCPs in Table 4.10 were obtained by assuming ~90 days as the age of Cyclone Noah. If Cyclone Noah indeed re-intensified by the time we proposed, then the real age of the water mass within the eddy core should be around 6 weeks. Thus, NCP results in Table 4.11 should serve as a conservative estimation, a low boundary of NCP estimation.

Please note that at station 13, the maximal salinity was approximately between 90 m (salinity = 35.0925) and 100 m (salinity = 35.0932) and began to decrease below 100 m (salinity = 35.0753 at 110 m) (Fig. 4.7B). Firstly, this indicates that at 100-110 m depth interval, water mass with lower salinity below the Subtropical Salinity Maximum Water already intruded into the bottom of the euphotic zone. Secondly, the maximal salinity at station 13 is significantly lower than other stations at the eddy center (Fig. 4.7B) and about ~0.036 lower than salinity of OUT_{deep} in Table 4.3. This further implies that the water mass with lower salinity (but higher DIC) may intrude into the 90-100 m depth interval as well, thus decreased the maximal salinity, and increased DIC. However, our salt-budget approach to estimate NCP does not include this situation. The much larger negative value of NCP_{DIC} below the mixed layer (Fig. 4.15C) and therefore much lower NCP_{DIC} in the whole euphotic zone (Table 4.10B) should be due to this intrusion of deeper water mass with much higher DIC/salinity ratio than the water mass above it.

Characteristics of NCP during the decay phase of Cyclone Noah

During E-Flux I, we only had the chance to sample two IN-stations (IN1 and IN2, Table 2.1) at the center of Cyclone Noah besides station 13, which was considered at the eddy center and sampled during Transect 2 (Table 2.1; Fig. 2.4). NCP estimates from these three stations

were presented in Table 4.10. Please note that there are no nutrients data for station 13 (Table 4.10). Although enhanced NCP and higher carbon export could be reasonably expected due to the enhanced nutrients supply at the eddy center, the situation during the decay phase of Cyclone Noah need to be closely examined. Over the mixed layer depth horizon, the NCPs from the mass balances of DIC and N+N are 7.4-8.4 and 2.3-3.9 mmol C m^{-2} d^{-1}, respectively (Table 4.10A). Over the entire euphotic zone (0-110 m), excluding station 13, the NCPs from DIC and N+N are 5.8-6.0 and 5.1-6.6 mmol C m^{-2} d^{-1}, respectively (Table 4.10B). These values are moderately higher than the average NCP at OUT-stations in the mixed layer (~0-90 m), 2.26±0.56 mmol C m^{-2} d^{-1} (Table 4.8).

Similar to Cyclone Opal, we plotted NCP over different depth intervals within the euphotic zone, i.e., within the mixed layer and lower euphotic zone (below the mixed layer depth), to better understand the NCP throughout the water column (Fig. 4.15). Please note that the NCP within the lower euphotic zone is actually the difference between the NCP within the mixed layer and that over the whole euphotic zone.

For Cyclone Noah, the vertical distributions of NCP_{DIC} and NCP_{N+N} are somewhat different (Fig. 4.15). Nevertheless, NCP estimates from both mass balances are all positive in the mixed layer, which is the same as the situation for Cyclone Opal. This is also supported by the positive dissolved oxygen anomaly in the mixed layer of the eddy center (Kuwahara et al., 2008). The positive NCP within the mixed layer is also consistent with modest enhancement of the ambient phytoplankton community with cyanobacteria indicated by a ~1.3-fold increase of total chlorophyll a concentration in the mixed layer (Rii et al., 2008).

Comparing mixed layer NCP_{DIC} to NCP_{N+N}, the estimates of NCP_{N+N} are much lower than NCP_{DIC} (Table 4.10A). Actually, this is also the case for the mixed layer of Cyclone Opal.

Part of the reason is because of the much larger uncertainties in NCP_{DIC} as we mentioned in Section 4.3. Furthermore, Cyclone Noah was already in relaxation (or decay phase) by the time of sampling and it is reasonable to deduce that upwelled N+N due to the active isopycnal uplift (during spin-up and mature phases) were depleted before the sampling period. On the other hand, we propose that the higher NCP_{DIC} might be supplied by other nitrogen inputs besides the eddy pumping from below, e.g., N_2 fixation and even terrestrial nitrogen input since Cyclone Noah was very close to the coast of Island of Hawaii (Kuwahara et al., 2008; Dickey et al., 2008). This implies that when Cyclone Noah evolved into the decay phase, the mixed layer NCP enhancement due to the contribution of eddy-induced nutrients pumping from below diminished correspondingly. However, this assumption need to be further examined in the future study. Besides, the discussion above is also possible for the case of the mixed layer of Cyclone Opal, although terrestrial nitrogen input is not likely since Cyclone Opal was much farther away from the islands and it was translating to the south, which is the opposite of the Hawaiian Islands.

In the lower euphotic zone (below the mixed layer), if only considering stations IN1 and IN2, there were close to zero NCP_{DIC} (Figs. 4.14A-B). This could be the similar reason as we discussed in case of Cyclone Opal that the enhanced grazing (small eukaryotes are one of the dominant planktons in the lower euphotic zone of Cyclone Noah) and subsequent remineralization could cancel out the photosynthetic carbon fixation there. These are consistent with the lack of enhancement of particle export at the center of Cyclone Noah (Rii et al., 2008). In contrast, NCPs from N+N in the lower euphotic zone are comparable to that within the mixed layer (Fig. 4.15A-B). Actually for station IN2, it is much larger in the lower euphotic zone. This is due to the significant consumption of extra "new" nutrients in the lower euphotic zone below the mixed layer, which also implies phytoplankton bloom may have already decayed since such a

depletion in nutrients may occur long time before the sampling time due to the lack of the active isopycnal uplift. The difference in the vertical distribution between NCP_{DIC} and NCP_{N+N} may reflects their different biogeochemical status in the euphotic zone, i.e., N+N is desired by biological activities and generally depleted in the euphotic zone, but DIC is abundant in the ocean. When heterotrophic metabolic activities release DIC and nutrients, nutrients will be absorbed by biological communities immediately while DIC will left over in the water column.

Section 4.5 Conclusions and significance

This chapter examined how wind-driven cyclonic eddies in their different life stages or phases (i.e., Cyclone Opal in its mature phase and Noah in its decay phase), influenced NCP. For Cyclone Opal, NCP estimates from mass balances of salt, DIC, N+N, TOC, and DON consistently suggest that on average, there was substantially enhanced NCP in the center of the eddy relative to that in the surrounding waters. In the average mixed layer (0-50 m) of the eddy center, NCP is 14.2 ± 9.2 mmol C m^{-2} d^{-1}; within the DCML (~ 0-75 m), NCP is 18.5 ± 10.7 mmol C m^{-2} d^{-1}; and for the euphotic zone, NCP is 14.1 ± 10.6 mmol C m^{-2} d^{-1}. In contrast, NCP for the mixed layer is 2.37±4.24 mmol C m^{-2} d^{-1} outside the eddy, which is equivalent to 80% NCP over the whole euphotic zone in the subtropical North Pacific gyre (Keeling et al., 2004). Enhanced NCP in the center of Cyclone Opal is consistent with earlier studies that new production depends on mixing and vertical advection processes (Eppley and Peterson, 1979; Mourino and McGillicuddy, 2006).

For Cyclone Noah, which was sampled in its decay phase, NCP estimates from mass balances of salt, DIC, and N+N consistently suggest that on average, there were enhanced NCPs in the center of the eddy relative to that in the ambient waters outside the eddy. However, the magnitude of NCP enhancement for Cyclone Noah is much less than that for Cyclone Opal. In

the mixed layer of the eddy center, NCPs from DIC and N+N are 8.0 ± 3.9 and 3.1 ± 1.1 mmol C m^{-2} d^{-1} respectively; and for the euphotic zone, NCPs from DIC and N+N are 5.9 ± 7.0 and 5.8 ± 2.3 mmol C m^{-2} d^{-1}, respectively. In contrast, NCP is 2.26±0.56 mmol C m^{-2} d^{-1} in the mixed layer outside the eddy. This implies that the enhancement in NCP within cyclonic eddies is indeed ephemeral and most intense enhancement in NCP should occur during the spin-up and mature phase. While in the decay phase, the *in situ* NCP within the eddy core may be not much different from the outside-eddy area. Simultaneously, the time-averaged NCP estimates would start to decrease since there is no active isopycnal uplift and therefore no extra "new" nutrients pumping into the well-lit zone by vertical advection. However, the NCP enhancement would still maintain for a while before the eddy area completely disappeared into the oligotrophic subtropical gyres.

Alternatively, a major difference between Cyclone Opal and Noah was their translation speeds (Dickey et al., 2008; Kuwahara et al., 2008; Nencioli et al., 2008). Cyclone Opal was substantially dynamic with significantly higher translation speed. According to hypothesis proposed by Nencioli et al. (2008), nutrients injection due to isopycnal uplift within Cyclone Opal might not be limited to a single injection at the time of its mature phase, thus multiple or continuous injections of extra "new" nutrients into the euphotic zone could occur along its propagation after the initial isopycnal uplift and caused more biological production. On the contrary, Cyclone Noah was relatively stationary with much lower translation speed, thus may exert less nutrients injection by the transport along the isopycnals below the portion of the solid body rotation after the initial isopycnal uplift. Thus, the total quantity of nutrients injection into the well-lit zone was much less and therefore the lower NCPs for Cyclone Noah. In Section 4.4, we proposed Cyclone Noah re-intensified ~6 weeks before our sampling time. If this is the case,

then it would further support the view that lower translational speed results in less nutrients injection. Comparing Cyclone Opal to Noah, Cyclone Opal was in mature phase after ~6 weeks since its formation while Cyclone Noah was already in decay phase after about the same time since its re-intensification.

Our models may involve significant uncertainties due to the lack of knowledge of initial conditions and future efforts should strive to incorporate additional biogeochemical constraints wherever possible. For example, NCP using a DIC budget would have been better estimated with the additional δ^{13}C-DIC estimates. In addition, efforts should be made to include all of the mass balance terms with better error control, even if less significant (see values in the brackets, Table 4.5).

Subtropical gyres show seasonal metabolic variation in the upper water column (Williams et al., 2004; Juranek and Quay, 2005). In situ NCP on four cruises to the Hawaii Ocean Time series (HOT) Station ALOHA during 2002-2003 was estimated to ~ 10 mmol C m^{-2} d^{-1} in the summer (Juranek and Quay, 2005). However, a neutral or net heterotrophic state was indicated by the winter data. Quay and Stutsman (2003) also determined much higher NCP at Station ALOHA during the summer, which is 7.2 ± 2.9 mmol C·m^{-2}·d^{-1}. Such net autotrophy in summer and net heterotrophy in winter was also suggested during a series of HOT cruises between May 2001 and May 2002 (Williams et al., 2004). Our NCP estimates in the center of the eddy are higher (for Cyclone Opal) or at least comparable (for Cyclone Noah) to the above NCP results in the subtropical Pacific Ocean in summer. Considering that our November 2004 and March 2005 cruises occurred just before winter or during the winter, this comparison also indirectly supports the view that NCP is substantially enhanced due to mesoscale eddies, at least in the mature phase, although mechanisms of NCP enhancement may differ from those at Station

ALOHA over the summer. Such an enhanced NCP within cyclonic eddies is also consistent with studies that mesoscale eddy-driven events are likely major mechanisms for supplying new nutrient to the upper ocean and hence, increased PP (McGillicuddy and Robinson, 1997; McGillicuddy et al., 1998).

For Cyclone Opal, our results suggest that the euphotic zone can be further divided into two layers: an upper layer (0-75 m) which is characterized with positive NCP and a lower layer (75-110 m) with NCP rates not significantly different from zero. Inside Cyclone Opal, enhanced NCP and shifting community structure (from pico-phytoplankton to diatom) suggested that a higher carbon export would be observed. Surprisingly, most of the enhanced NCP was stored in the surface water as DOC rather than exported as POC to the deep ocean. This suggests that eddies are not necessarily more efficient in exporting particulate organic matter to deep waters.

For Cyclone Noah, such two-layer structure is not as clear as that for Cyclone Opal, although NCPs are all positive in the mixed layer. The reasons are complicated. Firstly, there are only two different depth intervals conducted for Cyclone Noah because the mixed layer depth is different for individual IN-stations. Secondly, Cyclone Opal and Noah were in different eddy life stages. For Cyclone Opal, along-isopycnal transport of nutrients may still occur by the time of sampling, thus the nutrients in the lower layer may not have enough time to be consumed and therefore neutral NCP in the lower layer is acceptable if we even consider heterotrophic processes, such as remineralization, grazing, and excretion. While for Cyclone Noah, N+N was almost completely consumed within the entire euphotic zone, thus it is possible that the net NCP in the lower euphotic zone is also positive and even with a larger value relative to the mixed layer since the mixed layer depth only occupy a small proportion of the water column in the euphotic zone, not even mention the mixed layer depth for Cyclone Noah was much shallower at

IN-stations. Thirdly, the difference in the vertical distribution between NCP_{DIC} and NCP_{N+N} may reflects their different biogeochemical status in the euphotic zone.

Finally, every cyclone has its own unique physical, biological, and biogeochemical characteristics. As mentioned, Cyclone Noah is much closer to the coast of Island of Hawaii, we can not exclude the nutrients input from other pathways, for example, terrestrial injection. The physical properties between Cyclone Opal and Noah are also quite different. For example, their translation speeds were different from each other, which will also cause their difference in nutrient input rate. According to the hypothesis proposed by Rii et al. (2008), such different input rate of nutrients will subsequently favor different types of phytoplankton blooms. Therefore, the resulting average NCPs over time will be different.

Table 4.1 Average observed depth-integrated temperature and salinity over three depth horizons (0-50 m, 0-75 m, and 0-110 m) at (A) IN- and OUT-stations during E-Flux III, and (B) OUT-stations during E-Flux II.

(A) OUT-stations during E-Flux III

Stations	$Temperature_{obs}$ (°C)	$Salinity_{obs}$
In_{avg} (0-50 m)	23.647±0.056	35.044±0.013
OUT_{avg} (0-50 m)	24.723±0.056	34.882±0.030
In_{avg} (0-75 m)	23.234±0.081	35.071±0.016
OUT_{avg} (0-75 m)	24.627±0.016	34.900±0.041
In_{avg} (0-110 m)	22.631±0.100	35.089±0.012
OUT_{avg} (0-110 m)	24.448±0.057	34.929±0.038
OUT_{deep} (150 m)	21.738±0.179	35.122±0.009

(B) OUT-stations during E-Flux II

Stations	$Temperature_{obs}$ (°C)	$Salinity_{obs}$
In_{avg} (0-50 m)	23.647±0.056	35.044±0.013
OUT_{avg} (0-50 m)	25.259±0.107	34.858±0.015
In_{avg} (0-75 m)	23.234±0.081	35.071±0.016
OUT_{avg} (0-75 m)	25.189±0.123	34.875±0.024
In_{avg} (0-110 m)	22.631±0.100	35.089±0.012
OUT_{avg} (0-110 m)	24.844±0.154	34.926±0.026
OUT_{deep} (125 m)	22.308±0.369	35.131±0.010

Table 4.2 Average observed concentrations over three depth horizons (0-50 m, 0-75 m, and 0-110 m) at OUT-stations during E-Flux II and E-Flux III cruises. OUT_{deep} represents the Subtropical Salinity Maximum Water between 125 and 150 m at OUT-stations. E-Flux II data in this table were collected between January 16 and 26, 2005. E-Flux III data were collected between March 24 and 26, 2005.

	DIC (μmol kg^{-1})		Salinity		N+N (μM)		TOC (μM)		DON (μM)	
	E-Flux II (n=8)	E-Flux III (n=3)	E-Flux II (n=6)	E-Flux III (n=3)	E-Flux II (n=6)	E-Flux III (n=3)	E-Flux II (n=6)	E-Flux III (n=3)	E-Flux II (n=6)	E-Flux III (n=3)
OUT_{avg} (0-50 m)	1950.3±5.1	1956.0±3.2	34.858±0.015	34.882±0.030	0.04±0.03	0.28±0.08	72.40±0.42	73.19±0.38	4.56±0.34	4.11±0.05
OUT_{avg} (0-75 m)	1952.0±5.7	1956.8±4.4	34.875±0.024	34.900±0.041	0.04±0.03	0.25±0.07	72.08±0.79	72.80±0.28	4.51±0.32	4.09±0.11
OUT_{avg} (0-110 m)	1960.9±6.3	1960.6±3.4	34.926±0.026	34.929±0.038	0.13±0.07	0.22±0.05	70.35±0.78	71.88±0.35	4.45±0.33	4.16±0.13
OUT_{deep}	2025.3±4.8	2019.4±3.2	35.131±0.010	35.122±0.009	1.85±0.33	1.51±0.26	59.17±1.64	58.74±1.01	3.91±0.39	3.78±0.56

Table 4.3 Average observed depth-integrated temperature and salinity over two depth horizons ((A). 0-the mixed layer depth, and (B). 0-110 m (the euphotic zone)) at IN- and OUT-stations during E-Flux I.

(A) Mixed layer

Stations[a)]	**$Temperature_{obs}$ (°C)**	**$Salinity_{obs}$**
IN1 (49 m)	26.772	35.024
IN2 (33 m)	26.886	35.012
13 (30 m)	26.719	34.998
OUT_{avg} (n=3)	26.937±0.105	34.816±0.014
OUT_{deep} (150 m)	21.623±0.414	35.129±0.011

a). The number inside the parentheses is the mixed layer depth.

(B) 0-110 m

Stations	**$Temperature_{obs}$ (°C)**	**$Salinity_{obs}$**
IN1	25.099	35.052
IN2	24.237	35.072
13	24.415	35.039
OUT_{avg} (n=3)	26.359±0.057	34.861±0.019
OUT_{deep} (150 m)	21.623±0.414	35.129±0.011

Table 4.4 Selected average observed concentrations over three depth horizons (0-50 m, 0-75 m, and 0-110 m) at OUT-stations during E-Flux I, II and E-Flux III cruises. OUT_{deep} represents the Subtropical Salinity Maximum Water between 125 and 150 m at OUT-stations. E-Flux II data in this table were collected between January 16 and 26, 2005. E-Flux III data were collected between March 24 and 26, 2005.

	DIC (µmol kg^{-1})			Salinity			N+N (µM)		
	E-Flux I (n=8)	E-Flux II (n=8)	E-Flux III (n=3)	E-Flux I (n=6)	E-Flux II (n=6)	E-Flux III (n=3)	E-Flux I (n=2)	E-Flux II (n=6)	E-Flux III (n=3)
OUT_{avg} (0-50 m)	1953.6±4.9	1950.3±5.1	1956.0±3.2	34.816±0.014	34.858±0.015	34.882±0.030	0.09±0.06	0.04±0.03	0.28±0.08
OUT_{avg} (0-75 m)	1955.1±5.5	1952.0±5.7	1956.8±4.4	34.826±0.013	34.875±0.024	34.900±0.041	0.09±0.07	0.04±0.03	0.25±0.07
OUT_{avg} (0-110 m)	1961.5±6.0	1960.9±6.3	1960.6±3.4	34.861±0.019	34.926±0.026	34.929±0.038	0.15±0.04	0.13±0.07	0.22±0.05
OUT_{deep}	2020.5±5.0	2025.3±4.8	2019.4±3.2	35.129±0.011	35.131±0.010	35.122±0.009	1.58±0.05	1.85±0.33	1.51±0.26

a) E-Flux 2 data were collected between January 16 and 26, 2005. E-Flux 3 data were collected between March 24 and 26, 2005.

Table 4.5 OUT-stations (n=3) NCP and other net carbon flux terms in the mixed layer (95±7 m) from the budgets of DIC, N+N, TOC, and DON by using the mixed layer model during E-Flux III.

Term	Flux (mmol C m^{-2} d^{-1})			
	DIC	N+N	TOC	DON
Air-sea CO_2 exchange [a)]	2.90±1.84	NA	NA	NA
Horizontal advection [b)]	0 (1.64±3.30)	0	0	0
Vertical diffusion	2.73±0.34	0.84±0.16	0.64±0.07	0.78±0.35
POC export [c)]	NA	NA	1.25±0.51	NA
Time rate of change [d)]	0 (2.78±7.48)	0	0 (1.44±0.98)	0
NCP	5.63±1.88 (4.49±8.39)	0.84±0.16	1.89±0.51 (3.33±1.11)	0.78±0.35

a) Only for the mixed layer DIC budget. This flux is from Chen et al. (2007).

b) Estimate only available for DIC budget.

c) Only for the mixed layer TOC budget. POC flux is from Benitez-Nelson et al. (2007).

d) The values in the brackets are estimated by using the difference of *n* DIC between E-Flux II and II

Table 4.6 Average observed and expected concentrations as well as the fraction of Subtropical Salinity Maximum Water (f_{deep}) over three depth horizons (0-50 m, 0-75 m, and 0-110 m) from two end-member mixing model at IN-stations during E-Flux III.

Stations	**$f_{(deep)}$ (%)**	**$DIC_{IN(obs)}$ (µM)**	**$DIC_{IN(exp)}$ (µM)**	**$N+N_{IN(obs)}$ (µM)**	**$N+N_{IN(exp)}$ (µM)**	**$TOC_{IN(obs)}$ (µM)**	**$TOC_{IN(exp)}$ (µM)**	**$DON_{IN(obs)}$ (µM)**	**$DON_{IN(exp)}$ (µM)**
In_{avg} (0-50 m)	67.6±3.9	2031.6±3.2	2046.9±4.1	0.17±0.12	1.14±0.30	70.7±2.3	63.1±3.3	4.43±0.40	3.88±0.86
OUT_{avg} (0-50 m)	-	2002.9±3.3	-	0.28±0.08	-	73.2±0.4	-	4.11±0.05	-
In_{avg} (0-75 m)	77.0±5.7	2041.0±3.1	2053.3±5.3	0.31±0.14	1.26±0.37	68.9±2.5	61.6±4.0	4.34±0.38	3.85±0.84
OUT_{avg} (0-75 m)	-	2003.8±4.6	-	0.25±0.07	-	72.8±0.3	-	4.09±0.11	-
In_{avg} (0-110 m)	83.1±3.8	2053.5±2.6	2056.8±4.1	0.83±0.14	1.33±0.45	66.0±2	60.5±3.6	4.16±0.24	3.84±0.53
OUT_{avg} (0-110 m)	-	2007.6±3.5	-	0.22±0.05	-	71.9±0.3	-	4.16±0.13	-
OUT_{deep} (150 m)	-	2068.0±3.3	-	1.51±0.26	-	58.7±1	-	3.78±0.56	-

Table 4.7 The average as well as individual IN-station NCP estimates over three depth horizons ((A) 0-50 m; (B) 0-75 m; and (C) 0-110 m) from two end-member mixing model and mass balances of DIC, N+N, TOC, and DON during E-Flux III.

(A) 0 – 50 m

Stations	NCP_{DIC} (mmol C m^{-2} d^{-1})	NCP_{N+N} (mmol C m^{-2} d^{-1})	NCP_{TOC} (mmol C m^{-2} d^{-1})	NCP_{DON} (mmol C m^{-2} d^{-1})
IN0	35.6±19.6	10.4±7.5	-	-
IN1	7.7±12.2	-	-	-
IN2	30.5±10.3	10.8±7.6	19.6±10.2	23.9±11.5
IN3	27.4±9.8	9.8±7.4	12.3±9	5.0±10.4
IN4	27.2±8.4	9.8±7.4	11.4±8.8	8.1±10.6
IN5	44.2±37.2	9.4±7.4	10.9±8.7	8.0±10.6
IN6	18.3±6.9	7.0±6.9	11.1±8.8	5.4±10.4
IN7	-	8.8±7.3	10.1±8.6	11.9±10.9
INavg	24.3±9.5	9.1±7.2	12.6±9	10.7±10.8

(B) 0 – 75 m

Stations	NCP_{DIC} (mmol C m^{-2} d^{-1})	NCP_{N+N} (mmol C m^{-2} d^{-1})	NCP_{TOC} (mmol C m^{-2} d^{-1})	NCP_{DON} (mmol C m^{-2} d^{-1})
IN0	36.3±19.8	15.6±8.4	-	-
IN1	3.9±11.6	-	-	-
IN2	42.1±14.4	15.1±8.3	28.4±11.7	33.3±11.8
IN3	34.7±11.8	12.6±7.9	15.9±9.6	5.8±10.4
IN4	31.3±11.2	15.7±8.4	15.6±9.5	15.3±11.1
IN5	58.1±17.8	14.2±8.2	14.2±9.3	9.7±10.7
IN6	22.0±10.3	11.1±7.6	15.4±9.5	6.9±10.5
IN7	-	15.6±8.9	15.4±9.5	12.8±10.9
INavg	28.6±13.3	13.4±7.9	17.6±9.9	14.4±11

(C) 0 – 110 m

Stations	NCP_{DIC} (mmol C m^{-2} d^{-1})	NCP_{N+N} (mmol C m^{-2} d^{-1})	NCP_{TOC} (mmol C m^{-2} d^{-1})	NCP_{DON} (mmol C m^{-2} d^{-1})
IN0	1.8±11.2	11.5±7.7	-	-
IN1	-14.7	-	-	-
IN2	26.4±15.3	12.4±7.8	31.1±12.1	32.4±11.8
IN3	24.4±15	9.8±7.4	15.8±9.6	6.6±10.5
IN4	19.4±14.1	8.3±7.2	13.3±9.1	12.6±10.9
IN5	58.8±20.7	10.5±7.5	15.1±9.4	9.7±10.7
IN6	7.3±10.7	12.3±7.8	19.5±10.2	10.7±10.8
IN7	-	14.4±8.2	18.1±10	12.0±10.9
INavg	12.8±13.1	10.5±7.4	19.0±10.1	14.1±11

Table 4.8 OUT-stations (n=3) NCP and other net carbon flux terms in the mixed layer (89±6 m) from the budgets of DIC and N+N by using the mixed layer model during E-Flux I.

Term	Flux (mmol C m^{-2} d^{-1})	
	DIC	N+N
Air-to-sea CO_2 exchange [a)]	0.53±0.30	NA
Vertical diffusion	2.65±0.36	1.34±0.31
NCP	3.18±0.47	1.34±0.31

a) Only for the mixed layer DIC budget. This flux is from Section 3.2.

Table 4.9 Observed and expected concentrations as well as the fraction of Subtropical Salinity Maximum Water (f_{deep}) over two depth horizons ((A) Mixed layer and (B) 0-110 m) from two end-member mixing model at individual IN-stations during E-Flux I.

(A) Mixed layer

Stations[a)]	**$f_{(deep)}$ (%)**	**$DIC_{IN(obs)}$ (μM)**	**$DIC_{IN(exp)}$ (μM)**	**$N+N_{IN(obs)}$ (μM)**	**$N+N_{IN(exp)}$ (μM)**
IN1 (49 m)	66.4	2030.9	2046.2±8.9	0.02	1.07±0.32
IN2 (33 m)	62.6	2019.7	2043.5±10.5	0.05	1.01±0.33
13 (30 m)	58.2	2017.1	2040.5±10.4	N/A	N/A
OUT_{avg} (n=3)	-	2000.3±5.1	-	0.09±0.06	-
OUT_{deep} (150 m)	-	2069.3±5.1	-	1.58±0.05	-

a). The number inside the parentheses is the mixed layer depth.

(B) 0-110 m

Stations	**$f_{(deep)}$ (%)**	**$DIC_{IN(obs)}$ (μM)**	**$DIC_{IN(exp)}$ (μM)**	**$N+N_{IN(obs)}$ (μM)**	**$N+N_{IN(exp)}$ (μM)**
IN1	70.9	2046.4	2051.6±6.1	0.52	1.15±0.21
IN2	78.4	2051.1	2056.2±6.1	0.44	1.31±0.32
13	66.3	2047.2	2048.8±7.6	N/A	N/A
OUT_{avg} (n=3)	-	2008.5±6.2	-	0.15±0.04	-
OUT_{deep} (150 m)	-	2069.3±5.1	-	1.58±0.05	-

Table 4.10 The IN-station NCP estimates during E-Flux I. The results are over two depth horizons ((A) Mixed layer and (B) 0-110 m) from two end-member mixing model and mass balances of DIC and N+N.

(A) Mixed layer

Stations	NCP_{DIC} (mmol C m^{-2} d^{-1})	NCP_{N+N} (mmol C m^{-2} d^{-1})
IN1	8.1±4.7	3.9±1.3
IN2	8.4±3.7	2.3±0.8
13	7.4±3.3	N/A

(B) 0-110 m

Stations	NCP_{DIC} (mmol C m^{-2} d^{-1})	NCP_{N+N} (mmol C m^{-2} d^{-1})
IN1	6.0±7.0	5.1±2.1
IN2	5.8±6.9	6.6±2.4
13	1.6±7.6	N/A

Table 4.11 The corrected IN-station NCP estimates after considering the net effect of evaporation/precipitation during E-Flux I. The results are over two depth horizons ((A) Mixed layer and (B) 0-110 m) from two end-member mixing model and mass balances of DIC and N+N.

(A) Mixed layer*

Stations	NCP_{DIC} (mmol C m^{-2} d^{-1})	NCP_{N+N} (mmol C m^{-2} d^{-1})
IN1	5.8±3.8	3.4±1.2
IN2	6.8±3.3	1.8±0.7
13	5.2±2.9	N/A

* including the net effect of evaporation/precipitation.

(B) 0-110 m*

Stations	NCP_{DIC} (mmol C m^{-2} d^{-1})	NCP_{N+N} (mmol C m^{-2} d^{-1})
IN1	4.1±4.8	4.7±2.0
IN2	3.6±4.3	6.2±2.2
13	0±5.5	N/A

* including the net effect of evaporation/precipitation.

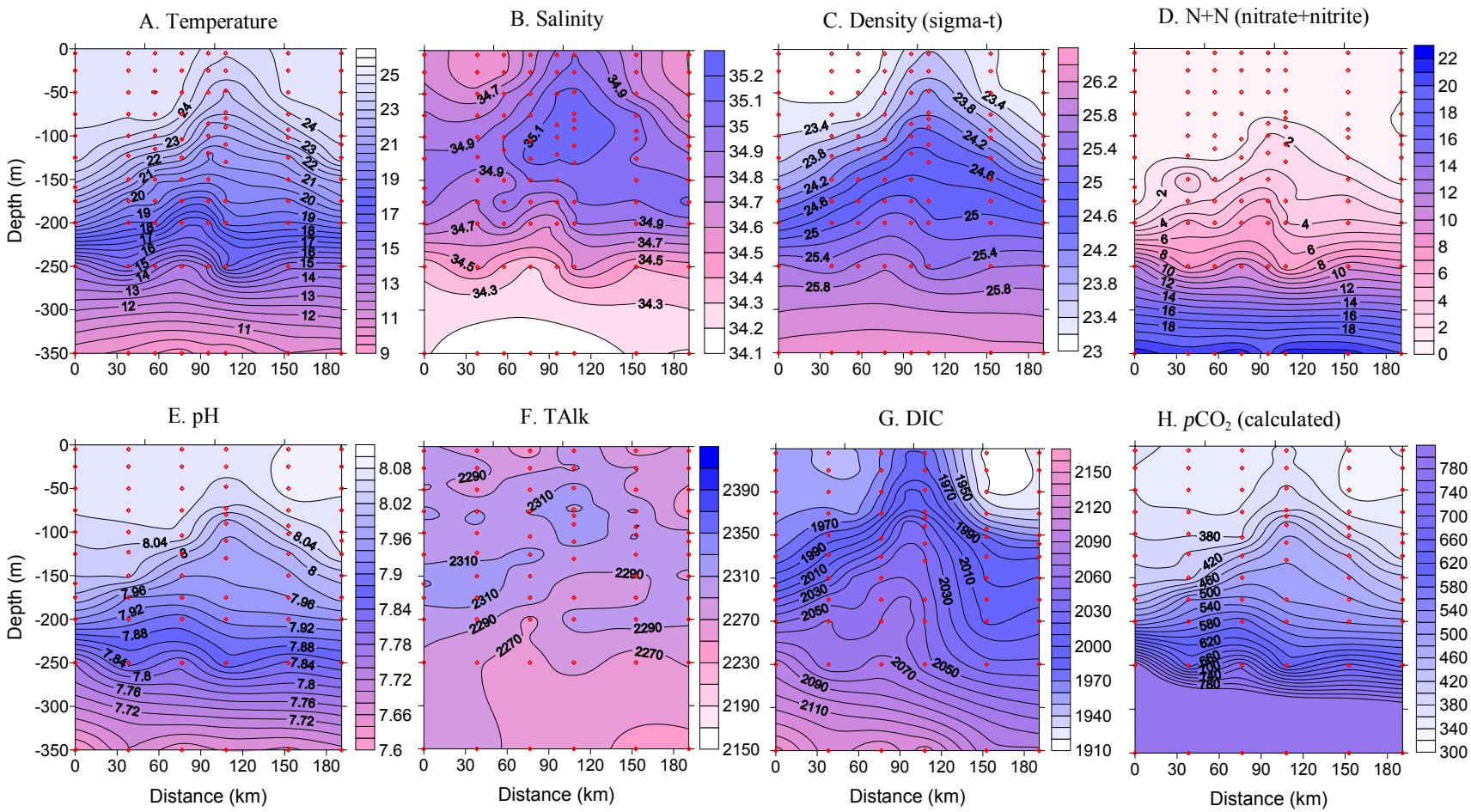

Fig. 4.1 Vertical sections (A. Temperature (°C); B. Salinity; C. Density (σ_t); D. N+N (μM); E. pH; F. TAlk (μmol·kg^{-3}); G. DIC (μmol·kg^{-3}); H. pCO_2 (μatm) (calculated from pH and DIC, coefficients come from documents (Mehrbach et al., 1973; Dickson and Millero, 1987)) for Transect 3 from station 26 through 36 (Red dots represent real data) during E-Flux III. For the horizontal axis label, station 26 is located where distance is zero, and station 36 is located on the other side. Note that temperatures were not corrected to potential temperature since the data discussed do not exceed 350 m and deviation resulted is less than 0.03 ºC.

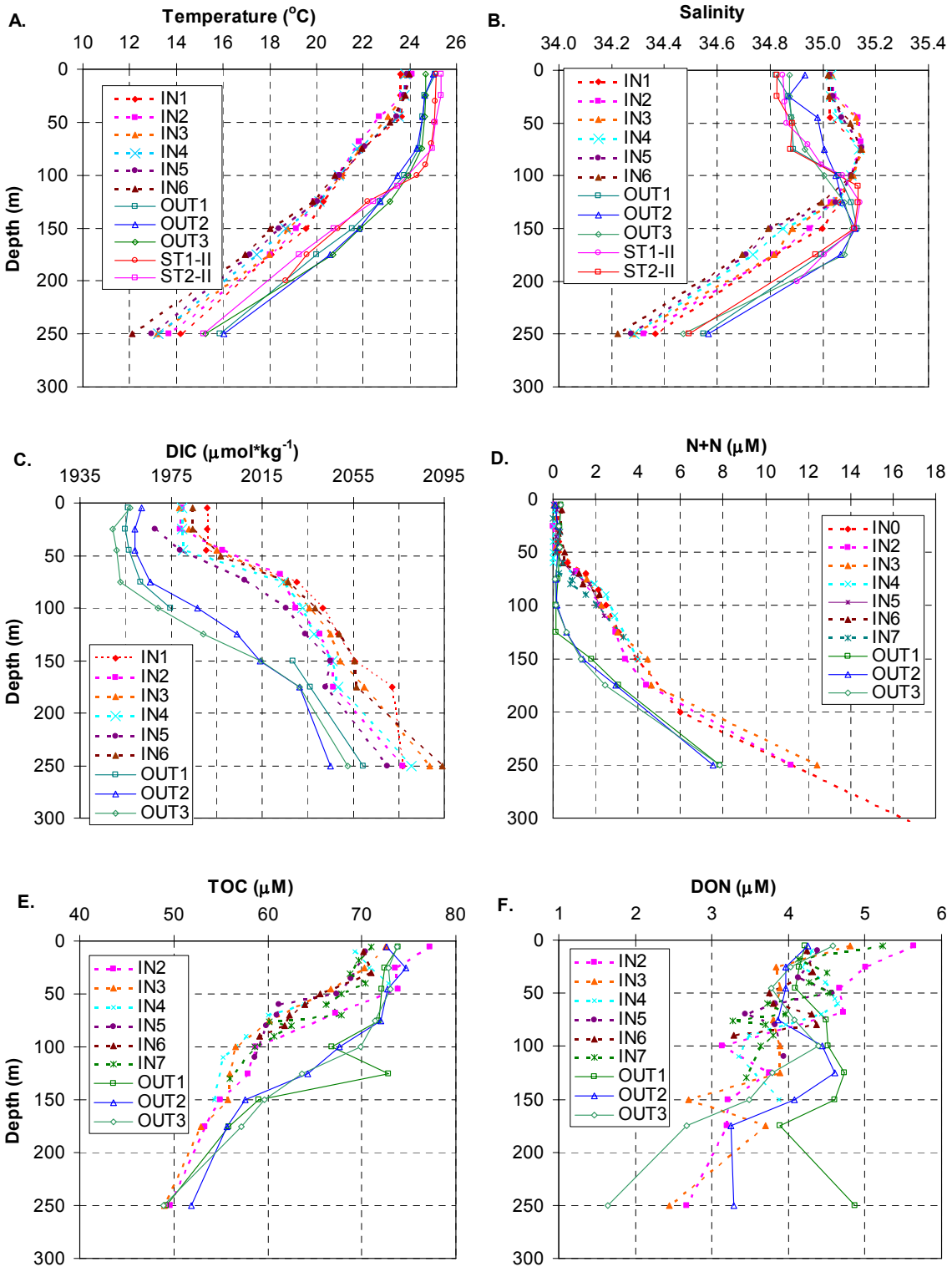

Fig. 4.2 Vertical profiles of (A) Temperature, (B) Salinity, (C) DIC, (D) Nitrate+nitrite (N+N), (E) TOC, and (F) DON vs. depth at IN- and OUT-stations during E-Flux III in March 2005. Please note that for (A) and (B), ST1-II and ST2-II correspond to two stations (IN3 and IN4) from E-Flux II cruise in January 2005.

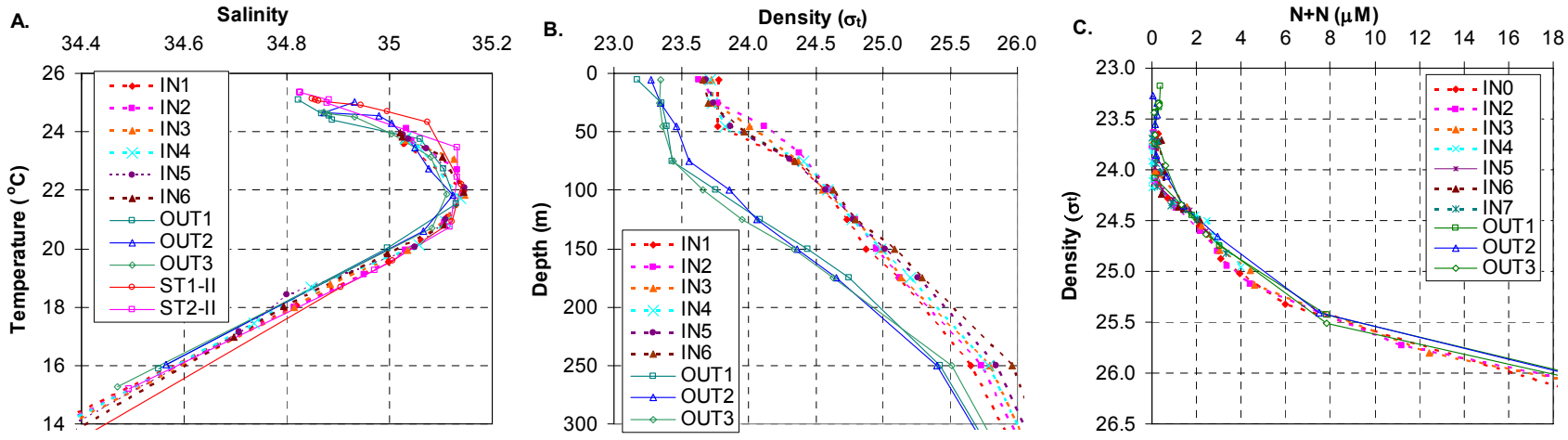

Fig. 4.3 (A) Diagram of salinity vs. temperature; (B) Profile of density vs. depth; and (C) Profile of N+N vs. density at IN-stations and OUT-stations during E-Flux III in March 2005. Please note that for (A), ST1-II and ST2-II correspond to two stations (IN3 and IN4) from E-Flux II cruise in January 2005.

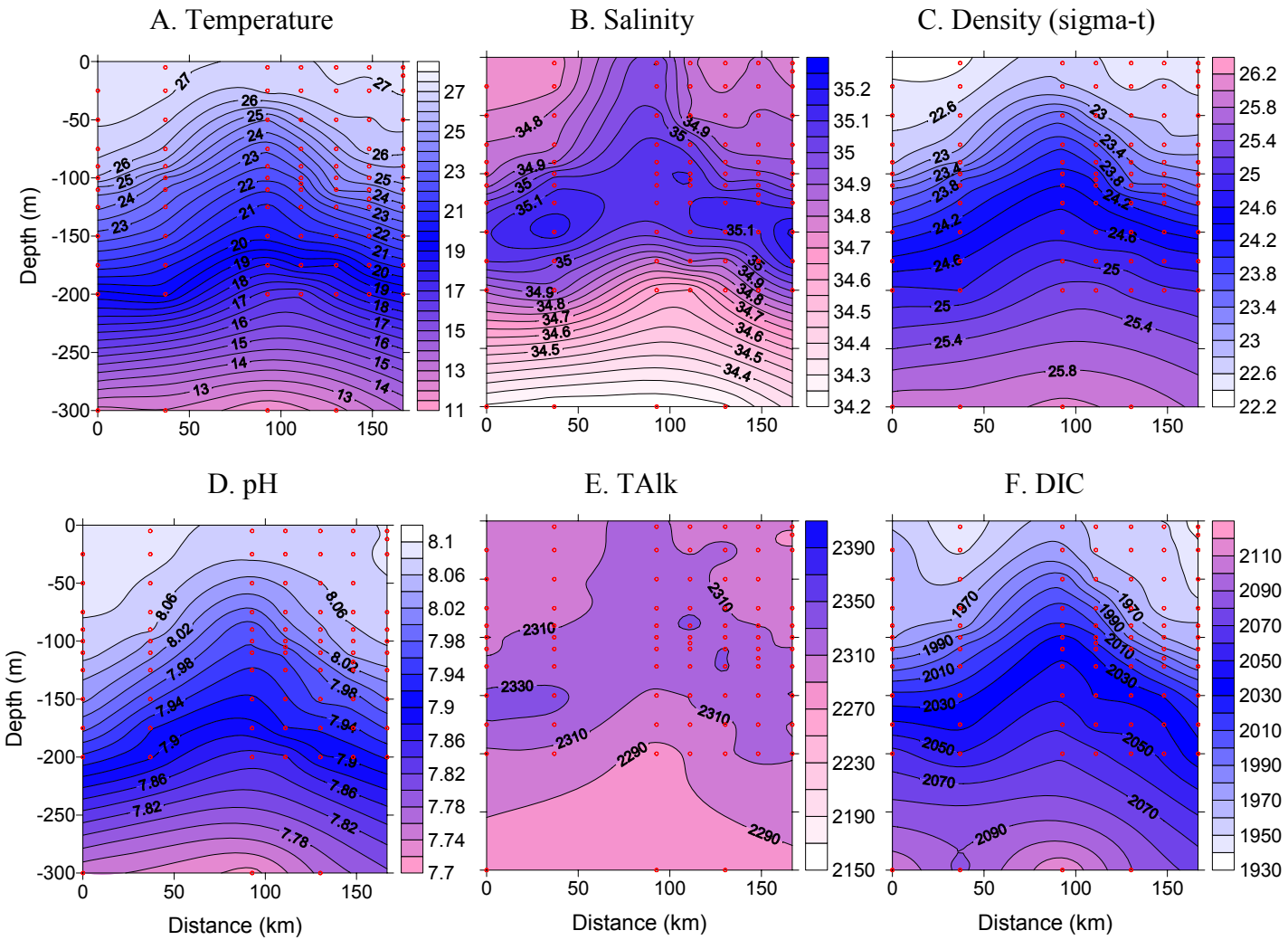

Fig. 4.4 Vertical sections (A. Temperature (°C); B. Salinity; C. Density (σ_t); D. pH; E. TAlk (μmol·kg^{-3}); F. DIC (μmol·kg^{-3}) for Transect 2 from station 8 through 17 (Red dots represent real data) during E-Flux I. For the horizontal axis label, station 8 is located where distance is zero, and station 17 is located on the other side. Note that temperatures were not corrected to potential temperature since the data discussed do not exceed 300 m and deviation resulted is less than 0.03 ºC.

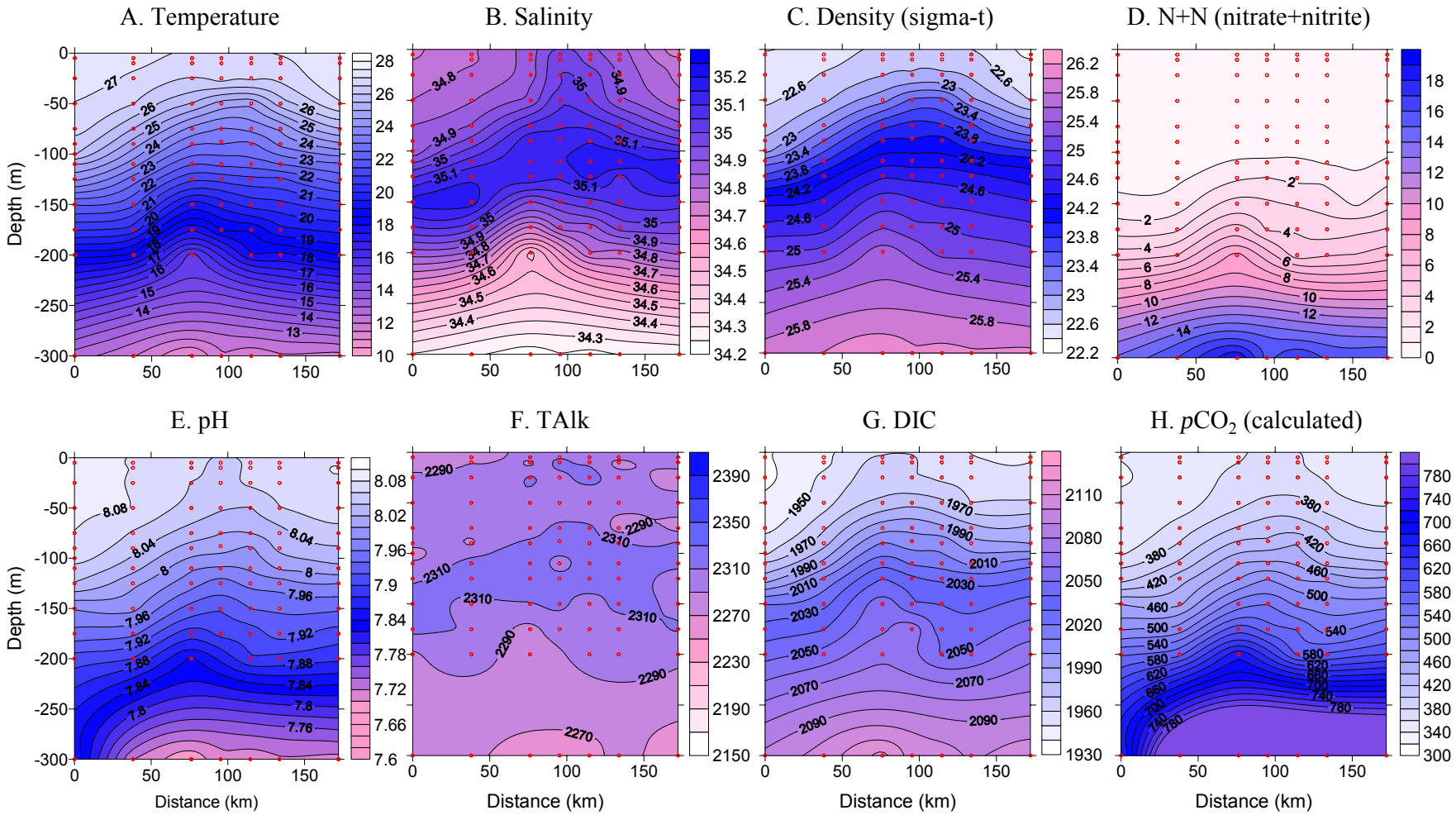

Fig. 4.5 Vertical sections (A. Temperature (°C); B. Salinity; C. Density (σ_t); D. N+N (μM); E. pH; F. TAlk (μmol·kg^{-3}); G. DIC (μmol·kg^{-3}); H. pCO_2 (μatm) (calculated from pH and DIC, coefficients come from documents (Mehrbach et al., 1973; Dickson and Millero, 1987)) for Transect 3 from station 18 through 27 (Red dots represent real data) during E-Flux I. For the horizontal axis label, station 18 is located where distance is zero, and station 27 is located on the other side. Note that temperatures were not corrected to potential temperature since the data discussed do not exceed 300 m and deviation resulted is less than 0.03 ºC.

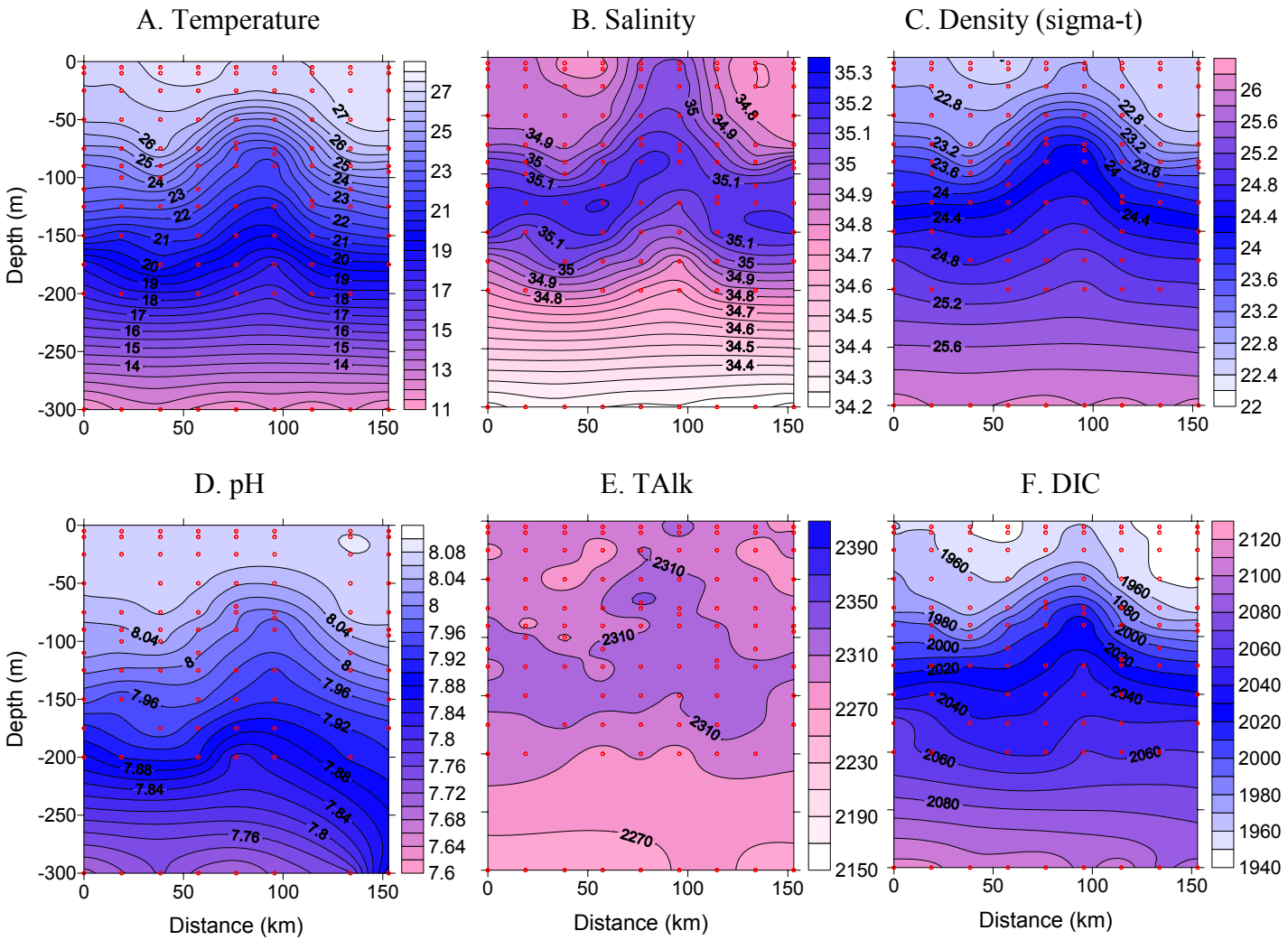

Fig. 4.6 Vertical sections (A. Temperature (°C); B. Salinity; C. Density (σ_t); D. pH; E. TAlk (μmol·kg^{-3}); F. DIC (μmol·kg^{-3}) for Transect 4 from station 29 through 38 (Red dots represent real data) during E-Flux I. For the horizontal axis label, station 29 is located where distance is zero, and station 38 is located on the other side. Note that temperatures were not corrected to potential temperature since the data discussed do not exceed 300 m and deviation resulted is less than 0.03 ºC.

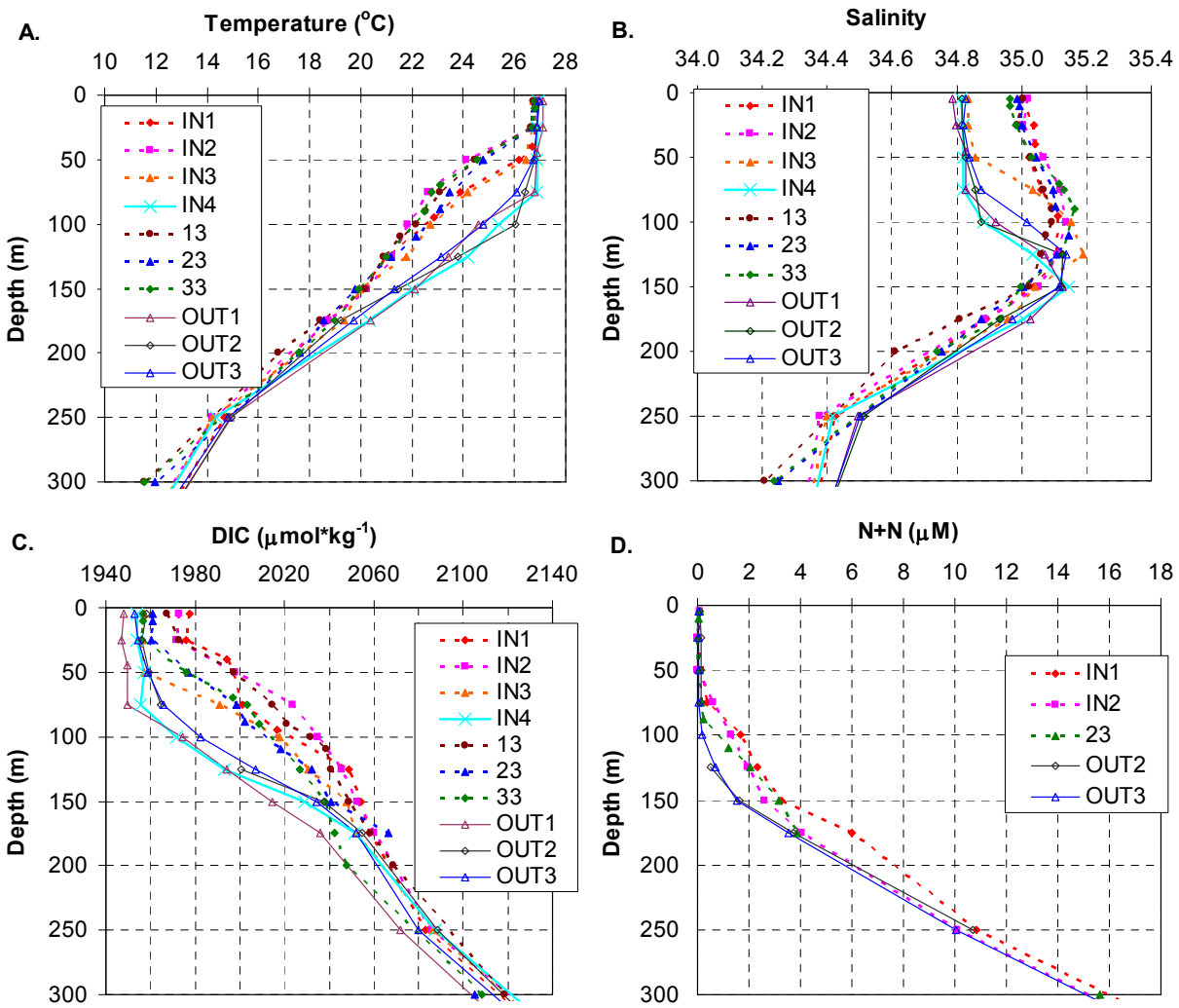

Fig. 4.7 Vertical profiles of (A) Temperature, (B) Salinity, (C) DIC, and (D) Nitrate+nitrite (N+N) vs. depth at IN- and OUT-stations during E-Flux I in November 2004.

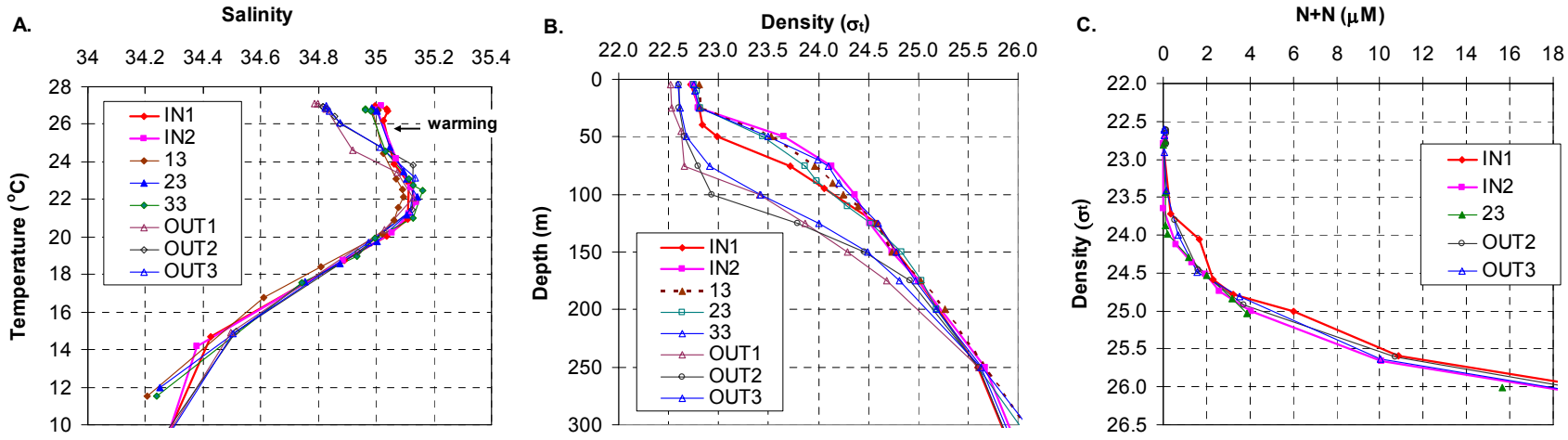

Fig. 4.8 (A) Diagram of salinity vs. temperature; (B) Profile of density vs. depth; and (C) Profile of N+N vs. density at IN-stations and OUT-stations during E-Flux I.

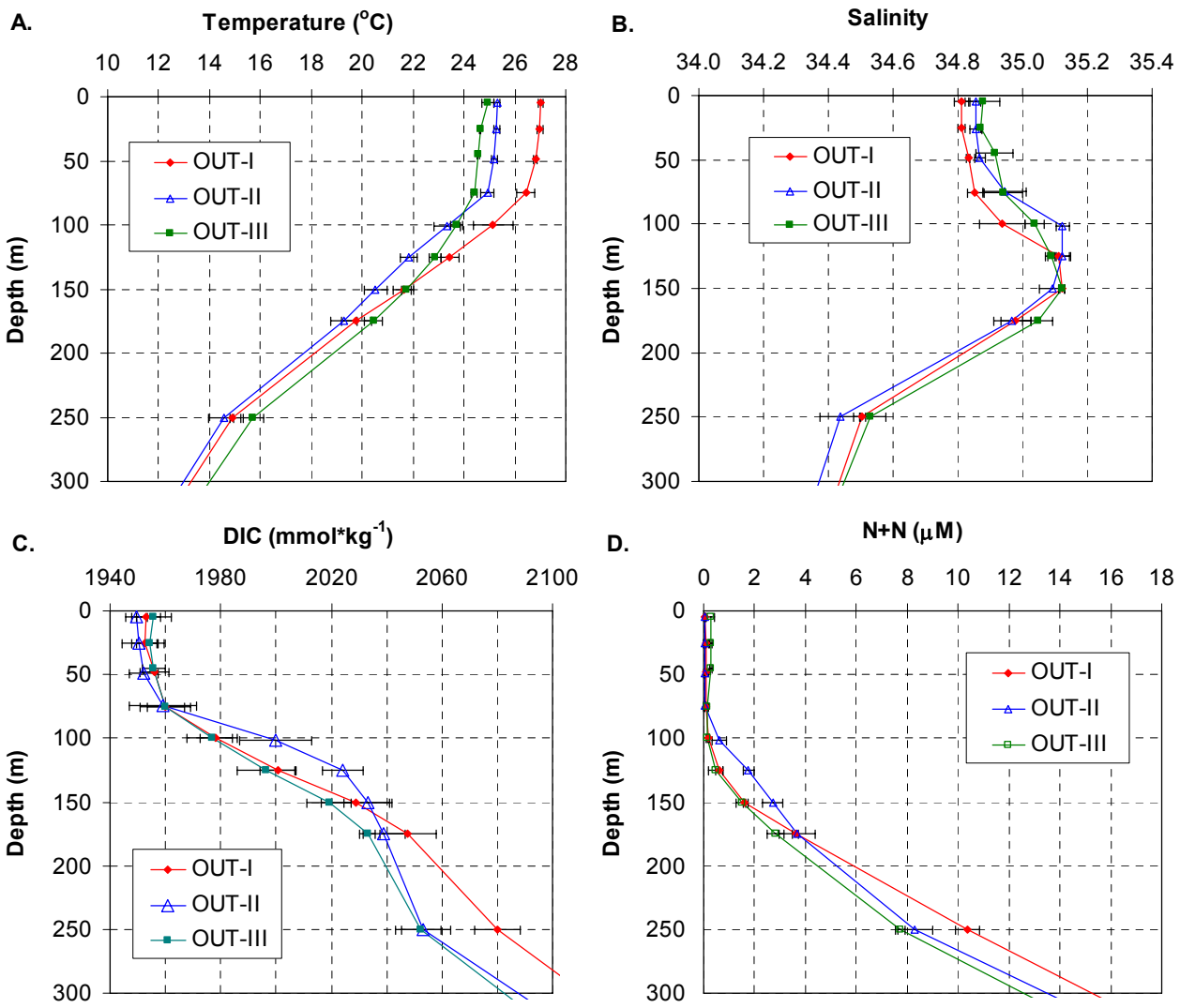

Fig. 4.9 Average vertical profiles of (A) Temperature, (B) Salinity, (C) DIC, and (D) Nitrate+nitrite (N+N) vs. depth at OUT-stations during three consecutive E-Flux cruises. OUT-I, OUT-II, and OUT-III represent OUT-stations from E-Flux I, II, and III, respectively.

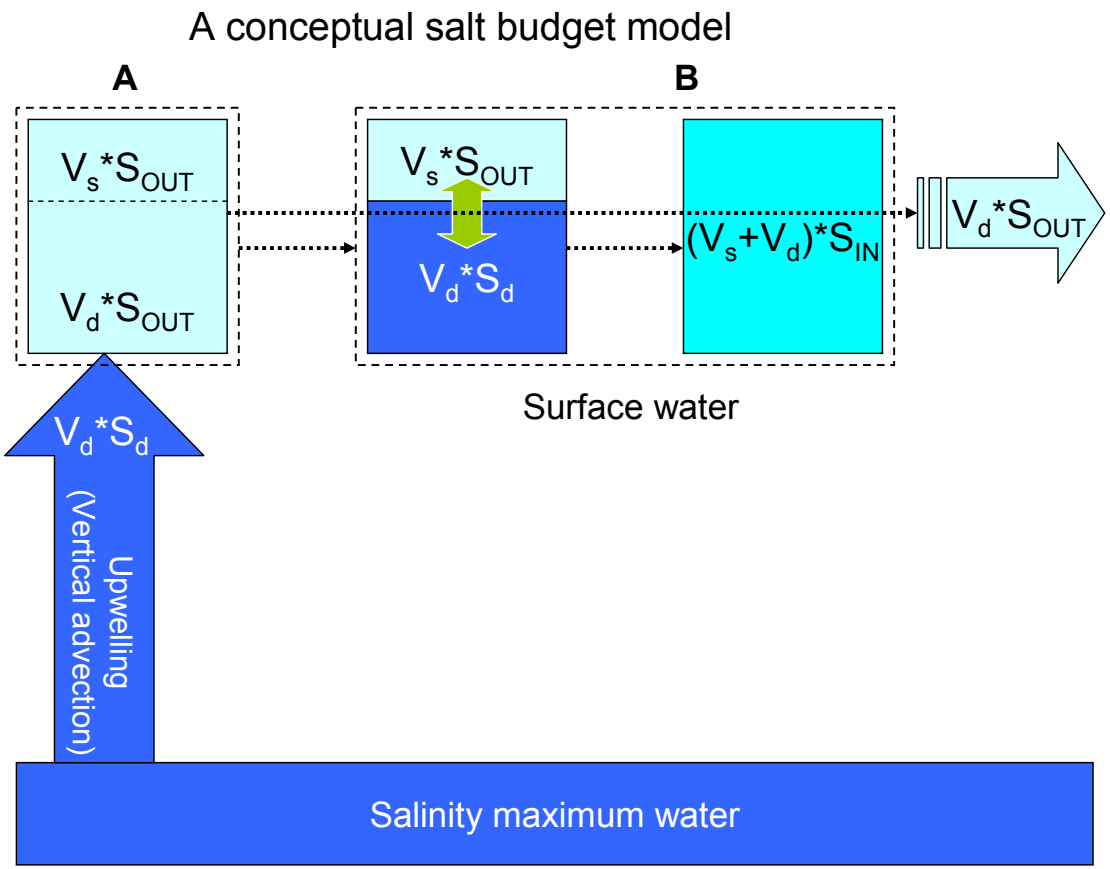

Fig. 4.10 Conceptual salt budget model for the eddy case: (A) Before subsurface salinity maximum water Intruding the surface layer inventory; (B) After the eddy-induced intrusion of salinity maximum deep water in the surface layer inventory. There are two balances here: (1) Water mass balance: $V_T = V_s + V_d$;
(2) Salt mass balance: $V_s \cdot S_{OUT} + V_d \cdot S_d = (V_s + V_d) \cdot S_{IN}$.

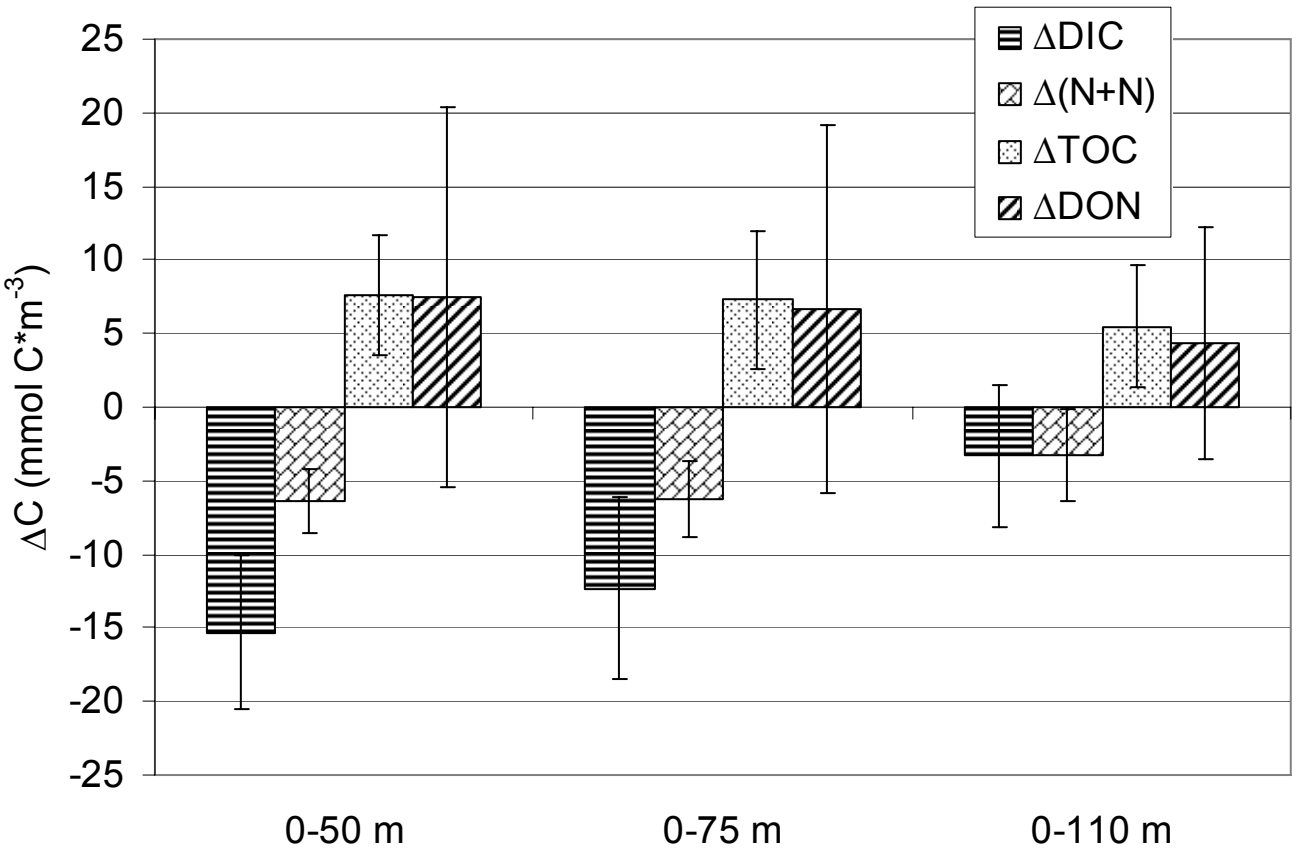

Fig. 4.11 Difference between average observed and expected concentrations of four biogeochemical parameters (ΔDIC, Δ(N+N), ΔTOC, and ΔDON) at IN-stations over three depth horizons (0-50 m, 0-75 m, and 0-110 m) from two end-member mixing model during E-Flux III. Please note that the units of Δ(N+N) and ΔDON were converted to carbon by using different C/N ratios (6.6 and 13.6 for particulate organic carbon and dissolved organic carbon, respectively).

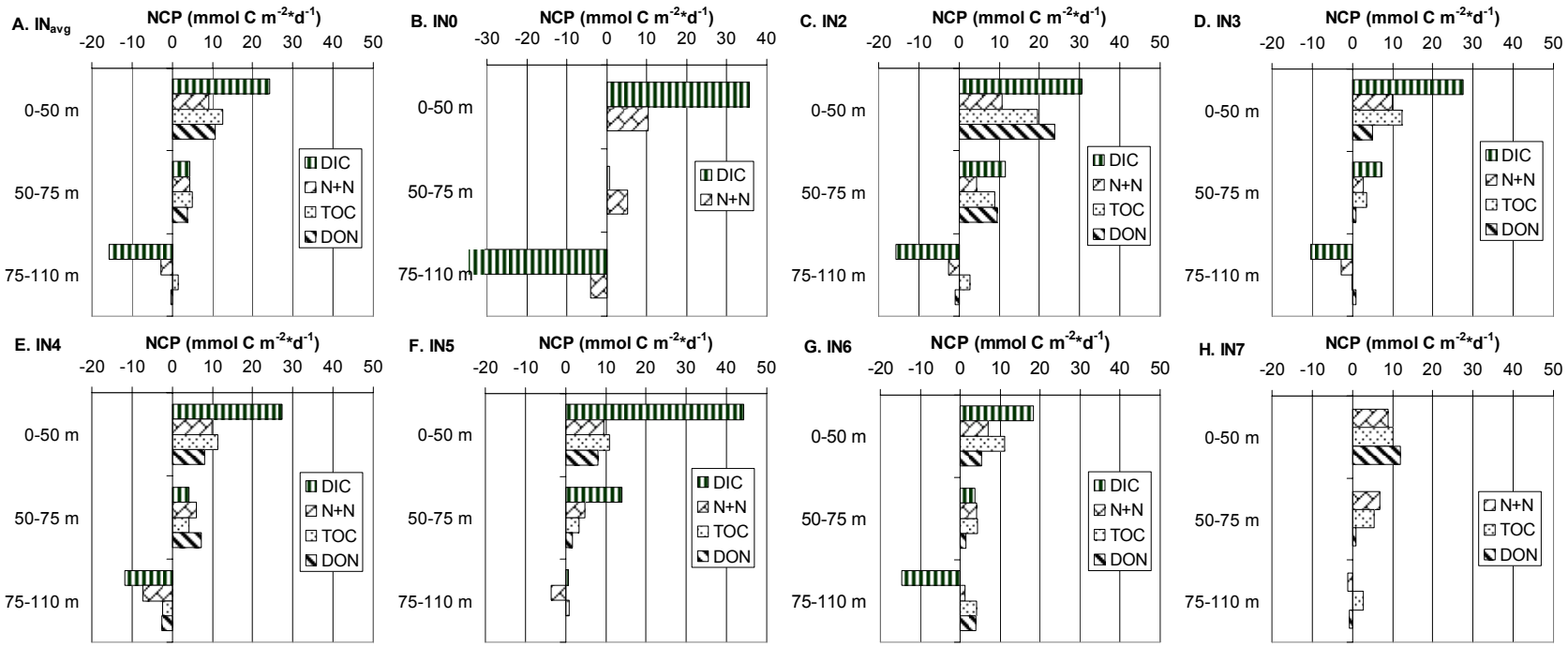

Fig. 4.12 Net community production (NCP) based on DIC, N+N, TOC, and DON mass balances in E-Flux III by using salt budget approach at three different depth intervals: 0-50 m, 50-75 m, and 75-110 m, respectively. (A) Average NCP estimate at IN-stations; (B-H) NCP estimates at individual IN-stations.

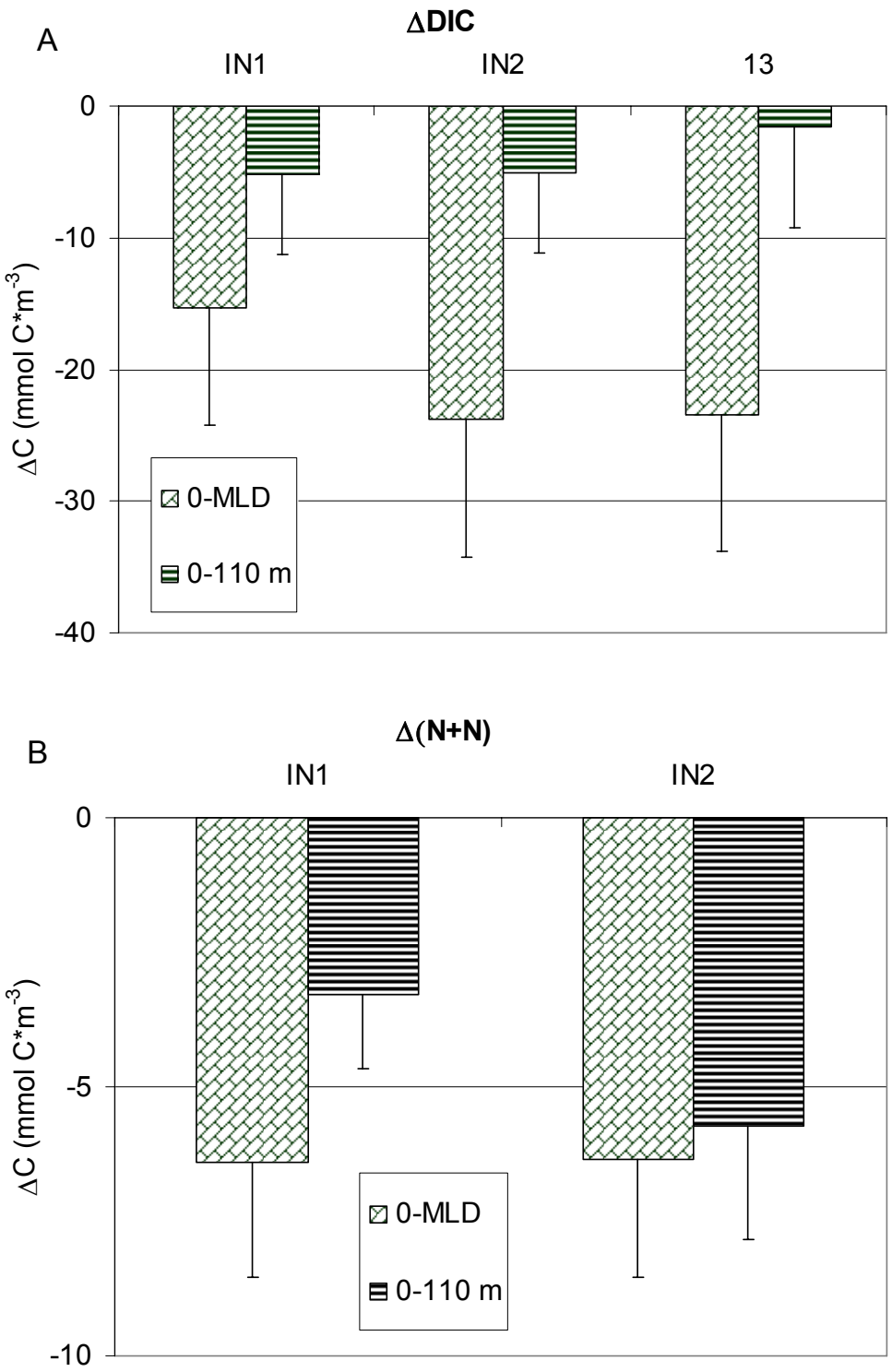

Fig. 4.13 Difference between average observed and expected concentrations of two biogeochemical parameters ((A) ΔDIC and (B) Δ(N+N)) at IN-stations over two depth horizons (0-MLD and MLD-110 m) from two end-member mixing model during E-Flux I. Please note that the unit of Δ(N+N) was converted to carbon by using different C/N ratios (6.6 for particulate organic carbon).

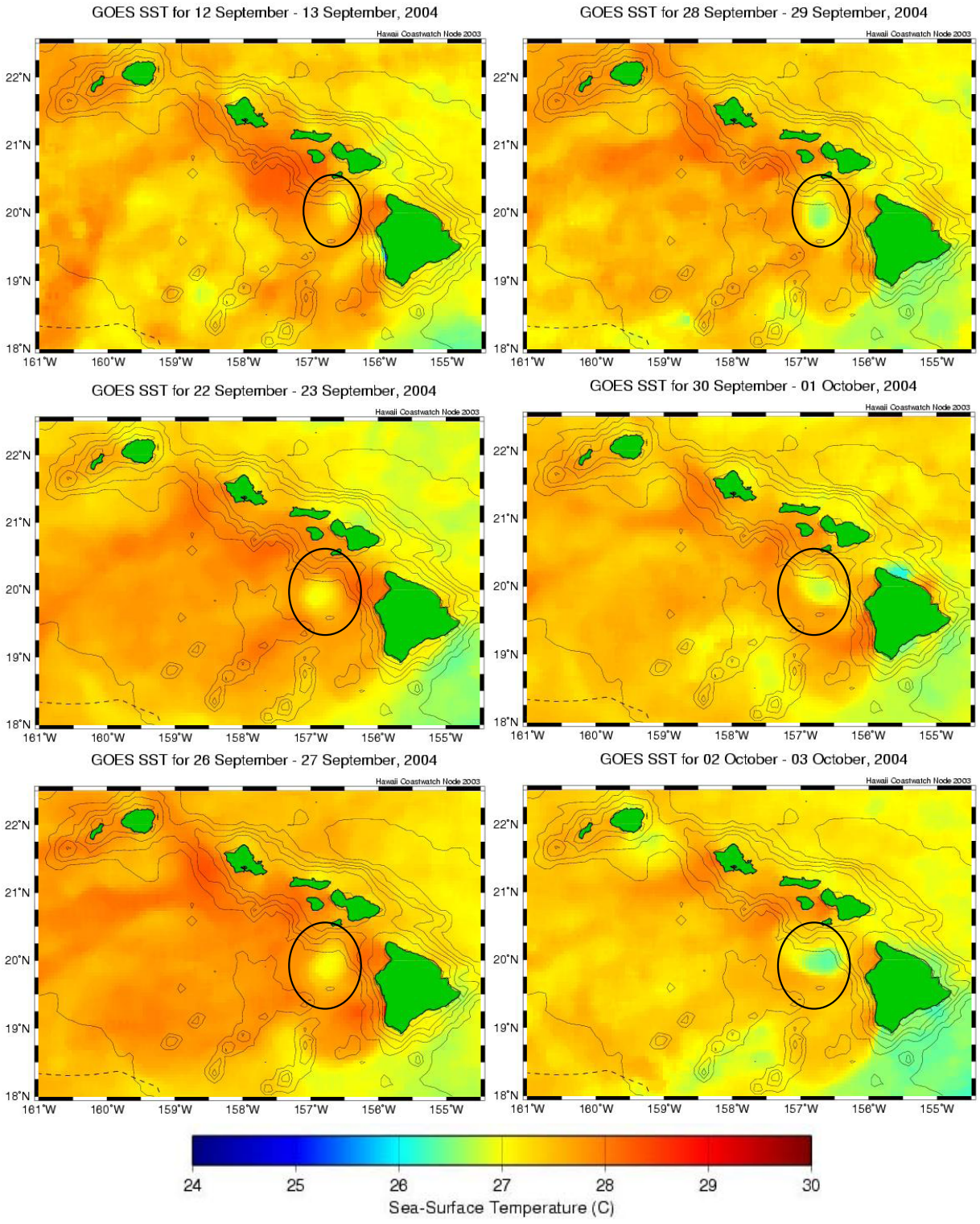

Fig. 4.14 Time-series remote sensing of GOES SST image in the lee of Hawaii area about one and a half months before the E-Flux I cruise. Black circles highlight the cold core of Cyclone Noah. It seems that Cyclone Noah was re-intensified by the end of September 2004.

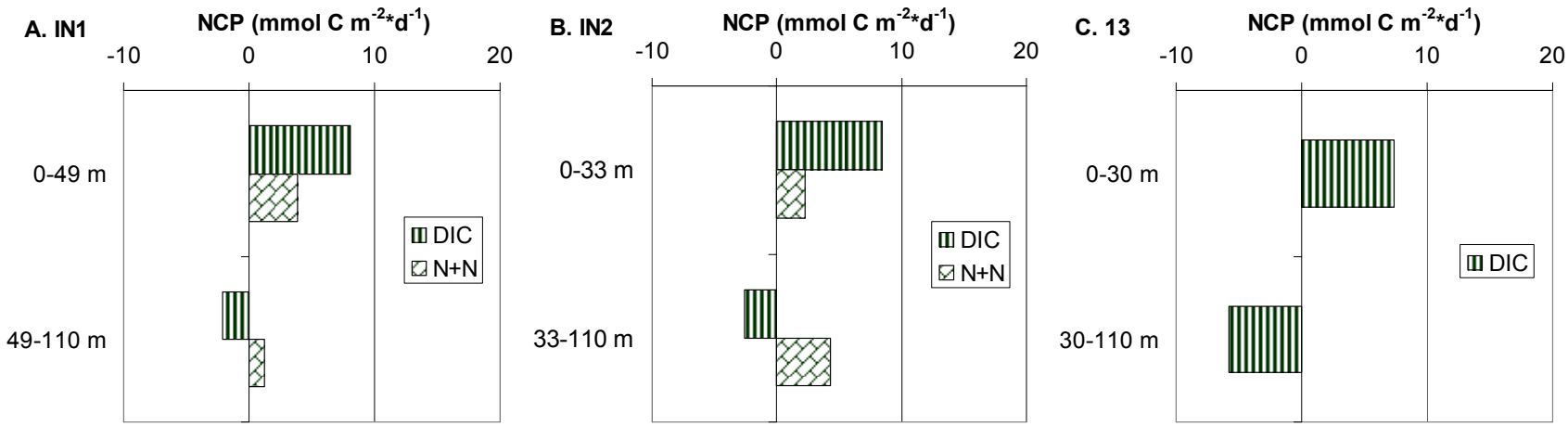

Fig. 4.15 Net community production (NCP) based on DIC and N+N mass balances in E-Flux I by using salt budget approach at two different depth intervals: 0-MLD and MLD-110 m, respectively. (A-E) NCP estimates at individual IN-stations.

CHAPTER 5 SUMMARY

Mesoscale eddies are ubiquitous features throughout the oceans and subtropical gyres which represent more than half of the global ocean area. In the oligotrophic oceans, NP is greatly constrained by the major nutrients from exogenous sources. Mesoscale eddies and other mesoscale processes were considered to be a major pathway for transporting new nutrients to the well-lit zone from nutrient-rich deep water from below. Quantifying the influence of the episodic mesoscale eddy events on air-sea CO_2 exchange and dissolved inorganic carbon cycling in the oligotrophic subtropical ocean will constrain the uncertainties in the estimation of global oceanic carbon fluxes.

In the worldwide open ocean, there are several common types of eddies. Combination of and dominant northeasterly trade winds and local steep sea-floor topography forms frequently wind-driven cyclone eddies in the lee of main Hawaii Islands in the subtropical North Pacific Gyre, and makes there an excellent field for eddy study. Two cyclonic eddies in their different life stages were sampled, i.e., Cyclone Opal in its mature phase and Noah in its spin-down or decay phase. My goals in this dissertation were to 1) improve the understanding of how biologically productive, cold-core cyclonic eddies affect sea surface pCO_2 in the lee of the main Hawaiian Islands in the subtropical North Pacific Gyre; 2) estimate the influence of cyclonic eddies on surface water CO_2 budget in the lee of Hawaii; 3) examine whether cold-core cyclonic eddies can significantly improve net community production due to the uplift of nutrients-rich deep water to the well-lit zone based on the inorganic carbon budget in the upper ocean.

In Chapter 3, we focused on how wind-driven cyclonic eddies affect sea surface pCO_2-SST relationships and air-sea CO_2 exchange. These findings help improve the accuracy of global

climatological distributions by assessing the role of mesoscale eddies. For Cyclone Opal, we identified three unique relationships between pCO_2 and sea surface temperature (SST). A positive correlation between pCO_2 and SST was observed in the waters surrounding the eddy suggesting surface CO_2 is controlled primarily by thermodynamics. In contrast, a negative relationship was observed within the eddy core as a result of the upwelling of CO_2-enriched subsurface waters. A third relationship existed throughout the rest of the eddy with reduced pCO_2 suggesting a combination of biological uptake, physical upwelling and thermodynamic controls. In the absence of an eddy, this region was a CO_2 sink, with the passage of the cold-core mesoscale eddy decreasing the magnitude of the sink by ~17%. However, if the general temperature correlation is used to predict pCO_2 inside the cold eddy, it would overestimate the CO_2 sink inside the eddy by 100%.

For Cyclone Noah, there was no difference in SST across the passage of Cyclone Noah due to near complete surface water warming which is consistent with its decay phase during the sampling period. Therefore, the observed SST-pCO_2 relationships are all positive and controlled primarily by thermodynamics, although sea surface pCO_2 within the eddy core was much higher than surrounding area due to the higher proportion of upwelled DIC-rich subsurface water from below. In the absence of Cyclone Noah, this area was a weak CO_2 sink. Within the eddy core, Cyclone Noah served as from neutral to weak CO_2 source by the time of sampling. Our preliminary estimates suggest although cyclonic eddies substantially enhance primary production, they do not necessarily enhance net CO_2 air-to-sea sink in subtropical ocean due to the balance of two competing mechanisms: vertical upwelling and biological uptake.

A plausible observation can be that cyclonic eddies serve as CO_2 sink during their spin-up or mature phase (as for Cyclone Opal) and neutral or weak CO_2 source during their decay

phase (as for Cyclone Noah). Of course, please note that for both cases, cyclone eddies reduced the intensity of net CO_2 sink within the center of cyclonic eddies. Alternatively, we propose that the magnitude of potential increase in SST within the eddy core is the primary factor to determine if a cyclonic eddy serves as a CO_2 sink or source. Such a magnitude is defined as the difference between the initial SST within the eddy core (when eddy core was just formed) and SST outside the eddy. This assumption is supported by the correlation between temporal decrease in SST and decrease in sea surface pCO_2 from two cyclonic eddies (Cyclone Opal and Noah), and further confirmed by a mechanistic understanding assessed by separating the relative roles of (1) upwelling induced mixing, (2) the thermodynamic effect (warming), (3) gas exchange, and (4) biological uptake.

In Chapter 4, we examined how wind-driven cyclonic eddies in their different life stages (i.e., Cyclone Opal in its mature phase and Noah in its decay phase), affect the dynamics of inorganic carbon and processes controlling net community production. For both eddies, within the eddy core, physical and biogeochemical properties suggested that nutrient- and DIC-rich deep waters were uplifted significantly (~80 m doming for Cyclone Opal and ~50 m for Noah) relative to surrounding waters, enhancing biological production. A salt budget indicates that the eddy core is a mixture of dominant part of deep water (with salinity maximum) and minor part of surface water.

For Cyclone Opal, NCP was estimated from mass balances of DIC, nitrate+nitrite, total organic carbon, and dissolved organic nitrogen, making rational inferences about the unobserved initial conditions at the time of eddy formation. Results consistently suggest that NCP in the center of the eddy was substantially enhanced relative to the surrounding waters outside the eddy. Within the eddy core, NCP ranged from 14.1 ± 10.6 (0 – 110 m: within the euphotic zone)

to 14.2 ± 9.2 (0 – 50 m: within the mixed layer) to 18.5 ± 10.7 (0 – 75 m: within the deep chlorophyll maximum layer) mmol C m^{-2} d^{-1} depending on the depth of integration. NCP in the ambient waters outside the eddy averaged about 2.37 ± 4.24 mmol C m^{-2} d^{-1} in the mixed layer (~0-95 m). Most of the enhanced NCP inside the eddy appears to have accumulated as dissolved organic carbon (DOC) rather than exported as particulate organic carbon (POC) to the mesopelagic. Our results for Cyclone Opal also suggest that the upper euphotic zone (0-75 m) above the deep chlorophyll maximum is characterized by positive NCP, while NCP in the lower layer (>75 m) is close to zero or negative.

In contrast, the magnitude of NCP enhancement for Cyclone Noah in its decay phase is much less than that for Cyclone Opal. In the mixed layer of the eddy center, NCPs from DIC and N+N are on average ~8.0 and ~3.1 mmol C m^{-2} d^{-1} respectively; and for the whole euphotic zone, NCPs from DIC and N+N are ~5.9 and ~5.8 mmol C m^{-2} d^{-1}, respectively. Thus, NCP within the eddy core of Cyclone Noah was only moderately enhanced comparing to that in the ambient waters outside the eddy (averaged 2.26±0.56 mmol C m^{-2} d^{-1}).

The lower NCP estimates during the decay phase of Cyclone Noah imply that the enhancement in NCP within cyclonic eddies is indeed ephemeral, which is consistent with the observed relaxation in physical, biological, and biogeochemical properties for Cyclone Noah. Firstly, most intense enhancement in NCP should occur during the mature phase. While in the decay phase, NCP enhancement should start to decrease since there is no active isopycnal uplift and therefore the growth-limited nutrient was depleted in the well-lit zone. Alternatively, Cyclone Opal was substantially dynamic with much higher translational speed than Cyclone Noah. Thus, multiple or even continuous nutrients injections were expected and therefore higher NCPs for Cyclone Opal. However, the possible re-intensification of Cyclone Noah about one and

a half months before the sampling time implies that our current NCP estimates for Cyclone Noah may be a conservative estimation. Further research is required to fully understand how different life stages (or age) and physical/chemical/biological characteristics of cyclonic eddies affect eddy NCP enhancement and air-sea CO_2 exchange.

REFERENCES

Allen, C.B., Kanda, J., Laws, E.A., 1996. New production and photosynthetic rates within and outside a cyclonic mesoscale eddy in the North Pacific subtropical gyre. Deep Sea Research (Part I, Oceanographic Research Papers) 43, 917-936.

Amiel, D., Cochran, J.K., Hirschberg, D.J., 2002. $^{234}Th/^{238}U$ disequilibrium as an indicator of the seasonal export flux of particulate organic carbon in the North Water. Deep-Sea Research Part Il-Topical Studies in Oceanography 49 (22-23, The International North Water Polynya Study), 5191-5209.

Anderson, R.A., Bidigare, R.R., Keller, M.D., Latasa, M., 1996. A comparison of HPLC pigment signatures and electron microscopic observations for oligotropic waters of the North Atlantic and Pacific Oceans. Deep-Sea Research (Part II, Topical Studies in Oceanography) 43, 517-537.

Bakker, D., Watson, A., 2001. A piece in the CO_2 jigsaw. Nature 410, 765-766.

Bates, N.R., Merlivat, L., Beaumont, L., Pequignet, A.C., 2000. Intercomparison of shipboard and moored CARIOCA buoy seawater fCO_2 measurements in the Sargasso Sea. Marine Chemistry 72 (2-4), 239-255.

Bates, N.R., Takahashi, T., Chipman, D.W., Knap, A.H., 1998. Variability of pCO_2 on diel to seasonal timescales in the Sargasso Sea near Bermuda. Journal of Geophysical Research-Oceans 103 (C8), 15567-15585.

Benitez-Nelson, C.R., Bidigare, R.R., Dickey, T., Landry, M.R., Leonard, C.L., Brown, S.L., Nencioli, F., Rii, Y.M., Maiti, K., Becker, J.W., Bibby, T.S., Black, W., Cai, W.-J., Carlson, C., Chen, F., Kuwahara, V.S., Mahaffey, C., McAndrew, P.M., Quay, P.D., Rappe, M., Selph, K.E., Simmons, M.P., Yang, E.J., 2007. Mesoscale eddies drive increased silica export in the subtropical Pacific Ocean. Science 316, 1017-1021.

Benner, R., Pakilski, J.D., McCarthy, M., Hedges, J.I., Hatcher, P.G., 1992. Bulk chemical characteristics of dissolved organic matter in the ocean. Science, pp. 1561-1564.

Bidigare, R.R., Benitez-Nelson, C., Leonard, C.L., Quay, P.D., Parsons, M.L., Foley, D.G., Seki, M.P., 2003. Influence of a cyclonic eddy on microheterotroph biomass and carbon export in the lee of Hawaii. Geophysical Research Letters 30 (6), 1318, doi: 1310.1029/2002GL016393.

Broenkow, W.W., 1965. The distribution of nutrients in the Costa Rica Dome in the eastern tropical Pacific Ocean. Limnology and Oceanography 10, 40-52.

Brown, S.L., Yang, E.J., Landry, M.R., Selph, K., 2008. Diatoms in the dissert. Deep Sea Research (Part II, Topical Studies in Oceanography) in press.

Cai, W.-J., Wang, Y., 1998. The chemistry, fluxes and sources of carbon dioxide in the estuarine waters of the Satilla and Altamaha Rivers, Georgia. Limnology and Oceanography 43, 657-668.

Capone, D.G., Zehr, J.P., Paerl, H.W., Bergman, B., Carpenter, E.J., 1997. *Trichodesmium*, a Globally Significant Marine Cyanobacterium Science 276 (5316), 1221-1229.

Carlson, C.A., Giovannoni, S.J., Hansell, D.A., Goldberg, S.J., Parsons, R., Vergin, K., 2004. Interactions between DOC, microbial processes, and community structure in the mesopelagic zone of the northwestern Sargasso Sea. Limnology and Oceanography 49, 1073-1083.

Chavanne, C., Flament, P., Lumpkin, R., Dousset, B., Bentamy, A., 2002. Scatterometer observations of wind variations by oceanic islands: Implications for wind driven ocean circulation. Can. J. Remote Sensing 28 (3), 466-474.

Chen, F., Cai, W.-J., Benitez-Nelson, C., Wang, Y., 2007. Sea surface pCO_2-SST relationships across a cold-core cyclonic eddy: Implications for understanding regional variability and air-sea gas exchange. Geophysical Research Letters 34 (L10603), doi:10.1029/2006GL028058.

Chen, F., Cai, W.-J., Wang, Y., Rii, Y.M., Bidigare, R.R., Benitez-Nelson, C.R., resubmitted. The carbon dioxide system and net community production within a cyclonic eddy in the lee of Hawaii. Deep Sea Research (Part II, Topical Studies in Oceanography).

Chierici, M., Miller, L.A., Whitney, F.A., Johnson, K.W., Wong, C.S., 2005. Biogeochemical evolution of the carbon dioxide system in the waters of long-lived mesoscale eddies in the Northeast Pacific Ocean. Deep Sea Research (Part II, Topical Studies in Oceanography) 52 (7-8), 955-974.

Cochran, J.K., Buesseler, K.O., Bacon, M.P., Livingston, H.D., 1993. Thorium isotopes as indicators of particle dynamics in the upper ocean: results from the JGOFS North Atlantic Bloom experiment. Deep Sea Research (Part I, Oceanographic Research Papers) 40 (8), 1569-1595.

Cosca, C.E., Feely, R.A., Boutin, J., Etcheto, J., McPhaden, M.J., Chavez, F.P., Strutton, P.G., 2003. Seasonal and interannual CO_2 fluxes for the central and eastern equatorial Pacific Ocean as determined from fCO_2-SST relationships. Journal of Geophysical Research-Oceans 108 (C8), 3278, doi:3210.1029/2000JC000677.

Crawford, W.R., Whitney, F., 1999. Mesoscale eddies aswirl with data in Gulf of Alaska Ocean. EOS, Transactions, American Geophysical Union 80, 365-370.

Dandonneau, Y., 1995. Sea-Surface Partial-Pressure of Carbon-Dioxide in the Eastern Equatorial Pacific (August 1991 to October 1992) - a Multivariate-Analysis of Physical and Biological Factors. Deep-Sea Research Part Ii-Topical Studies in Oceanography 42 (2-3), 349-364.

Denman, K., Gargett, A., 1983. Time and space scales of vertical mixing and advection of phytoplankton in the upper ocean. Limnology and Oceanography 28 (5), 801-805.

Dickey, T., Marra, J., Sigurdson, D.E., Weller, R.A., Kinkade, C.S., Zedler, S.E., Wiggert, J.D., Langdon, C., 1998. Seasonal variability of bio-optical and physical properties in the Arabian Sea: October 1994 - October 1995. Deep Sea Research (Part II, Topical Studies in Oceanography) 45, 2001-2025.

Dickey, T., Nencioli, F., Kuwahara, V.S., Leonard, C.L., Black, W., Bidigare, R.R., Rii, Y.M., Zhang, Q., 2008. Physical and bio-optical observations of oceanic cyclones west of the Island of Hawai'i. Deep Sea Research (Part II, Topical Studies in Oceanography) in press.

Dickson, A.G., Millero, F., 1987. A comparison of the equilibrium constants for the dissolution of carbonic acid in seawater media. Deep-Sea Research (Part A, Oceanographic Research Papers) 34, 1733-1743.

Dore, J.E., Lukas, R., Sadler, D.W., Karl, D.M., 2003. Climate-driven changes to the atmospheric CO_2 sink in the subtropical North Pacific Ocean. Nature 424 (6950), 754-757.

Dugdale, R.C., Goering, J.J., 1967. Uptake of new and regenerated forms of nitrgen in primary productivity. Limnology and Oceanography 12, 196-206.

Eppley, R.W., Peterson, B.J., 1979. Particulate organic matter flux and planktonic new production in the deep ocean. Nature 282, 677-680.

Falkowski, P.G., Ziemann, D., Kolber, Z., Bienfang, P.K., 1991. Role of eddy pumping in enhancing primary production in the ocean. Nature 352 (6330), 55-58.

Fischer, A.S., Weller, R.A., Rudnick, D.L., Lee, C.C., Brink, K.H., Fox, C.A., Leben, R.R., 2002. Mesoscale eddies, coastal upwelling, and the upper-ocean heat budget in the Arabian Sea. Deep-Sea Research (Part II, Topical Studies in Oceanography) 49 (12), 2231-2264.

Goldman, J.C., 1993. Potential role of large oceanic diatoms in new primary production. Deep Sea Research II 40, 159-168.

Gordon, L.I., Jennings, J.C., Ross, A.A., Krest, J.M., 1994. A suggested protocol for continuous flow analysis of seawater nutrients (Phosphate, Nitrate, Nitrite, and Silicic Acid) in the WOCE Hydrographic Program and Joint Global Ocean Fluxes Study. WHP Office Report 91-1.

Gruber, N., Keeling, C.D., Stocker, T.F., 1998. Carbon-13 constraints on the seasonal inorganic carbon budget at the BATS site in the northwestern Sargasso Sea. Deep-Sea Research (Part I, Oceanographic Research Papers) 45 (4-5), 673-717.

Haury, L.R., 1984. An offshore eddy in the California current system Part IV: Plankton distributions. Progress In Oceanography 13, 95-111.

Honjo, S., Dymond, J., Prell, W., Ittekkot, V., 1999. Monsoon-controlled export fluxes to the interior of the Arabian Sea. Deep-Sea Research (Part II, Topical Studies in Oceanography) 46 (8-9), 1859-1902.

Inoue, H.Y., Matsueda, H., Ishii, M., Fushimi, K., Hirota, M., Asanuma, I., Takasugi, Y., 1995. Long-Term Trend of the Partial-Pressure of Carbon-Dioxide (pCO_2) in Surface Waters of the Western North Pacific, 1984-1993. Tellus Series B-Chemical and Physical Meteorology 47 (4), 391-413.

Jacobson, D.M., Anderson, D.M., 1996. Widespread phagocytosis of ciliates and other protists by marine mixotrophic and heterotrophic thecate dinoflagellates. Journal of Phycology 32 (2), 279-285.

Jenkins, W.J., 1988. Nitrate flux into the euphotic zone near Bermuda. Nature 331, 521-523.

Jenkins, W.J., Goldman, J.C., 1985. Seasonal oxygen cycling and primary production in the Sargasso Sea. Journal of Marine Research 43 (2), 465-491.

Jeong, H.J., Yoo, Y.D., Kim, S.T., Kang, N.S., 2004. Feeding by the heterotrophic dinoflagellate Protoperidinium bipes on the diatom Skeletonema costatum. Aquatic Microbial Ecology 36 (2), 171-179.

Juranek, L.W., Quay, P.D., 2005. In vitro and in situ gross primary and net community production in the North Pacific Subtropical Gyre using labeled and natural abundance isotopes of dissolved O_2. Global Biogeochemical Cycles 19 (GB3009), doi: 10.1029/2004GB002384.

Keeling, C.D., Brix, H., Gruber, N., 2004. Seasonal and long-term dynamics of the upper ocean carbon cycle at Station ALOHA near Hawaii. Global Biogeochemical Cycles 18 (GB4006), doi: 10.1029/2004GB002227.

Kuwahara, V.S., Nencioli, F., Dickey, T., Rii, Y.M., Bidigare, R.R., 2008. Physical dynamics and biological implications of Cyclone *Noah* in the lee of Hawai'i during E-Flux I. Deep Sea Research (Part II, Topical Studies in Oceanography) in press.

Landrum, L.L., Gammon, R.H., Feely, R.A., Murphy, P.P., Kelly, K.C., Cosca, C.E., Weiss, R.F., 1996. North Pacific Ocean CO_2 disequilibrium for spring through summer, 1985-1989. Journal of Geophysical Research-Oceans 101 (C12), 28539-28555.

Landry, M.R., Brown, S.L., Rii, Y.M., Selph, K.E., Bidigare, R.R., Yang, E.J., Simmons, M.P., 2008. Depth-stratified phytoplankton dynamics in Cyclone Opal, a subtropical mesoscale eddy. Deep Sea Research (Part II, Topical Studies in Oceanography) in press.

Lee, K., 2001. Global net community production estimated from the annual cycle of surface water total dissolved inorganic carbon. Limnology and Oceanography 46 (6), 1287-1297.

Lee, K., Wanninkhof, R., Takahashi, T., Doney, S.C., Feely, R.A., 1998. Low interannual variability in recent oceanic uptake of atmospheric carbon dioxide. Nature 396 (6707), 155-159.

Lefevre, N., Aiken, J., Rutllant, J., Daneri, G., Lavender, S., Smyth, T., 2002. Observations of pCO_2 in the coastal upwelling off Chile: Spatial and temporal extrapolation using satellite data. Journal of Geophysical Research-Oceans 107 (C6), 3055, doi:3010.1029/2000JC000395.

Lefevre, N., Andrie, C., Dandonneau, Y., Reverdin, G., Rodier, M., 1994. pCO_2, Chemical-Properties, and Estimated New Production in the Equatorial Pacific in January-March 1991. Journal of Geophysical Research-Oceans 99 (C6), 12639-12654.

Lefevre, N., Taylor, A., 2002. Estimating pCO_2 from sea surface temperatures in the Atlantic gyres. Deep-Sea Research Part I-Oceanographic Research Papers 49 (3), 539-554.

Letelier, R.M., Karl, D.M., Abbott, M.R., Flament, P., Freilich, M., Lukas, R., Strub, T., 2000. Role of later winter mesoscale events in the biogeochemical variability of the upper water column of the North Pacific Subtropical Gyre. Journal of Geophysical Research-Oceans 105 (C12), 28723-28740.

Li, Y.-H., Karl, D.M., Winn, C.D., Mackenzie, F.T., Gans, K., 2000. Remineralization ratios in the subtropical North Pacific gyre. Aquatic Geochemistry 6, 65-86.

Liss, P.S., Merlivat, L., 1986. Air-sea gas exchange rates: Introduction and synthesis. In: The role of air-sea exchange in geochemical cycling (ed. P. Buat-Menard). D. Reidel, 113-127.

Lohrenz, S.E., Cai, W.-J., 2006. Satellite ocean color assessment of air-sea fluxes of CO_2 in a river-dominated coastal margin. Geophysical Research Letter 33.

Lumpkin, C.F., 1998. Eddies and currents of the Hawaiian Islands. Ph.D. Dissertation, Univ. Hawaii, 281 p.

Mahadevan, A., Archer, D., 2000. Modeling the impact of fronts and mesoscale circulation on the nutrient supply and biogeochemistry of the upper ocean. Journal of Geophysical Research-Oceans 105 (C1), 1209-1225.

Mahadevan, A., Levy, M., Memery, L., 2004. Mesoscale variability of sea surface pCO_2: What does it respond to? Global Biogeochemical Cycles 18 (1), GB1017, doi:1029/2003GB002102.

Mahaffey, C., Benitez-Nelson, C.R., Bidigare, R.R., Rii, Y.M., Karl, D.M., 2008. Nitrogen dynamics within a wind-driven eddy. Deep Sea Research (Part II, Topical Studies in Oceanography) in press.

Maiti, K., Benitez-Nelson, C.R., Rii, Y.M., Bidigare, R.R., 2008. The influence of a mature cyclonic eddy on particle export in the lee of Hawaii. Deep Sea Research (Part II, Topical Studies in Oceanography) in press.

McGillicuddy, D.J., Jr., Anderson, D.J., Doney, S.C., Maltrud, M.E., 2003. Eddy-driven sources and sinks of nutrients in the upper ocean: results from a 0.1° resolution model of the North Atlantic. Global Biogeochemical Cycles 17 (2) (1035), doi: 10.1029/2002GB001987.

McGillicuddy, D.J., Jr., Anderson, L.A., Bates, N.R., Bibby, T., Buesseler, K.O., Carlson, C.A., Davis, C.S., Ewart, C., Falkowski, P.G., Goldthwait, S.A., Hansell, D.A., Jenkins, W.J., Johnson, R., Kosnyrev, V.K., Ledwell, J.R., Li, Q.P., Siegel, D.A., Steinberg, D.K., 2007. Eddy/wind interactions stimulate extraordinary mid-ocean plankton blooms. Science 316, 1021-1026.

McGillicuddy, D.J., Jr., Robinson, A.R., 1997. Eddy-induced nutrient supply and new production in the Sargasso Sea. Deep Sea Research (Part I: Oceanographic Research Papers) 44 (8), 1427-1450.

McGillicuddy, D.J., Jr., Robinson, A.R., Siegel, D.A., Jannasch, H.W., Johnson, R., Dickey, T.D., McNeil, J., Michaels, A.F., Knap, A.H., 1998. Influence of mesoscale eddies on new production in the Sargasso Sea. Nature 394 (6690), 263-266.

McGillis, W.R., Edson, J.B., Ware, J.D., Dacey, J.W.H., Hare, J.E., Fairall, C.W., Wanninkhof, R., 2001. Carbon dioxide flux techniques performed during GasEx-98. Marine Chemistry 75 (4), 267-280.

McNeil, J.D., Jannasch, H.W., Dickey, T., McGillicuddy, D., Brzezinski, M., Sakamoto, C.M., 1999. New chemical, bio-optical and physical observations of upper ocean response to the passage of a mesoscale eddy off Bermuda. Journal of Geophysical Research. C. Oceans 104 (C7), 15537-15548.

Mehrbach, C., Culberson, C.H., Hawley, J.E., Pytkowicz, R.M., 1973. Measurement of the apparent dissociation constants of carbonic acid in seawater at atmospheric pressure. Limnology and Oceanography 18, 897-907.

Metzl, N., Poisson, A., Louanchi, F., Brunet, C., Schauer, B., Bres, B., 1995. Spatio-temporal Distributions of Air-Sea Fluxes of CO_2 in the Indian and Antarctic Oceans - a First Step. Tellus Series B-Chemical and Physical Meteorology 47 (1-2), 56-69.

Minas, H.J., Minas, M., Packard, T.T., 1986. Productivity in upwelling areas deduced from hydrographic and chemical fields. Limnology and Oceanography 31 (6), 1182-1206.

Mourino, C.B., McGillicuddy, D.J., Jr., 2006. Mesoscale variability in the metabolic balance of the Sargasso Sea. Limnology and Oceanography 51 (6), 2675-2689.

Nelson, N.B., Bates, N.R., Siegel, D.A., Michaels, A.F., 2001. Spatial variability of the CO_2 sink in the Sargasso Sea. Deep-Sea Research Part Ii-Topical Studies in Oceanography 48 (8-9), 1801-1821.

Nencioli, F., Kuwahara, V.S., Dickey, T., Rii, Y.M., Bidigare, R.R., 2008. Physical dynamics and biological implications of a mesoscale eddy in the lee of Hawaii: Cyclone Opal observations during E-Flux III. Deep Sea Research (Part II, Topical Studies in Oceanography) in press.

Nightingale, P.D., Liss, P.S., Schlosser, P., 2000a. Measurements of air-sea gas transfer during an open ocean algal bloom. Geophysical Research Letters 27, 2117-2120.

Nightingale, P.D., Malin, G., Law, C.S., Watson, A.J., Liss, P.S., Liddicoat, M.I., Boutin, J., Upstill-Goddard, R.C., 2000b. In situ evaluation of air-sea gas exchange parameterizations using novel conservative and volatile tracers. Global Biogeochemical Cycles 14 (1), 373-387.

Officer, C.B., 1980. Box Model Revisited. In: Hamilton, P., Macdonald, K.B. (Eds.), Estuarine and Wetland Processes. Plenum Press, New York.

Olaizola, M., Ziemann, D.A., Bienfang, P.K., Walsh, W.A., Conquest, L.D., 1993. Eddy-induced oscillations of the pycnocline affect the floristic composition and depth distribution of phytoplankton in the subtropical Pacific. Marine Biology 116, 533-542.

Olsen, A., Trinanes, J.A., Wanninkhof, R., 2004. Sea-air flux of CO_2 in the Caribbean Sea estimated using in situ and remote sensing data. Remote Sensing of Environment 89 (3), 309-325.

Ono, T., Saino, T., Kurita, N., Sasaki, K., 2004. Basin-scale extrapolation of shipboard pCO_2 data by using satelliate SST and Chla. International Journal of Remote Sensing 25 (19), 3803-3815.

Oschlies, A., 2002. Can eddies make ocean deserts bloom? Global Biogeochemical Cycles 16 (4), 1106, doi:1110.1029/2001GB001830.

Oschlies, A., Garcon, V., 1998. Eddy-induced enhancement of primary production in a model of the North Atlantic Ocean. Nature 394, 266-269.

Patzert, W.C., 1969. Eddies in Hawaiian Islands. Report No. HIG-69-8, Hawaii Institute of Geophysics, . University of Hawaii, Honolulu, HI.

Peixoto, J.P., Oort, A.H., 1992. Observed mean state of the atmosphere. In: Physics of climate. American Institue of Physics, New York, pp. 131-175.

Platt, T., Harrison, W.G., Lewis, M.R., Li, W.K.W., Sathyendranath, S., Smith, R.E., Vezina, A.F., 1989. Biological production in the oceans: the case for a consensus. Marine Ecology Progress Series 52, 77-88.

Quay, P., Stutsman, J., 2003. Surface layer carbon budget for the subtropical N. Pacific: $\delta^{13}C$ constraints at Station ALOHA. Deep-Sea Research (Part I, Oceanographic Research Papers) 50 (9), 1045-1061.

Quay, P.D., Tilbrook, B., Wong, C.S., 1992. Oceanic Uptake of Fossil-Fuel CO_2 - C-13 Evidence. Science 256 (5053), 74-79.

Redfield, A.C., 1958. The biological control of chemical factors in the environment. Am. Sci. 46, 206-226.

Rii, Y.M., Brown, S.L., Nencioli, F., Kuwahara, V.S., Dickey, T.D., Karl, D.M., Bidigare, R.R., 2008. The transient oasis: Nutrient-phytoplankton dynamics and particle export in Hawaiian lee cyclones. Deep Sea Research (Part II, Topical Studies in Oceanography) in press.

Robinson, A.R., 1983. Overview of eddy science. In: Robinson, A. R. (Ed.), Eddies in Marine Science. Springer, Berlin, pp. 3-15.

Sabine, C.L., Feely, R.A., Gruber, N., Key, R.M., Lee, K., Bullister, J.L., Wanninkhof, R., Wong, C.S., Wallace, D.W.R., Tilbrook, B., Millero, F.J., Peng, T.H., Kozyr, A., Ono, T., Rios, A.F., 2004. The oceanic sink for anthropogenic CO_2. Science 305 (5682), 367-371.

Sabine, C.L., Mackenzie, F.T., Winn, C., Karl, D.M., 1995. Geochemistry of carbon dioxide in seawater at the Hawaii Ocean time series station, Aloha. Global Biogeochemical Cycles 9 (4), 637-651.

Sarmiento, J.L., Gruber, N., 2002. Sinks for anthropogenic carbon. Physics Today 55 (8), 30-36.

Savidge, G., Williams, P.J.l.B., 2001. The PRIME 1996 cruise: an overview. Deep-Sea Research II 48, 687-704.

Seki, M.P., Polovina, J.J., Brainard, R.E., Bidigare, R.R., Leonard, C.L., Foley, D.G., 2001. Biological enhancement at cyclonic eddies tracked with GOES thermal imagery in Hawaiian waters. Geophysical Research Letters 28 (8), 1583-1586.

Shulenberger, E., Reid, J.L., 1981. The Pacific shallow oxygen maximum, deep chlorophyll maximum, and primary productivity, reconsidered. Deep-Sea Research 28, 901-920.

Siegel, D.A., McGillicuddy, D.J., Jr., Fields, E.A., 1999. Mesoscale eddies, satellite altimetry, and new production in the Sargasso Sea. Journal of Geophysical Research. C. Oceans 104 (C6), 13359-13379.

Stephens, M.P., Samuels, G., Olson, D.B., Fine, R.A., 1995. Sea-Air Flux of Co2 in the North Pacific Using Shipboard and Satellite Data. Journal of Geophysical Research-Oceans 100 (C7), 13571-13583.

Sweeney, E.N., McGillicuddy, J.D.J., Buesseler, K.O., 2003. Biogeochemical impacts due to mesoscale eddy activity in the Sargasso Sea as measured at the Bermuda Atlantic Time-series

Study (BATS). Deep Sea Research Part II: Topical Studies in Oceanography 50 (22-26), 3017-3039.

Takahashi, T., Feely, R.A., Weiss, R.F., Wanninkhof, R.H., Chipman, D.W., Sutherland, S.C., Takahashi, T.T., 1997. Global air-sea flux of CO_2: An estimate based on measurements of sea-air pCO_2 difference. Proceedings of the National Academy of Sciences, USA 94 (16), 8292-8299.

Takahashi, T., Olafsson, J., Goddard, J.G., Chipman, D.W., Sutherland, S.C., 1993. Seasonal-Variation of CO_2 and Nutrients in the High-Latitude Surface Oceans - a Comparative-Study. Global Biogeochemical Cycles 7 (4), 843-878.

Takahashi, T., Sutherland, S.C., Sweeney, C., Poisson, A., Metzl, N., Tilbrook, B., Bates, N., Wanninkhof, R., Feely, R.A., Sabine, C., Olafsson, J., Nojiri, Y., 2002. Global sea-air CO_2 flux based on climatological surface ocean pCO_2, and seasonal biological and temperature effects. Deep-Sea Research II 49 (9-10), 1601-1622.

Tans, P.P., Fung, I.Y., Takahashi, T., 1990. Observational constraints on the global atmospheric CO_2 budget. Science 247, 1431-1438.

Vaillancourt, R.D., Marra, J., Seki, M.P., Parsons, M.L., Bidigare, R.R., 2003. Impact of a cyclonic eddy on phytoplankton community structure and photosynthetic competency in the subtropical North Pacific Ocean. Deep Sea Research (Part I, Oceanographic Research Papers) 50 (7), 829-847.

Wang, Z.A., Cai, W.J., 2004. Carbon dioxide degassing and inorganic carbon export from a marsh-dominated estuary (the Duplin River): A marsh CO_2 pump. Limnology and Oceanography 49 (2), 341-354.

Wanninkhof, R., 1992. Relationship between Wind-Speed and Gas-Exchange over the Ocean. Journal of Geophysical Research-Oceans 97 (C5), 7373-7382.

Wanninkhof, R., Feely, R.A., 1998. fCO_2 dynamics in the Atlantic, South Pacific and South Indian oceans. Marine Chemistry 60 (1-2), 15-31.

Wanninkhof, R., McGillis, W.R., 1999. A cubic relationship between air-sea CO_2 exchange and wind speed. Geophysical Research Letters 26 (13), 1889-1892.

Watson, A.J., Robinson, C., Robinson, J.E., Williams, P.B., Fasham, M.J.R., 1991. Spatial variability in the sink for atmospheric carbon dioxide in the North Atlantic. Nature 350 (6313), 50-53.

Weiss, R.F., 1974. Carbon dioxide in water and seawater: The solution of a non-ideal gas. Mar. Chem. 2, 203-215.

Williams, P.J.l.B., 1993. On the definition of plankton production terms. ICES Marine Science Symposium 197, 9-19.

Williams, P.J.l.B., Morris, P.J., Karl, D.M., 2004. Net community production and metabolic balance at the oligotrophic ocean site, Station ALOHA. Deep Sea Research (Part I, Oceanographic Research Papers) 51, 1563-1578.

Williams, R.G., Follows, M.J., 1998. Eddies make ocean deserts bloom. Nature 394, 228-229.

Winn, C.D., Li, Y.H., Mackenzie, F.T., Karl, D.M., 1998. Rising surface ocean dissolved inorganic carbon at the Hawaii Ocean Time-series site. Marine Chemistry 60 (1-2), 33-47.

Winn, C.D., Mackenzie, F.T., Carrillo, C.J., Sabine, C.L., Karl, D.M., 1994. Air-sea carbon dioxide exchange in the North Pacific Subtropical Gyre: Implications for the global carbon budget. Global Biogeochemical Cycles 8 (2), 157-163.

Wyrtki, K., Kilonsky, B., 1984. Mean water and current structure during the Hawaii-to-Tahiti shuttle experiment. journal of Physical Oceanography 14, 242-254.